TÉCNICO LISBOA

Effects of Head-Mounted Virtual Reality and Haptics in Upper-Limb Brain–Computer Interface Training

Diogo Filipe Simões Batista

Thesis to obtain the Master of Science Degree in

Biomedical Engineering

Supervisors: Prof. Athanasios Vourvopoulos
Prof. Patrícia Margarida Piedade Figueiredo

Examination Committee

Chairperson: Prof. João Miguel Raposo Sanches
Supervisor: Prof. Athanasios Vourvopoulos
Member of the Committee: Prof. Sergi Bermúdez i Badia

November 2022

This work was created using LaTeX typesetting language
in the Overleaf environment (www.overleaf.com).

Preface

The work presented in this thesis was performed at the Evolutionary Systems and Biomedical Engineering Lab (LaSEEB) of Instituto Superior Técnico (Lisbon, Portugal), from December 2021 to October 2022, under the supervision of Prof. Athanasios Vourvopoulos and Prof. Patrícia Figueiredo.

I declare that this document is an original work of my own authorship and that it fulfills all the requirements of the Code of Conduct and Good Practices of the Universidade de Lisboa.

Acknowledgments

This thesis is the culmination of six years of hard work, which was done in a journey that I did not endeavor on my own. There are many people whom I cherish and want to thank for having been by my side during these years.

First, I want to thank my mom and dad, Maria Benedita and Luís, who love me unconditionally. They have always been there for me whenever I felt down, and will always be. I've not always been a good son, and it may seem at times that I don't appreciate just how much they have given me, but I do. As I grow up and become more mature, I hope I'll be able to give back to my parents and be there for them in the years to come.

Next, I want to thank my maternal grandparents, Assunção and Luís, and paternal grandparents, Ana and Joaquim, as well as my cousins Jorge, Sérgio, Sofia, and Afonso, who bring a sense of familiarity into my life and with whom I can spend time whenever we come together. My great-aunt Jesus also comes to mind. She understands me and my drive to make a name for myself well, and I want to thank her for believing in me.

I also want to thank my high-school friends, in no particular order: Rui, Rodrigo, Bruno Silva, Bruno António, Diogo, and Henrique. We always have lots of fun together, and we're certainly a tight bunch that'll withstand the test of time, even as we move on with our lives. In addition, my two friends from college, Edgar and Raul, made school much more bearable, especially when we worked together or went to the movies. I hope that our friendship will be long-lasting, too.

Of course, this thesis could not also have been done without the help of my supervisors, Prof. Vourvopoulos and Prof. Figueiredo, who provided indispensable help in overcoming the hurdles of such a monumental task. Conducting the experiments for the study were done not only with Prof. Vourvopoulos's help but Gustavo's as well, who also works at LaSEEB.

Lastly, I want to dedicate this thesis to my late aunt, Alcina. She was very proud of me, of how far I had come, and would have certainly been joyful to see me graduate.

Abstract

Brain–computer interfaces (BCIs) can provide a non-muscular channel for communication and control to patients for assistive or restorative use. Motor-imagery-based BCIs can be augmented with virtual reality (VR) and haptics to provide stroke patients with insufficient motor ability an alternative to conventional therapy. Two questions are addressed in this thesis: (1) What BCI–VR feedback configurations lead to the strongest, most lateralized brain activation in stroke rehabilitation? (2) What conditions and machine-learning algorithms lead to the most robust features and most accurate models? To achieve this, 19 healthy subjects performed motor-imagery training through five conditions with different combinations of abstract vs. realistic feedback through *NeuRow*, head-mounted display vs. monitor, and with or without haptic feedback. The power of alpha and beta rhythms following the motor tasks (event-related desynchronizations [ERDs]) and their hemispheric lateralization (lateralization indices [LIs]) were extracted for analysis. The subjects also answered questionnaires on motor-imagery ability and sense of embodiment. Seven machine-learning algorithms and several hyperparameters were tested for each condition. The results were benchmarked against motor execution. The data suggested that the use of haptic feedback and a virtual environment such as *NeuRow* lead to stronger brain activation, which could become important components in stroke rehabilitation. The support-vector classifier and multilayer perceptrons performed better but are not necessarily more adequate for stroke rehabilitation. The common spatial patterns used to train the models did not correlate significantly with the LIs for the most part, suggesting different features to be used in stroke rehabilitation.

Keywords

Brain–computer interfaces; Upper-limb stroke rehabilitation; Head-mounted virtual reality; Haptic feedback; Machine learning

Resumo

As interfaces cérebro–computador (BCIs) fornecem um canal não-muscular de comunicação e controlo a pacientes para uso de apoio ou restaurador. BCIs baseados na imaginação motora com realidade virtual (VR) e *haptics* podem dar as pacientes de AVCs com capacidade motora insuficiente uma alternativa à terapia convencional. Duas questões são abordadas nesta tese: (1) Que configurações de retroalimentação BCI–VR levam à ativação cerebral mais forte e lateralizada na reabilitação de AVC? (2) Que condições e algoritmos de aprendizagem automática levam aos *features* mais robustos e os modelos mais precisos? Dezanove indivíduos saudáveis realizaram imaginação motora através de cinco condições com diferentes combinações de retroalimentação abstrata vs. realista através de *NeuRow*, *head-mounted display* vs. monitor, e com ou sem *haptics*. As potências dos ritmos alfa e beta após as tarefas motoras (*event-related desynchronizations* [ERDs]) e as suas lateralizações hemisféricas (*lateralization indices* [LIs]) foram analisadas. Os sujeitos responderam a questionários sobre imaginação motora e corporização. Sete algoritmos de aprendizagem automática e vários hiperparâmetros foram testados para cada condição. Os resultados foram comparados com execução motora. Os dados sugeriram que o uso de *haptics* e de ambientes virtuais como *NeuRow* levam a uma ativação cerebral mais forte, podendo se tornarem em componentes importantes na reabilitação de AVC. O *support-vector classifier* e os *multilayer perceptrons* tiveram melhor desempenho, mas não são necessariamente mais adequados para a reabilitação de AVC. Os *common spatial patterns* usados para treinar os modelos não se correlacionaram significativamente com os LIs, sugerindo diferentes features devem ser usados na reabilitação.

Palavras-chave

Interfaces cérebro–máquina; Reabilitação de AVC dos membros superiores; Realidade virtual montada na cabeça; Retroalimentação háptica; Aprendizagem automática

Contents

List of Figures

List of Tables

List of Abbreviations

AdaBoost	Adaptive Boosting
ANOVA	analysis of variance
BCI	brain–computer interface
CAR	common average reference
CNN	convoluted neural network
CSP	common spatial pattern
ECG	electrocardiography
ECoG	electrocorticography
EEG	electroencephalography
EMG	electromyography
EOG	electrooculography
ERD	event-related desynchronization
ERS	event-related synchronization
ERSP	event-related spectral perturbation
EVI	external visual imagery
FES	functional electrical stimulation
FMA	Fugl-Meyer Assessment
fMRI	functional magnetic resonance imaging
HMD	head-mounted display
ICA	independent component analysis
IVI	internal visual imagery
LSL	Lab Streaming Layer

KI	kinesthetic imagery
***k*-NN**	*k*-nearest neighbors
LDA	linear discriminant analysis
LI	lateralization index
MEG	magnetoencephalography
mERD	mean event-related desynchronization
MLP	multilayer perceptron
PPG	photoplethysmography
REINVENT	Rehabilitation Environment using the Integration of Neuromuscular-based Virtual Enhancements for Neural Training
SNR	signal-to-noise ratio
SVC	support-vector classifier
VMIQ-2	Vividness of Movement Imagery Questionnaire-2
VR	virtual reality

1

Introduction

Contents

Stroke is a leading cause of mortality and disability worldwide [1], and its incidence is predicted to increase throughout the world as the population ages. Victims commonly lose their motor capability, which disrupts their ability to carry out their daily routines. To date, rehabilitation for stroke survivors with severe motor impairments is burdensome, since most current rehabilitation options require some volitional movement to retrain the affected limbs. However, prior research has shown that patients receive increased benefits by combining traditional therapy with emerging technologies like brain–computer interfaces (BCIs) [2] and virtual reality (VR) [3]. In particular, upper-limb rehabilitation of severely affected stroke patients comes with challenges that can be overcome through a technology-based approach.

A BCI can be described as a pattern-recognition system that utilizes the physiological activity from the brain to control external devices (e.g., a prosthesis) [4]. Although various signal-acquisition modalities can monitor brain activity, electroencephalography (EEG) is the most commonly employed, due to its relatively low cost, portability, high temporal resolution, and noninvasiveness [5]. Modulation of EEG in a closed loop can promote plastic changes in the brain, making BCIs an appealing tool for neurorehabilitation [6]. Specifically, motor-imagery-based BCIs (i.e., the subject imagines the movement of their limbs) help promote recovery from brain lesions—particularly in stroke patients [7]—by converting motor imagery into real events, such as exoskeleton [8] or avatar movement [6, 9].

It is, thus, a suitable candidate for the rehabilitation of stroke patients with a motor ability too atrophied to make use of conventional therapy. Nevertheless, the interfaces by themselves may not provide sufficiently engaging feedback to the patient, which can be augmented with, for example, VR.

Thanks to VR technology, patients are able to interact with engaging virtual environments through a plethora of devices, be it visual, auditory, or haptic. These include screens, head-mounted displays (HMDs), video-capture systems, data gloves, hand controllers, etc. With a vast array of apparatuses that increase the patient's immersion and sense of embodiment, the ability to design engaging motor-related tasks, and superior recovery when combined with conventional therapy [3], virtual rehabilitation seems to be the natural successor to the current rehabilitation paradigm. However, the more severe cases of stroke still prohibit patients from moving and engaging with VR-based rehabilitation. Nevertheless, combining it with BCIs can provide the best of both worlds and fill the bill.

Combining motor-imagery-based BCIs and VR can improve treatment results by directly training the central nervous system [2], providing embodied feedback through avatars, and offering engaging tasks that increase adherence to the treatment. Some, but not that many, studies have tested this synergistic duo with promising results. Nevertheless, given the recency of this field of research, fundamental questions still linger. A couple of these are identified and targeted by this thesis, which hopes to shed some light on them. One such question asks what configurations (i.e., sets of equipment that provide multimodal feedback) lead to the strongest, most lateralized brain activation during motor imagery. A trade-off emerges between the added immersion and equipment cost, which adds to the complexity of

the question; however, this thesis strictly compares the brain activation between different configurations.

The use of haptics is scarce and not as prevalent as VR, yet there have been studies assessing its potential in stroke rehabilitation [10]. Together with BCIs and VR, the trio is capable of providing both visual and haptic feedback through a non-muscular channel connecting the patient's motor intention to the avatar's limbs. As such, haptics are taken into consideration in the search for the best configurations.

Another issue is the use of machine-learning algorithms in BCIs, which make the translation between motor imagery and avatar movement possible. Notwithstanding the typical usage of the linear discriminant analysis (LDA) and the support-vector classifier (SVC), there is no standardized combination of algorithms and BCI–VR configurations that lead to the most accurate and robust machine-learning models. Therefore, the second fundamental question appears: what algorithms and configurations lead to the most accurate models?

1.1 Thesis objectives

Given the two aforementioned questions arising from the field's recency, the objective of this thesis is, thus, twofold.

1.1.1 What BCI–VR configurations lead to the strongest, most lateralized brain activation?

To tackle this question, several subjects performed motor imagery in different combinations of HMD vs. non-HMD and haptic vs. non-haptic configurations, called *conditions*, through either Graz-based abstract feedback [11] or *NeuRow* [12]'s realistic feedback. A sixth condition had the subjects perform motor execution to benchmark the motor-imagery conditions against it. Their EEG signals were analyzed by interpreting a common phenomenon in motor imagery and execution, the event-related desynchronization (ERD) [13]. The spatial distributions of these desynchronizations were also analyzed through the lateralization indices (LIs).

1.1.2 What BCI–VR configurations and machine-learning algorithms lead to the most accurate models?

Different algorithms and hyperparameters were tested with the EEG signals recorded during the aforementioned experiment. The traditionally used LDA and SVC were included, as well as linear and nonlinear alternatives such as the multilayer perceptrons (MLPs), Gaussian naive Bayes, and the random-forest classifier. The different conditions were likewise compared across the algorithms.

1.2 Thesis outline

The thesis is split into six chapters, including the current one, Introduction. The following chapter, Background, succinctly contextualizes BCIs and VR in stroke rehabilitation and describes the state of the art. Then, the methods of the experiment and subsequent data analysis are described in Methods, and the results and discussion in Results and Discussion, respectively. Lastly, the conclusions taken from the study are laid out in Conclusion.

Additionally, two appendices can be found at the end of the thesis. Appendix A includes the questionnaires, while Appendix B contains figures from results that were only briefly mentioned in Results.

2

Background

Contents

2.1 Stroke

Nowadays, one of the most prevalent causes of death and disability worldwide is the cerebrovascular accident, also known as *stroke* (see Figure 2.1) [1]. Strokes can be classified as ischemic, which occur when blood flow to a region of the brain is blocked, depriving the cells of oxygen and nutrients and prompting their deaths; or hemorrhagic, which occur when there is a rupture of an intracranial blood vessel that causes blood to overflow and damage the surrounding brain tissue [14, 15].

There are 101 million people worldwide who have suffered a stroke at some point in their lives, and over 143 million daily-adjusted life years are lost each year due to stroke-related death and disability, at a global cost of US$721 billion [16]. Strokes can cause a myriad of cognitive and motor impairments that affect the victim's ability to perform activities of daily living, such as eating, dressing, and bathing [14]. Particularly, spasticity and weakness are the main motor impairments that the victim experiences post-stroke [17], with hemiparesis, which is the partial paralysis of one side of the body, affecting 80% of the victims acutely and 40% chronically [18].

As the European population continues to age and the survival rates increase, the number of people with sequelae of stroke is estimated to rise 27% within the next 30 years [19]; specifically, the incidence in Portugal is predicted to increase by 31% by 2035 [20]. Older people, in particular, are more susceptible to ischemic strokes, particularly those above the age of 50 [1].

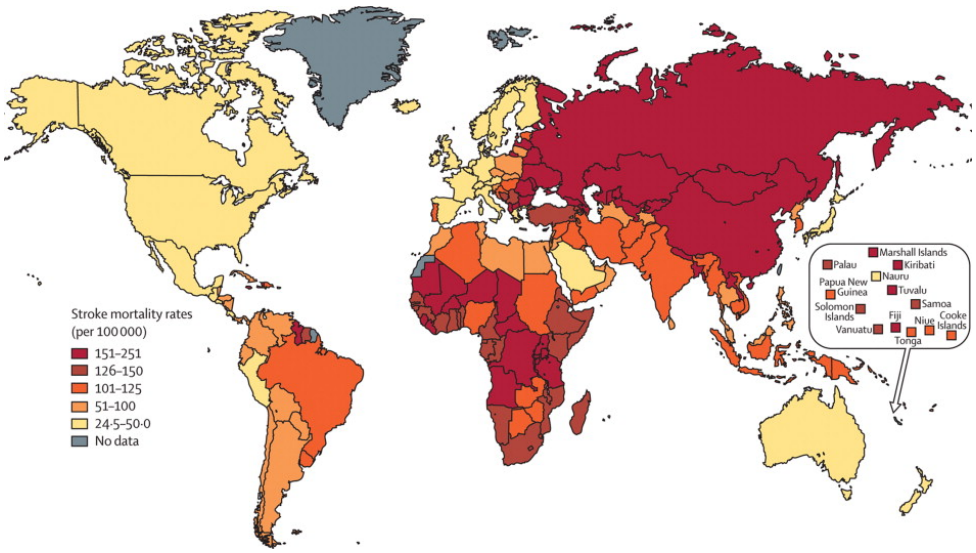

Figure 2.1: Age- and sex-adjusted stroke mortality rates per 100,000 [21]

2.1.1 Conventional rehabilitation

The basis for rehabilitation is the fact that the brain remains plastic even after the stroke [22, 23]. Most victims lose function in their upper limbs during the stroke, and between half and three-quarters remain

(a) Physical therapy [31] **(b)** Occupational therapy [32]

Figure 2.2: Conventional stroke rehabilitation

afflicted for the rest of their lives if left untreated [24]. However, recovery is possible through rehabilitation, in which the brain cortex is stimulated and reorganizes itself by having alternate regions take over the functions lost due to the subsequent lesion in the cortical tissue [23].

Conventional motor rehabilitation is done through physical therapy, where the patient performs movement exercises targeting the affected limbs [25], and occupational therapy, which is a holistic approach that seeks to recover the patient's motor function by performing activities relevant to their daily life and occupation [26] (see Figure 2.2).

Upper-limb rehabilitation, in particular, allows the recovery of arm movement and in-hand manipulation. One of the advantages it has over lower-limb rehabilitation is that the patient can remain seated during the exercises and the recovery allows them to perform a host of daily activities that require object manipulation.

While patients can recover around 70% of their lost function within months, on average, the more severe cases are more unpredictable, showing no or a very strong recovery [27]. The functional recovery of these cases should not be expected after the first 5 months [28]; that is, with conventional rehabilitation. Recently, technology-based alternatives have been attempting to overcome its limitations through the use of, for example, robotics [29] and brain–computer interfaces [30].

2.2 Brain–computer interfaces

Brain–computer interfaces (BCIs) appeared in the 1970s [33] as assistive technology in, for example, word-processing programs for people with locked-in syndrome [4]. But beginning in the early 2000s, researchers began to test BCIs for stroke rehabilitation, specifically for patients with severe neuromuscular disorders [34], and have recently started to experiment synergizing the interfaces with virtual reality (VR) and, to a lesser extent, haptics [10, 30].

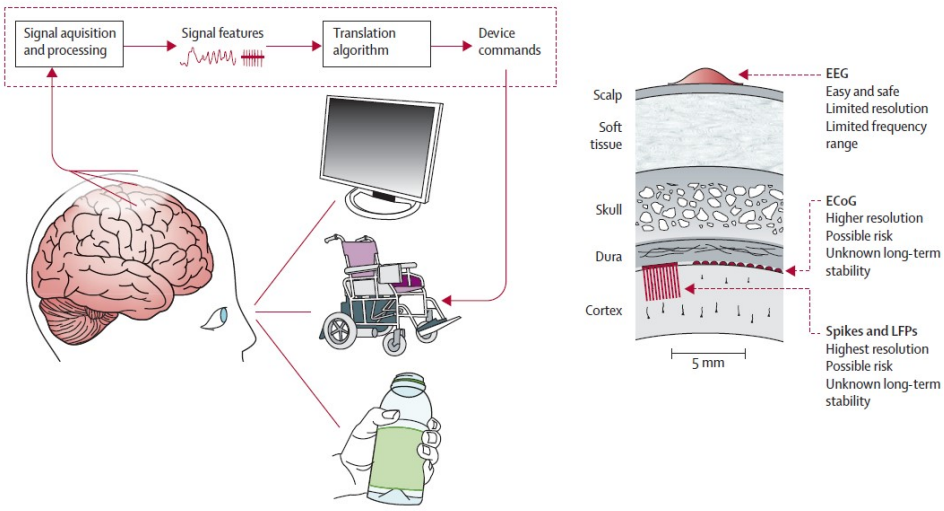

Figure 2.3: Overview of a BCI system [7]

A BCI may be divided into six phases: physiologic brain signals are first (A) acquired and then (B) processed to (C) extract features; afterward, the features are used to (D) build machine-learning models that predict the user's intent and establish a non-muscular channel to (E) communicate and manipulate computer-controlled external devices [4] (see Figure 2.3). The following description of the six phases refers to motor-imagery-based BCIs, as these are, by far, the most commonly used in stroke-rehabilitation research.

2.2.1 Signal acquisition

The most commonly used modality for brain-signal extraction is, by far, electroencephalography (EEG), due to its portability, simplicity, high temporal resolution, and noninvasiveness [4, 5, 35]. While there are other modalities that can be used in BCIs (e.g., electrocorticography (ECoG), functional magnetic resonance imaging (fMRI), and MEG), most require equipment that is expensive when compared to EEG's selection of low-cost systems ranging from €100 to €1,000 [35].

The disadvantages of using EEG signals are the fact that they are nonstationary (i.e., their statistical characteristics change over time), often noisy, and have low spatial resolution [5, 35]. The last two disadvantages are caused by how the signals are extracted: an array of electrodes, which may require conducting gel to reduce impedance, is placed on the scalp to detect electrical signals coming from the neurons in the cortex [5]. The electrical signals have to transverse through different layers of tissue (cerebrospinal fluid, bone, muscles, and skin) to reach the electrodes, and an electrical signal does not necessarily travel straight toward the electrode above its source (volume conduction) [5, 36].

The 10–20 system for electrode placement is the most commonly used (see Figure 2.4(a)). Electrodes

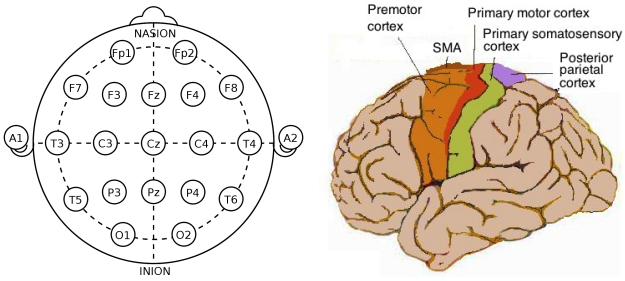

(a) 10–20 scheme for the electrode placement [38]

(b) Sensorimotor cortex [39]

Figure 2.4: Electrode placement and the sensorimotor cortex

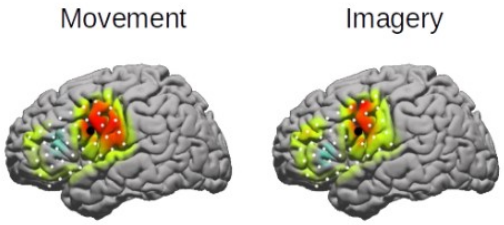

Figure 2.5: Brain regions activated during motor execution and imagery [40]

C3 and C4 are the most important for motor rehabilitation, as they are placed over the primary motor cortex (see Figure 2.4(b)). Since the latter activates similar brain regions to the former, including the primary motor cortex [37] (see Figure 2.5), it is possible to stimulate cortical reorganization and, thus, promote motor recovery for the more severe cases of impairment without requiring movement.

2.2.2 Signal processing

The EEG signals are usually processed due to their tendency to be contaminated with internal and external artifacts (spillover from other biosignals, body movement, etc.) and their tremendous data size derived from high sampling frequencies and a large number of electrodes. Therefore, a series of processing steps are performed to make the data more suitable for feature extraction.

2.2.2.A Temporal filtering

Temporal filtering involves the use of filters that remove components from the signal's frequency spectrum. They can be low-pass, high-pass, band-pass, or band-stop. In the case of EEG, certain artifacts or features one wishes to analyze have characteristic frequencies that can be removed or isolated, respectively.

On one hand, there is the power line artifact, for example, which is present in the overall signal in the 50 Hz or 60 Hz frequencies; therefore, it can be filtered with a band-stop filter. On the other hand, the EEG signals contain behavior-modulating oscillatory rhythms that can be isolated for analysis with a band-pass filter: delta (1–4 Hz), theta (4–8 Hz), alpha (8–12 Hz), beta (13–30 Hz), and gamma (40–100 Hz) [35].

For motor-imagery-based BCIs, the alpha and beta rhythms are particularly interesting; therefore, a band-pass filter that isolates their and the surrounding frequencies (e.g., from 1 Hz to 40 Hz) to remove low- and high-frequency artifacts and noise.

Additionally, the data can be compressed through downsampling, which does not lose information if the brain rhythms and the sampling theorem are taken into account when choosing the new sampling frequency.

2.2.2.B Spatial filtering

Spatial filtering helps tackle the volume-conduction problem owing to the current flow characteristic to the EEG, as well as increase the signal-to-noise ratio. For example, surface Laplacians and common average reference (CAR) are commonly used techniques.

The surface Laplacian algorithm can assign weights to the electrodes surrounding the sensorimotor cortex and enhance EEG spatial resolution by filtering out spatially broad features among nearest-neighbor (small Laplacian) or next-nearest-neighbor electrodes (large Laplacian) [41]. This is especially useful to mitigate the volume-conduction issue.

The CAR method, on the other hand, can be used to re-reference the electrodes and allow the signals' amplitudes to not be relative to a single reference electrode but to their average at any time point. The common activity of the electrodes is subtracted from their signals, which helps remove noise that is prevalent in many of the electrodes.

Additionally, independent component analysis (ICA) can be used, in its broadest description, to remove intrusive signals such as the electrocardiography (ECG), electromyography, and electrooculography from the original signal while keeping the EEG component. The number of independent components (i.e., with distinguishable non-Gaussian distributions, an assumption made by the method) is equal to the number of electrodes. Tools such as ICLabel[1] can help label the components and remove unwanted ones with discretion.

2.2.3 Feature extraction

The feature extraction is done not only to train the machine-learning models that predict the user's intent but to also perform offline analysis of relevant metrics such as the event-related desynchronizations (ERDs). Therefore, in stroke rehabilitation, the BCI should be robust enough to accurately predict if (i.e.,

[1] https://github.com/sccn/ICLabel

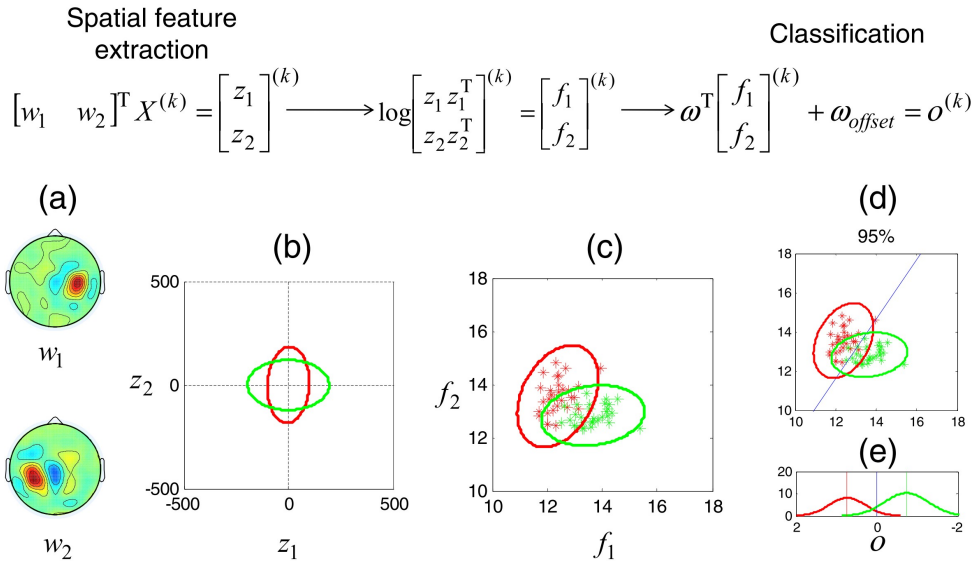

Figure 2.6: A conventional CSP and LDA model: the spatial filters (a) create surrogate channels based on weights attributed to the original electrodes so as to (b) project the signal variances on a plane that best distinguishes left- from right-hand movement. The variances are (c) projected to a new plane by using their log values. Then, a hyperplane is computed by the LDA to separate the two classes, and the (e) classifier's outputs are determined by the two classes' distributions relative to the hyperplane [44]

in a self-paced setting) and of which arm the patient wants to perform motor imagery, but also allow the therapist to assess the patient's recovery afterward.

Although ERDs can be used for the offline analysis and as features in the prediction [42], common spatial patterns (CSPs) are the most commonly used feature-extraction method [43] (see Figure 2.6). They can effectively separate channels created from the original electrodes to have the two classes (left- and right-hand movement) be differentiated based on the signal variances, and the volume conduction issue is overcome. Given that brain activation is contralateral to motor execution, the spatial distribution of the desynchronization will look different between the two sides.

2.2.3.A Event-related desynchronizations

A power suppression in the alpha and beta waves occurs in motor-related tasks, which activate the sensorimotor cortex; this phenomenon is called an *event-related desynchronization* (ERD) [45]. The desynchronization is typically larger and more sustained in the alpha waves, whereas the beta equivalent recuperates much earlier [46]. This power suppression is dependent on the baseline activity prior to the motor activation. It should also be said that desynchronization happens in anticipation of the stimulus (e.g., a cue asking the person to move their hand) [13]. A few seconds later, the rhythms rebound, in what is called an *event-related synchronization* (ERS).

That said, motor-imagery-based BCIs make special use of these features since ERDs are also invoked in motor imagery [37] (see Figure 2.7). They correlate with cortical activation [47], which can be analyzed

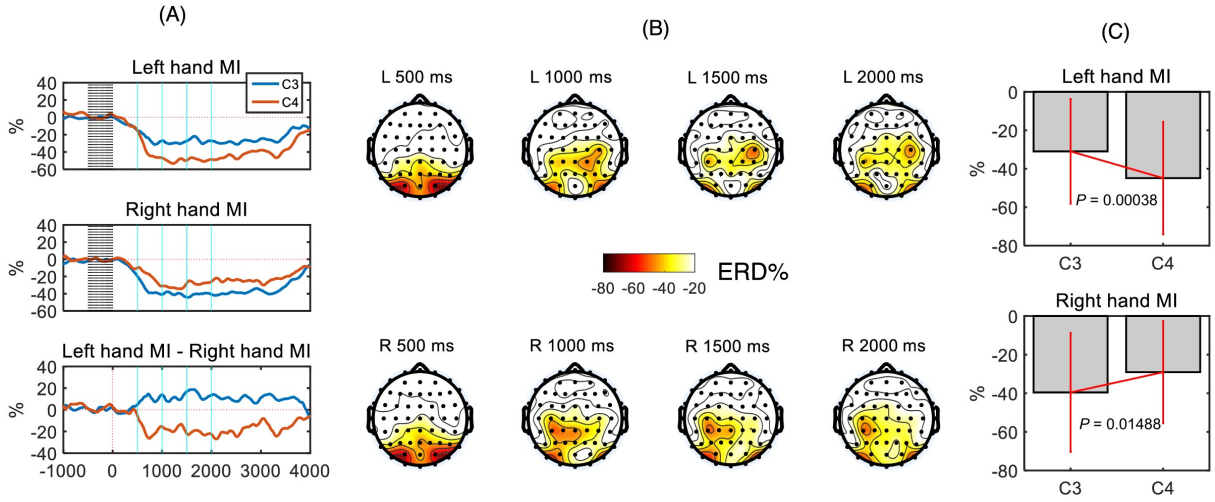

Figure 2.7: An example of an ERD of the somatosensory rhythm (8–14 Hz) averaged for 38 subjects. (A) The first two rows show the desynchronization of the C3 and C4 electrodes for left- and right-hand motor imagery. (B) Topographic plots of the desynchronizations spreading toward electrodes C3 and C4. (C) A paired *t*-test showing significant difference between both ERDs [48]

to compare the quality of the desynchronizations between any conditions being studied (e.g., under different feedback configurations or motor-related tasks).

2.2.4 Prediction

To predict the patient's intent, the most common machine-learning algorithms used are the linear discriminant analysis (LDA) (see Figure 2.6) and the support-vector classifier (SVC). They can be used on an individual basis and for a short time period, given the EEG's nonstationary nature. The models' accuracy is also affected by the user's ability to control their brain's electrical signal, which is directly correlated with the quality of the features [4, 7].

Given the prediction must be in real time, these two algorithms are most commonly used to provide a quick classification model without a high computational cost. While LDA is inherently linear, the SVC can be implemented with nonlinear kernels, despite the standard kernel being linear. Nevertheless, other algorithms such as convoluted neural network (CNN) can also be used [49].

2.2.5 Output

Generally speaking, the output can assist the user in performing actions that can vary from simple tasks such as switching the lights on and off, regulating the room temperature, or using word-processing programs to more complex tasks like operating a robotic arm or a neuroprosthetic limb that enables the movement of a paralyzed limb [7]. For motor-imagery-based BCIs, the output can be used in stroke rehabilitation by providing neurofeedback to the patient. This feedback takes on multiple forms, but when

joined with other technologies, it enriches the patient's experience and immersion. In the case of VR, the act of observing an avatar moving its limbs when the patient correctly performs motor imagery has a positive effect on the recovery [50].

2.3 Virtual reality

With the advent of more sophisticated hardware and software, the adoption of VR in stroke rehabilitation (virtual rehabilitation) has become a subject of discussion in regard to its efficiency and effectiveness over conventional therapy. Supporting evidence for the use of this technology is the fact that the brain's plasticity can be exploited through the mirror-neuron system for motor recovery by offering embodied feedback—the display of avatar limbs that move according to the patient's intent [51, 52]—and the possibility of designing engaging tasks that increase the patient's adherence to the treatment, which is important for the therapy to work.

Virtual reality can be implemented with a multitude of different interface configurations that can provide visual, auditory, and even tactile feedback (i.e., through haptics). The main advantage that VR brings to stroke rehabilitation is the virtual environment that the patients immerse themselves in and, ultimately, enhances recovery.

The most common way of providing visual feedback (i.e., to show the VR environment to the patient) is through screens (see Figures 2.8(b) and 2.8(c)), due to their low cost and ubiquity. Nonetheless, head-mounted displays (HMDs) can be used instead (see Figure 2.8(a)), which is usually what a layperson may understand as actual VR. Still, the use of computer-generated graphics to create a virtual environment is the definition of VR, without necessarily requiring the use of a VR headset to visualize it. Other devices such as projectors can also be used to the same extent. Moreover, headphones and speakers can provide auditory feedback, be it ambiance sounds or sound effects reminiscent of video games which provide positive or negative feedback based on the patient's performance. Haptic feedback may also be provided to the patient, most commonly through vibrotactile stimulation. Lastly, the patients can interact with the virtual environment through data gloves (see Figure 2.8(b)), video-capture systems, hand controllers (see Figure 2.8(a)), or even limb controllers (see Figure 2.8(c)).

Now, more than ever, the spread of VR development has seen considerable strides, in large part thanks to the video game and cinema industry, which have allowed researchers to develop their own VR settings through beginner-friendly game engines such as Unity[2]. Researchers have also made use of video games instead of custom-built environments to study virtual rehabilitation [53].

Virtual reality has thereby shown to be able to increase the effectiveness and efficiency of upper-limb stroke rehabilitation when combined with conventional therapy [3, 51], as well as increase the patients'

[2] https://unity.com/

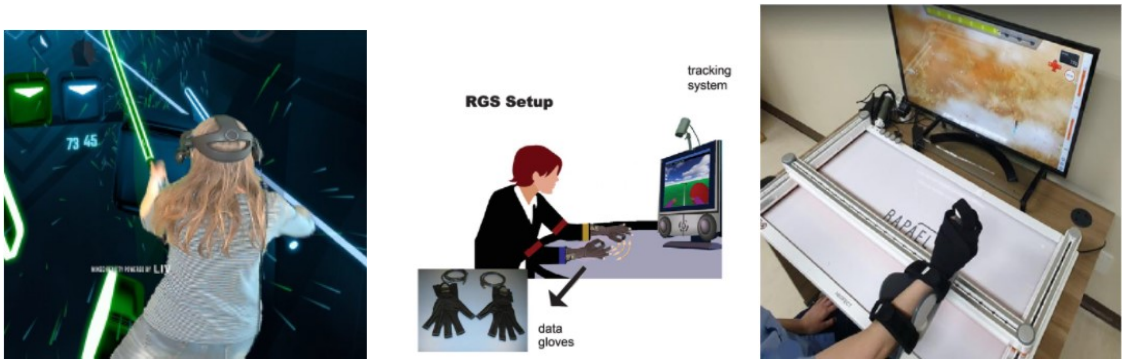

(a) HTC Vive HMD and hand controllers to play *Beat Saber* [53]

(b) Rehabilitation Gaming System to play *Spheroids* [51]

(c) Limb controller and a monitor part of the *Rapael Smart Board* [54]

Figure 2.8: VR experimental setups

engagement [54, 55] and social participation [56, 57] compared to exclusively conventional therapy [55]. However, virtual rehabilitation has a major limitation affecting the more severe cases of stroke, which is that all patients are required to have some limb functionality to perform the tasks (i.e., to interact with the virtual environment). Consequently, there is a substantial group of patients incapable of taking part in this technology-based rehabilitation due to their inferior motor ability.

2.4 Brain–computer interfaces and virtual reality

As some stroke victims suffer severe loss of motor function in their upper limbs, conventional therapy or virtual rehabilitation can become outright impossible. Yet, as BCIs become more reliable, their use in stroke rehabilitation has become an attractive solution to overcome this challenge. In order to enhance recovery, motor-imagery-based BCIs can be used in tandem with VR to both train the central nervous system directly [2]—without requiring any movement—and provide embodied feedback to the patient after performing motor imagery of their affected limbs (see Figure 2.9). Not only that, but VR itself also confers ecological validity to studies that contextualize their virtual tasks into the real world. Since the repetitive practice of motor imagery induces changes in the brain (i.e., a cortical reorganization whereby alternative brain regions take over the lost functions), rehabilitation on the basis of motor-imagery-based BCIs leads to recovery [58].

Given the recency of the BCI–VR field, there have only been a few studies on the viability of this synergistic duo, with some involving healthy subjects and others stroke patients. Some studies use custom-built equipment, while others use commercial equipment such as recoveriX[3] (g.tec medical

[3] https://recoverix.com/

engineering GmbH, Schiedlberg, Austria). A handful of studies have shown promising results but there are still fundamental questions to be answered. Next, a brief timeline follows on the literature review of BCI–VR systems in stroke rehabilitation.

2.4.1 Timeline of BCI–VR systems in stroke rehabilitation

Fifteen years ago, Pfurtscheller et al. [59] recruited nine healthy subjects to perform motor imagery of finger flexion and extension while observing a virtual hand, as well as a rotating cube, with an HMD. It was one of the early, if not the earliest, BCI–VR systems to be investigated. They noticed, as expected, a desynchronization of the alpha and central beta rhythms when performing motor imagery; however, the desynchronization was stronger when the virtual hand was shown rather than the cube.

Five years later, Badia et al. [60] investigated a BCI–VR system by complementing the Rehabilitation Gaming System [61], a VR system, with a BCI. The system would let the subjects intercept flying spheres inside the virtual environment by performing motor imagery of their hands. Using a linear classifier, the nine subjects managed to intercept the incoming spheres with a median accuracy of 85%; nevertheless, they reported the avatar's arms to be hard of controlling, suggesting dissatisfaction with the system's accuracy. On the plus side, most subjects enjoyed the experiment and the motor imagery seemed feasible for a BCI–VR system.

Three years later, Pichiorri et al. [6] recruited 28 stroke patients to a different study, but with the same goal: to assess the feasibility of a motor-imagery-based BCI for stroke rehabilitation. A VR component was also included, albeit more straightforward, which was a virtual hand projected onto a sheet covering the subject's hands (see Figure 2.9). The patient would be able to control the virtual hand through motor imagery, and they did so with an improved functional recovery compared to patients who only received conventional therapy. The system was similarly reported as demanding, which could be considered advantageous for keeping the subject engaged in the task.

Another study, this time involving the flexion and extension of a virtual arm, was done by Achanccaray et al. [62] in 2017, further showing the potential of BCI–VR systems. Eight healthy male subjects were recruited, and the prediction performance had a minimum accuracy of 77%, going for as high as 89% in the online phase. The absence of stroke patients undermined the promising performance of the system, but future studies would make up for that.

Indeed, there were a series of studies starting in 2018 that would make use of the commercial system recoveriX and study its effectiveness in stroke rehabilitation. All subjects participating in these studies had the assistance of an avatar and electrical stimulation of their hands (a common modality called *functional electrical simulation* [FES]). Being a set of four studies using the same system, the common task was to perform motor imagery of wrist dorsiflexion. Cho et al. [63] studied the functional recovery of seven patients, which saw a significant increase that was above the minimal clinically important

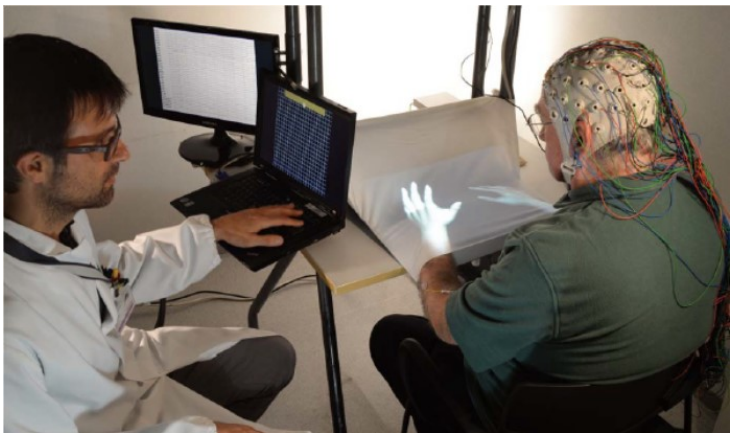

Figure 2.9: A BCI–VR experimental setup with the projection of virtual hands providing visual assistance to the subject and a monitor allow the therapist to track the subject's performance [6]

difference. Sebastián-Romagosa et al. [64], on the other hand, sought to find any correlations between the lateralization indices of the ERDs and clinical scales and concluded that there was a positive trend between the indices and the Fugl-Meyer Assessment (FMA). Miao et al. [65] saw patients improve more with recoveriX than just traditional therapy. Lastly, there was a study by Voinas et al. [66] that tested a novel feature-extraction method: wavelet packet decomposition combined with higher-order statistics. The random-forest classifier was used to compare the method with the commonly used CSPs and filter bank CSPs, with which the novel method managed to achieve a mean accuracy of 70% compared to the other's 66% and 69%, respectively.

Three years before Voinas et al. [66] did their study, Karácsony et al. [49] investigated not a feature-extraction method but a new machine-learning algorithm. The three-class CNN, which classified left- and right-hand movements and a resting state (i.e., a self-paced BCI), led to an average online accuracy of 60%. Additionally, this study had been, so far, the first to have HMD devices instead of screens or projectors; the subjects had fun while catching falling fruit in the VR environment and found it interesting and immersive. The downside of the experiment was the absence of stroke patients; the subjects were, instead, healthy individuals in their 20s.

A study by Juliano et al. [67] followed up on the HMD clue by assessing the added immersiveness of said device in the Rehabilitation Environment using the Integration of Neuromuscular-based Virtual Enhancements for Neural Training (REINVENT). The subjects were asked to control a virtual hand through motor imagery by observing it first through a monitor and then a VR headset. This was possibly one of the few studies where the focus was on the subject's immersion and sense of embodiment. As far as the literature review goes, there are very few papers addressing this matter. And it paid off, as the preliminary results suggested a positive correlation between embodiment and neurofeedback performance. Now, one of the fundamental questions begins to surface: what is the BCI–VR configuration that leads to an optimal balance between strong brain activation and immersion improved by complex,

Figure 2.10: A BCI–VR experimental setup that uses the Oculus Rift VR headset, headphones, and hand controllers generating vibrotactile stimulation to interface the subject with the VR environment *NeuRow* [9]

more expensive equipment?

2.4.1.A Haptic feedback

A relevant component to the immersion in BCI–VR is that of haptics: a sense of touch experienced by the subject through mechanically or electronically generated movement as part of an interface. It can be hand controllers, data gloves, or FES, for example. The aforementioned studies that used recoveriX also included haptics through FES, and other studies featuring haptics are mentioned below.

Back in 2018, Lupu et al. [68] had seven patients use the TRAVEE [69] system, which includes an HMD and FES, to perform motor imagery of hand or finger flexion and extension. The subjects were able to achieve low control errors, with a mean of 26%, and were generally encouraged to improve their recovery with the proposed system.

The REINVENT system had previously been used in 2019 in a study before Juliano et al. [67] conducted theirs. Vourvopoulos et al. [70] had not only used that system but had also complemented it with hand controllers providing vibrotactile stimulation. In the same year, Vourvopoulos et al. [9] did a pilot study with a stroke patient using a similar setup by featuring a HMD and hand controllers that provided vibrotactile stimulation (see Figure 2.10). Both papers reported noteworthy benefits for the more debilitated patients, who could show important motor improvements with these BCI–VR systems.

A couple of years later, a study by Achanccaray et al. [71] similarly flirted with the idea of using a HMD with haptic feedback, but through FES instead. The SVC classifier was used to predict the user's intent, and the accuracies reached 4% to 6% more with FES than with only visual feedback. The subjects were healthy individuals, however, which naturally perform better than stroke patients.

Sebastián-Romagosa et al. [72] used a custom-built BCI–VR system with FES but, unlike the aforementioned studies, a monitor was used instead of an HMD. The results showed that the patients with motor-imagery accuracies above 80% increased their FMA scores by 3.16 points more than those with

accuracies below that threshold.

Finally, given the scarce use of haptics, it is still worth mentioning a couple of related studies that did not make use of VR. One is by Shu et al. [73] and another by Zhong et al. [74]. While the former only employed motor execution with stroke patients as the subjects, the latter employed motor imagery with healthy subjects. Both studies did, however, use CSPs to analyze the performance accuracies. They noticed significant increases in the accuracies of the conditions that used haptics, which further pushes the idea that haptic feedback may be an important element for a strong brain activation, also aided by Zhong et al. [74]'s analysis of the ERDs.

2.4.2 Machine learning

Most studies employ linear algorithms such as the LDA and the SVC, but some do experiment with either the feature extraction, which is usually done with CSPs, or the algorithm. A simple but serviceable algorithm is usually preferred over a more complex one, since there needs to be a calibration phase before the online phase more often than not. The subject has to first train the model by letting their EEG signals be recorded during motor imagery, which are then used to train the models. This can be time consuming, especially considering the nonstationary nature of EEG signals that make the calibration recurrent if the subject habitually uses the BCI system, such as in several therapy sessions.

Nevertheless, the evolution of hardware with time speeds up the training times that open a wide array of nonlinear algorithms that may or may not have a better performance over the two linear algorithms aforementioned. That is the other fundamental question: what is the machine-learning algorithm that leads to the most robust, most accurate models? The first question also creeps into the second, since the extracted features influence the accuracies intimately. As such, the question splinters off: what is the best BCI–VR configuration that leads to the most accurate models? These are the questions this thesis hopes to shed some light on.

3

Methods

Contents

This chapter begins by describing the subjects who took part in the study and the experimental procedure for the data acquisition. Then, the data analysis is described in length, of both the EEG and the machine-learning models resulting thereof, as well as analysis of the questionnaires and correlations with the other data. The statistical tests used in this study are also mentioned.

3.1 Participant demographics

A total of 21 healthy volunteers were recruited for the study, three of whom took part in pilot studies. As such, the subjects were labeled from P01 to P03 and from S01 to S18. However, the data of two subjects, S10 and S11, had been corrupted due to a hardware malfunction, impeding its analysis. Therefore, the data analysis included 19 subjects in total.

The subjects had a mean age of 24.79 years (SD = 3.54 years), with the youngest being 21 years old and the oldest 36 (see Figure 3.1(a)). The cohort was 68% male and 32% female (see Figure 3.1(b)). In terms of education, 16% had attended only high school, while 32% had a bachelor's degree, 42% a master's degree, and 11% a doctorate (see Figure 3.1(c)). Subjects S06 up to S18 were also asked to rate their prior experience with BCIs and VR from 1 (nonexistent) to 5 (plenty): the mean scores were 1.36 (SD = 0.67) and 1.73 (SD = 0.65), respectively (see Figures 3.1(d) and 3.1(e)). Given the nature of the motor-imagery task, some subjects (starting with S06) were asked if they had any rowing experience. At least five subjects had some, while at least four did not.

3.2 Experimental procedure

3.2.1 Conditions

The experiment consisted in having the subjects perform motor imagery of a bimanual rowing task with two individual paddles, one in each hand, under five experimental conditions. Four of these conditions used *NeuRow* [12]—a VR environment made in Unity[1] t renders a set of virtual arms from a first-person perspective—while the other condition used abstract feedback based on the BCI-Graz paradigm [11]. A sixth condition had the subjects perform motor execution, also with the abstract feedback. These last two acted as control conditions. All six conditions and their acronyms are described below:

1. **grazMI:** The standard motor-imagery training, with a fixation cross and directional arrows on a black background guiding the subjects through the experiment (see Figure 3.3(a)).

2. **neurowMIMO:** A motor-imagery training paradigm using *NeuRow*, with a fixation cross and directional arrows overlaid on the VR environment, which was displayed through a monitor (see

[1] https://unity.com/

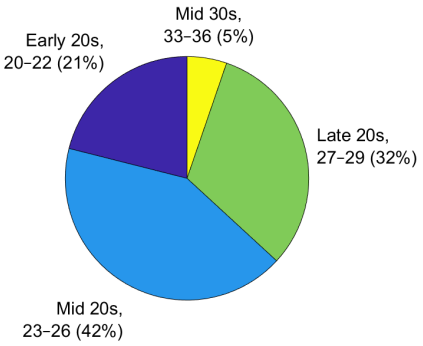

(a) Age percentages

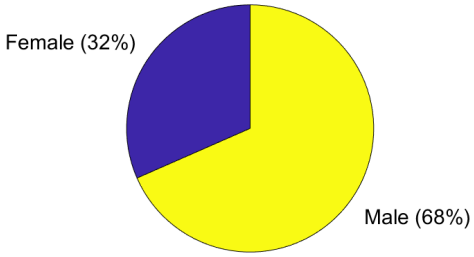

(b) Sex percentages

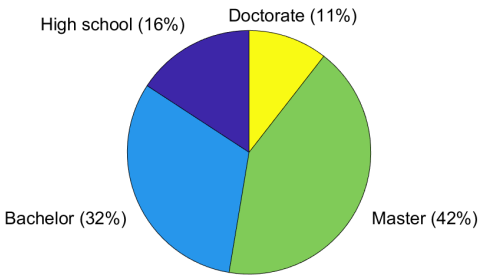

(c) Education-level percentages

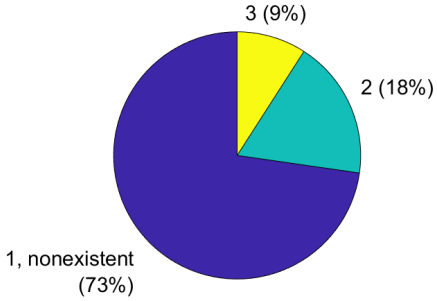

(d) BCI-experience percentages

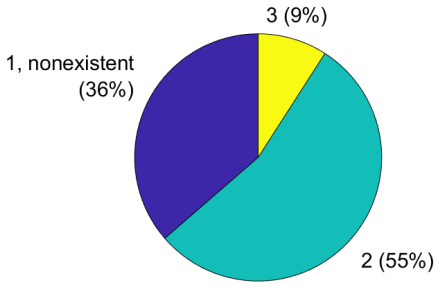

(e) VR-experience percentages

Figure 3.1: Sample demographics

Figure 3.3(b)).

3. **neurowMIMOHP:** A motor-imagery training paradigm using *NeuRow*, with a fixation cross and directional arrows overlaid on the VR environment, which was displayed through a monitor. Hand controllers also provided haptic feedback through vibrotactile stimulation Figure 3.3(b)).

4. **neurowMIMOVR:** A motor-imagery training paradigm using *NeuRow*, with a fixation cross and directional arrows overlaid on the VR environment, which was displayed through a VR headset Figure 3.3(c)).

5. **neurowMIMOVRHP:** A motor-imagery training paradigm using *NeuRow*, with a fixation cross and directional arrows overlaid on the VR environment, which was displayed through a VR headset. Hand controllers also provided haptic feedback through vibrotactile stimulation Figure 3.3(c)).

6. **grazME:** A fixation cross and directional arrows were displayed on a black background through a monitor and guide the subjects through the experiment by having them tap their fingers on the table accordingly Figure 3.3(d)).

The condition order was randomized for each subject to minimize any latent effects originating from preceding conditions that could skew the results. An initial version of the sixth condition, *grazME*, had the subjects perform a circular arm motion similar to the avatar's movement in *NeuRow*. A later version had the subjects then tap their fingers on the desk, as it would be sufficient to induce a similar ERD while avoiding movement artifacts. Nevertheless, the desynchronizations between the two types of movement were not compared to ascertain the similarity. The results from *grazME* were compared against those obtained with motor imagery in the subsequent data analysis. However, the condition was only implemented after S07's session, so only subjects S08 to S18 performed it.

3.2.2 Setup

A 32-channel EEG cap (actiCAP; Brain Products GmbH, Gilching, Germany) was used to extract the brain's electrical signals with a wireless EEG amplifier (LiveAmp; Brain Products GmbH, Gilching, Germany) with a sampling rate of 500 Hz, which included active electrodes for improving the signal-to-noise ratio. The spatial distribution of the electrodes used the 10–20 system.

ECG, photoplethysmography (PPG), and respiration were also acquired as auxiliary signals. The ECG was acquired by placing two electrodes under the collarbones and the ground electrode on the lower end of the sternum. The PPG was measured with a clip on the left index finger. The respiration was measured through a respiratory band placed under the chest where the rib cage is the most prominent. The recordings of the auxiliary signals were not analyzed in the context of this study.

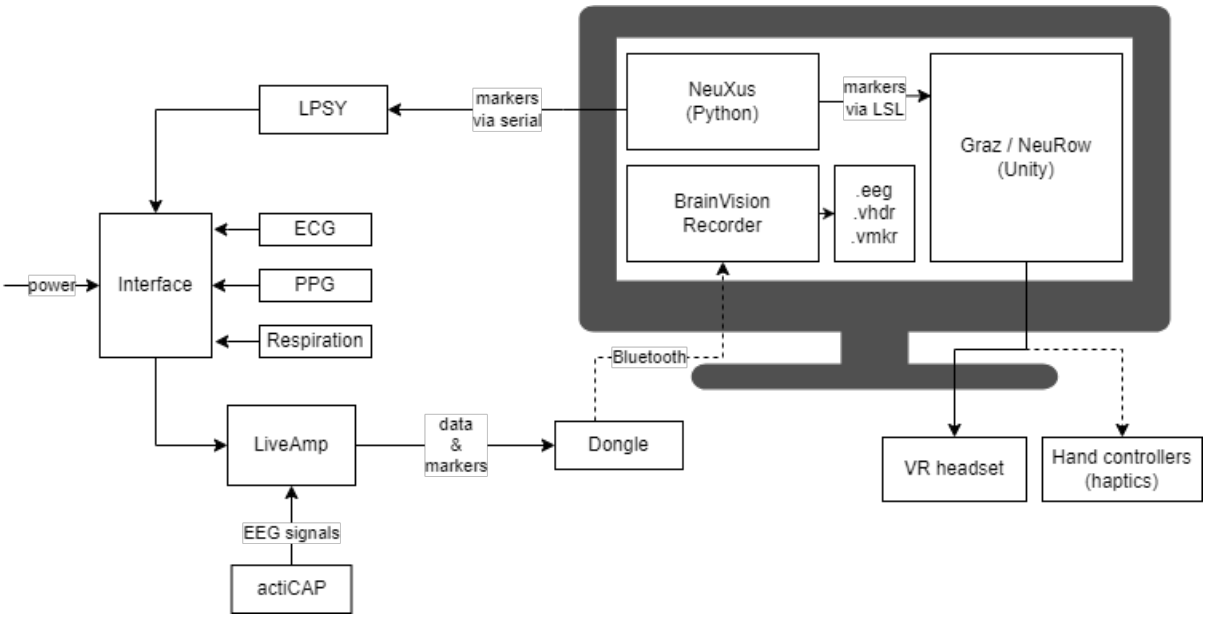

Figure 3.2: Software–hardware pipeline, where full lines outside the screen represent cable connections and dashed lines represent wireless connections

Visual feedback was provided through a monitor in all conditions except in *neurowMIMOVR* and *neurowMIMOVRHP*, in which an Oculus Rift CV1 headset (Reality Labs, formerly Facebook, Inc., CA, USA) was used instead. Haptic feedback was provided through vibrotactile stimulation from Oculus Rift hand controllers.

3.2.3 Software–hardware pipeline

The data acquisition started by running a batch file that would launch either the Graz-based program or *NeuRow*, depending on the condition. A Python script launched by the batch file would use NeuXus [75], a modular toolbox in Python for real-time biosignal processing and pipeline design, to send markers to either program via Lab Streaming Layer (LSL)[2] with timestamps indicating when the left- or right-hand movement cue should appear to the subject, and via serial communication through LPSY, a custom-made interface that merges the incoming markers with the auxiliary signals in the interface where all three auxiliary signals were collected. The markers would also signal the avatar in *NeuRow* to row the kayak with the targeted arm. The EEG signal detected through the actiCAP was amplified with LiveAmp and sent, together with the auxiliary signals and the time markers, to BrainVision Recorder (v1.22; Brain Products GmbH, Gilching, Germany) via Bluetooth. The data would be stored in different files (in VHDR, EEG, and VMKR formats) to be analyzed later. A pipeline diagram is shown in Figure 3.2.

[2] https://github.com/sccn/labstreaminglayer

3.2.4 Protocol

The experiment was divided into three parts. The first part was acquiring data from the subject that would not be affected by the experimental conditions (e.g., demographics), together with informed consent, and setting up the hardware. The second part was the BCI interaction and acquisition of data across all conditions. Lastly, the third part was the acquisition of data that was related to the experimental conditions (e.g., the sense of embodiment).

3.2.4.A Initial questionnaires and hardware setup

The subject would begin by filling in the consent form to participate in the study. Given the informed consent, their blood pressure and resting heart rate were measured with a blood-pressure monitor. Afterward, the subject would answer the 12-item version of the Edinburgh Handedness Inventory questionnaire [76] (Appendix A.1) and the Vividness of Movement Imagery Questionnaire-2 (VMIQ-2) [77] (Appendix A.2). While the former evaluates one's handedness in different tasks, the latter has the subjects assess their ability to perform motor imagery of different tasks in three different ways: by observing the movements through one's eyes (internal visual imagery [IVI]), by observing one's body performing the movements through an external point of view (external visual imagery [EVI]), or by feeling the movements being performed (kinesthetic imagery [KI]).

The 32-channel EEG cap would then be placed on the subject's head. The electrode holes were swabbed with isopropyl alcohol to clean the skin and expose the scalp for optimal gel implementation. The electrodes were attached to the cap, and viscous conductive gel (SuperVisc: HighViscosity Electrolyte Gel for Active Electrodes; EASYCAP GmbH, Wörthsee-Etterschlag, Germany) was injected between the scalp and the electrodes to lower the impedance to below 15 kΩ. The impedance check was done through BrainVision Recorder. Afterward, the equipment for the auxiliary signals—ECG, PPG, and respiration—was put on the subject, so those signals could be recorded anonymously for public databases. The subject held the hand controllers throughout all conditions except *grazME*, and later subjects would also have a towel underneath to dampen the clattering between the controllers and the desk in conditions with haptic feedback. All subjects remained seated throughout their sessions and were asked to avoid moving and talking, and to have a relaxed posture, so the number of artifacts in the data could be minimized (see Figure 3.3).

3.2.4.B Interacting with the brain–computer interfaces

The order of the motor-imagery conditions was randomized for each subject to prevent any latent effects of previous conditions from skewing the data. Every condition except *grazME* was approximately eight minutes long, while *grazME* was around five. All of them showed a cross at the beginning of a new trial so

(a) grazMI

(b) *neurowMIMO* or *neurowMIMOHP*

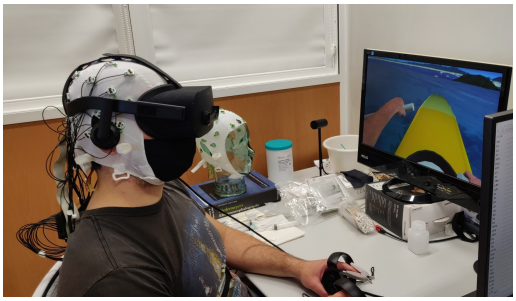

(c) *neurowMIMOVR* or *neurowMIMOVRHP*

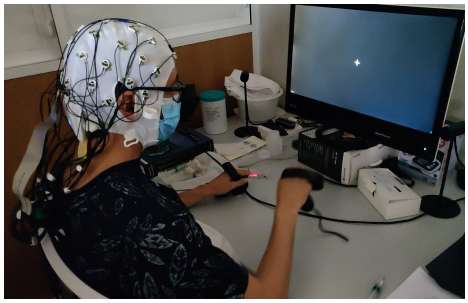

(d) *grazME* in its initial version, in which the subject would perform a circular arm movement similar to the one shown in *NeuRow*

Figure 3.3: Different setups for the conditions of the experimental procedure

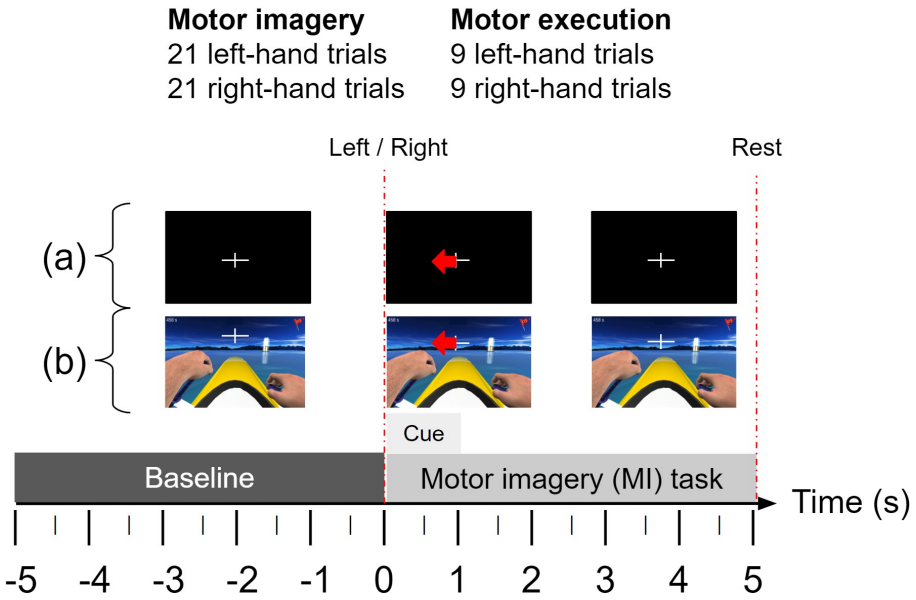

Figure 3.4: Experimental diagram showing the (a) Graz-based abstract feedback (*grazMI* and *grazME*) and (b) realistic feedback via *NeuRow* (*neurowMIMO*, *neurowMIMOHP*, *neurowMIMOVR*, and *neurowMIMOVRHP*)

the subject could focus on it and minimize eye movement. A left or right arrow would appear five seconds later for one second, in three consecutive trials, telling the subject to begin performing motor imagery for the targeted arm. There were 42 trials in total: 21 left- and 21 right-hand movements. The subject would stop the motor-imagery task when the cross disappeared, ending the trial (see Figure 3.4). After running all five motor-imagery conditions, the subjects performed a motor-execution task, *grazME*, for five minutes. In its initial version, the subjects would perform a circular arm motion similar to the avatar's movement in *NeuRow*, but the later version had the subjects tap their fingers on the desk instead, to prevent artifacts caused by the arm movements. The condition had 18 trials in total, also evenly split. The brain activity recorded during motor imagery could then be benchmarked against the activity recorded during motor execution.

3.2.4.C Final questionnaires and hardware removal

After running through all six conditions, the equipment for the signal acquisition was removed from the subject, starting with the auxiliary signals. Lastly, the subjects answered two more questionnaires: one on condition preference and another on the sense of embodiment experienced with *NeuRow* [78] (see Appendices A.3 and A.4).

3.3 Data analysis

3.3.1 Electroencephalography

3.3.1.A Data preprocessing

The data was analyzed in MATLAB (R2021b and R2022a; The MathWorks, Inc., Natick, MA, USA) with the EEGLAB toolbox[3] (v2022.0; Swartz Center for Computational Neuroscience, San Diego, CA, USA). Only the EEG data was analyzed, as the auxiliary signals were recorded for public databases. The locations of the electrodes were mapped by the standard 10–20 system provided by the toolbox. The electrodes were re-referenced using a CAR, which subtracts the average electrical signal of all electrodes at all time points. The sampling frequency was downsampled from 500 Hz to 125 Hz to reduce the data size without losing information, according to the sampling theorem, since frequencies above 62.5 Hz were not analyzed. A band-pass filter from 1 Hz to 40 Hz was applied to the data to include the alpha waves (8–12 Hz) and the beta waves (13–30 Hz). The trials were epoched between five seconds before the arrow cue and five seconds after. ICA was used to decompose the signals into several components and remove those labeled as eye and muscle movements by ICLabel[4] (Swartz Center for Computational

[3] https://github.com/sccn/eeglab
[4] https://github.com/sccn/ICLabel

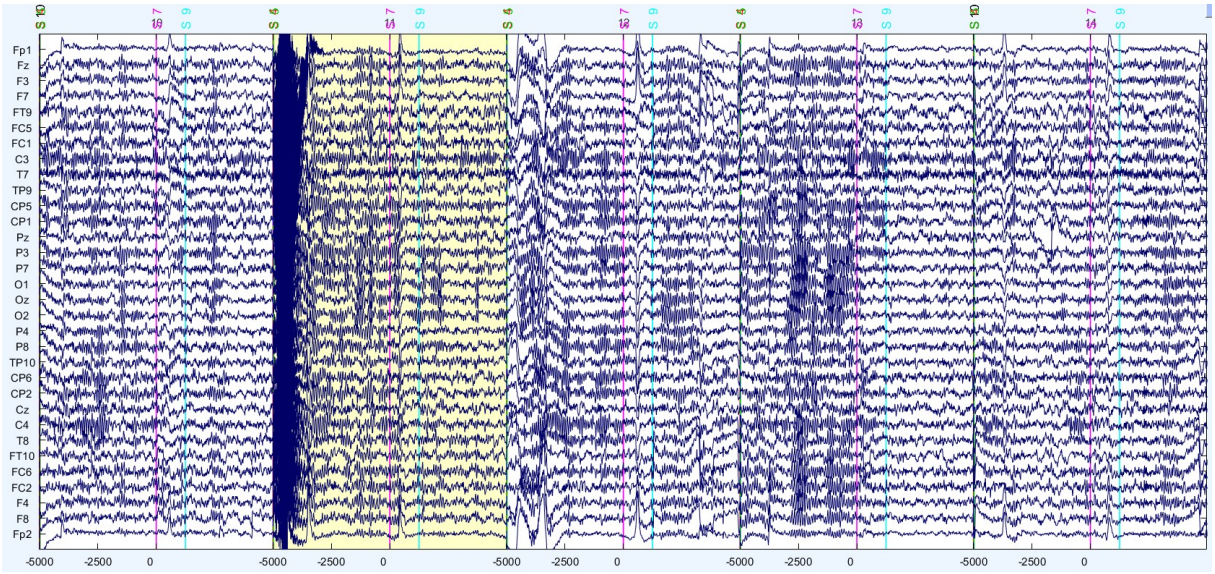

Figure 3.5: Trial rejection (highlighted in yellow) of P02's *neurowMIMO* run

Neuroscience, San Diego, CA, USA) with a confidence percentage between 90% and 100%. Trials with artifacts still present after the initial preprocessing were manually removed from the analysis through EEGLAB's interface (see Figure 3.5).

3.3.1.B Data rejection

Some EEG signals could not be analyzed due to artifacts or equipment malfunctions. Subject P02's *grazMI* and *neurowMIMOVR* runs could not be used due to displaying a single, indecipherable signal across all electrodes (see Figure 3.6), while S10's and S11's data did not include the markers with the timestamps due to a hardware malfunction (the LPSY was not connected to the interface). Thus, S10's and S11's runs were discarded, as well as P02's *grazMI* and *neurowMIMOVR* runs. Subject S13's *neurowMIMOVRHP* run was lost and could not be recovered (the EEG file went missing). All the remaining runs (one per subject) were analyzed: 19 runs for *neurowMIMO* and *neurowMIMOHP*; 18 runs for *grazMI*, *neurowMIMOVR*, and *neurowMIMOVRHP*; and 10 runs for *grazME*.

3.3.1.C Data processing

The ERD values were computed as percentages of the baseline through the event-related spectral perturbation (ERSP) values, in decibels, through the formula [79]

$$\text{ERD (\%)} = \left(10^{\text{ERSP}/10} - 1\right) \times 100, \tag{3.1}$$

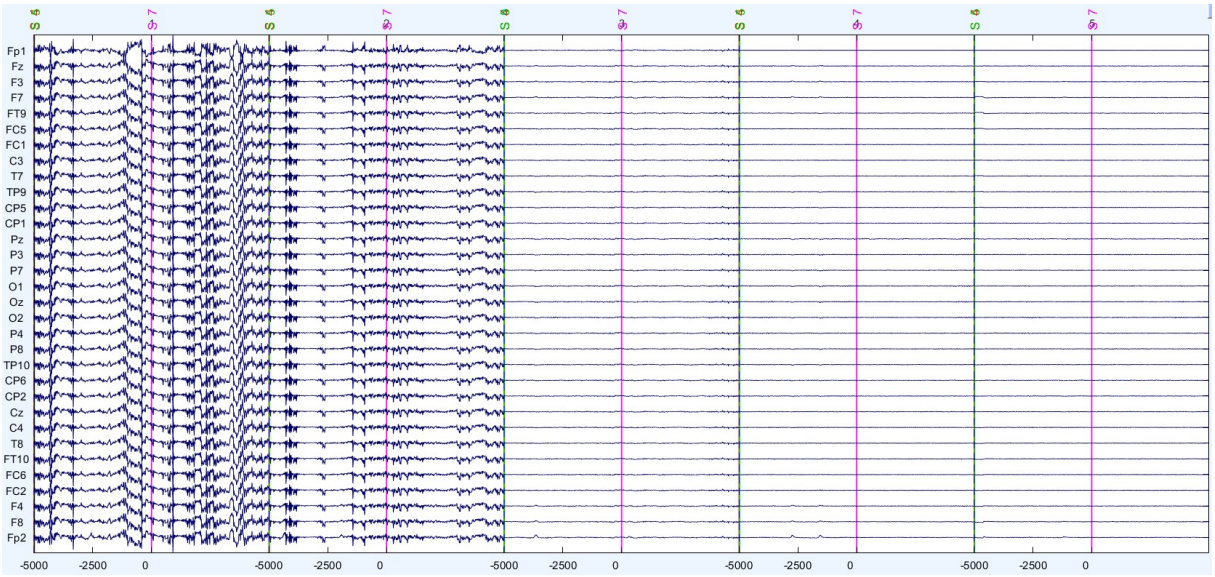

Figure 3.6: P02's corrupted *grazMI* run

which were negative if there was indeed an ERD, null at the baseline, or positive if it was, in fact, an ERS. For the sake of simplicity, the percentages are addressed as ERDs unless they are explicitly positive, in which case they are addressed as ERSs instead.

The mean event-related desynchronizations (mERDs) and lateralization indices (LIs) were computed from the time–frequency ERD maps of each electrode. The alpha waves' mERDs were computed between 8 Hz and 12 Hz, and the beta waves' mERDs were computed between 13 Hz and 30 Hz, from one second after the arrow cue until the end of the trial, as there was usually a delay between the cue and the ERD. The alpha and beta LIs were computed for each condition using the formula

$$\mathrm{LI} = \frac{(\mathrm{mERD}_{\text{left, C3}} - \mathrm{mERD}_{\text{left, C4}}) + (\mathrm{mERD}_{\text{right, C4}} - \mathrm{mERD}_{\text{right, C3}})}{2}, \tag{3.2}$$

which is positive if the brain activation is mostly contralateral to the arm movement during motor imagery, or negative if it is ipsilateral.

The percentages of the motor-imagery mERD medians relative to *grazME*'s were also analyzed using the formula

$$\text{Relative median mERD (\%)} = \frac{\mathrm{mERD}_{\textit{Mdn, MI}}}{\mathrm{mERD}_{\textit{Mdn, ME}}} \times 100, \tag{3.3}$$

which is the fraction of *grazME*'s mERD median for a given motor-imagery condition.

3.3.1.D Data visualization

The mERDs were displayed in box plots for electrodes C3 and C4, alpha and beta waves, and all conditions. The distributions were analyzed with left- and right-hand trials separated and together (i.e., in

contra- and ipsilateral sample groups).

The time–frequency ERD maps, from 1 Hz to 30 Hz, of electrodes C3 and C4 averaged for all runs were analyzed (but not shown in Results), as well as topographic plots of alpha and beta mERDs. Subtraction topographic plots between the motor-imagery conditions and *grazME* were also analyzed. The EEG signals from electrodes C3 and C4, which are placed over the sensorimotor region of the brain, were the main object of the analysis; however, the topographical plots included the mERD of all 32 electrodes so its spatial distribution could be analyzed.

The lateralization indices of each condition were analyzed in box plots. The average ERD values in time (i.e., all ERD values from 1 Hz to 30 Hz were averaged at all time points), which were also averaged for all runs, were plotted for the contralateral electrodes C3 or C4, alpha and beta waves, and each condition.

3.3.2 Machine learning

A Python script was written in Google Colab (adapted from David S. Batista [80]) which measures the algorithms' accuracies, as well as fitting times and precisions and recalls for left- and right-arm motor imagery. The algorithms picked for the script were the LDA, SVC, multilayer perceptron (MLP), *k*-nearest neighbors (*k*-NN), Gaussian naive Bayes, random forest, and Adaptive Boosting (AdaBoost).

3.3.2.A Algorithms and hyperparameters

Several hyperparameters were tested to determine the configurations with the highest accuracies by using the *GridSearchCV* function from Scikit-learn[5]:

1. Linear discriminant analysis (LDA):

   Solver: singular-value decomposition, least-squares solution, or eigenvalue decomposition.

   Shrinkage: automatic, 0.1, 0.2, or 0.5.

2. Support-vector classifier (SVC):

   Kernel: Linear or radial basis function.

   Regularization parameter: 1 or 10.

   Kernel coefficient: 1×10^{-3} or 1×10^{-4}.

3. Multilayer perceptron (MLP):

   Number of hidden layers: 1.

   Number of neurons: 50, 100, or 150.

[5] https://scikit-learn.org/

Activation function: Rectified linear unit, logistic function, or hyperbolic tan function.

Learning rate: Constant or adaptive.

Early stopping: Enabled or disabled.

4. *k*-nearest neighbors (*k*-NN):

   Number of neighbors: 3, 5, or 7.

   Weight function: Uniform or distance-based.

5. Gaussian naive Bayes

6. Random forest:

   Number of estimators: 10, 100, or 150.

   Criterion: Gini impurity or entropy.

7. Adaptive Boosting (AdaBoost):

   Number of estimators: 10, 100, 150.

   Learning rate: 0.5, 0.8, 1.0, or 1.2.

   Boosting algorithm : SAMME or SAMME.R.

The hyperparameters were chosen so as to have some variety in the configurations while also keeping the script runtime within a couple of hours. The algorithms feature a mix of linear and nonlinear algorithms. For this study, the Google Colab script was adapted in Python (Python 3.9; Python Software Foundation, Wilmington, DE, USA) to read the EEG data obtained from the experiments and analyze the model accuracies for each algorithm under different conditions, as well as between algorithms by considering the median accuracies of a given algorithm for all conditions.

3.3.2.B Data preprocessing and feature extraction

The data preprocessing was different than the one done for the EEG analysis in MATLAB. A band-pass filter between 8 Hz and 30 Hz was used to include just the alpha and beta waves. Afterward, a CSP filter with four components was used, which is the most commonly used feature-extraction tool in BCIs [43]. The data was split into epochs of left- and right-hand trials. For the accuracies, which were offline, 20% of the data was divided into 10 groups of shuffled epochs to b used in all the algorithms.

3.3.2.C Data visualization

The model accuracies were plotted in box plots. Scatter plots of the accuracies and the LIs were also analyzed to assess correlations, since the models should not only be accurate but also promote

contralateral brain activation in stroke patients. A bar chart with the number of correlations was also created.

3.4 Statistical tests

Because the sample size was small—ranging from 10 to 19 subjects, depending on the condition—the Kruskal–Wallis test, which is the nonparametric equivalent of the one-way analysis of variance (ANOVA), was used to determine statistically significant differences between the conditions in the mERD and LI sample groups, and conditions or algorithms in the machine-learning accuracy sample groups, for a significance level of 0.05 ($p < 0.05$). The LI sample groups were also compared to a null lateralization index (LI = 0) to determine if the brain activation was significantly lateralized in any conditions.

Whenever the null hypothesis was rejected—that the samples from some conditions or algorithms did not come from the same distribution—a post hoc analysis was performed. The analysis consisted of pairwise comparisons using Dunn's test, as it typically follows the Kruskal–Wallis test due to computing the same ranks.

3.5 Questionnaires

3.5.1 Edinburgh Handedness Inventory

The Edinburgh Handedness Inventory [76] (see Appendix A.1) was used to determine the subjects' hand dominance. The questionnaire had 12 items, of which the first 10 were directly related to hand dominance. A laterality quotient can be extracted from the answers,

$$\text{Laterality quotient (\%)} = \frac{R-L}{R+L} \times 100, \tag{3.4}$$

where R is the sum of the points attributed to the right hand—one point for each "Right +" and two for each "Right ++"—and L to the left hand—one point for each "Left +," and two points for each "Left ++." A plus sign means that the subject prefers to use a specific hand, while two mean that the subject uses the specific hand exclusively for the given task unless forced to use the other. If the subject is indifferent to using any of their hands, they could answer simultaneously with "Left +" and "Right +." A positive laterality quotient implies right-hand dominance, while a negative quotient implies left-hand dominance.

Given the subjects' handedness was not of particular interest to this study, neither the questionnaire answers nor the laterality quotients were reported in Results.

3.5.2 Vividness of Movement Imagery Questionnaire-2

The VMIQ-2 [77] (see Appendix A.2) has the subjects evaluate their ability to perform motor imagery for 12 tasks including walking, running, throwing a stone, etc. The evaluation is done in three ways: by observing the movements through one's eyes (IVI) and from an outside perspective (EVI), and by feeling the movement (KI). The answers were used in a correlation analysis with the EEG metrics.

3.5.3 Condition preference

The subjects answered a questionnaire ranking the five motor-imagery conditions from most (first place) to least preferred (fifth place) (see Appendix A.3). An average score from 1 to 5 was attributed to each condition to rank them in a bar chart. For each condition, every first-place vote counted 5 points, second-place 4 points, and so on till fifth-place votes, which counted 1 point. The average score for a condition was given by the formula

$$\text{Average score} = \frac{5 \times N_{1\text{st}} + 4 \times N_{2\text{nd}} + 3 \times N_{3\text{rd}} + 2 \times N_{4\text{th}} + 1 \times N_{5\text{th}}}{19}, \tag{3.5}$$

where $N_{i\text{-th}}$ is the number of votes for the i-th position.

3.5.4 Embodiment questionnaire

The embodiment questionnaire [78] (see Appendix A.4) had several statements that the subject had to answer between "strongly agree" and "strongly disagree" on a seven-point Likert scale. Those statements referred to four different areas concerning embodiment, whose scores—ranging from 1 (low) to 7 (high)—were defined as follows [78]:

$$\text{Appearance} = \frac{\text{Q8} + \text{Q13} + \text{Q15} + \text{Q16} + \text{Q17} + \text{Q18} + \text{Q20} + \text{Q21}}{8}, \tag{3.6}$$

$$\text{Response} = \frac{\text{Q12} + \text{Q17} + \text{Q20} + \text{Q21} + \text{Q22} + \text{Q24}}{6}, \tag{3.7}$$

$$\text{Ownership} = \frac{\text{Q1} + \text{Q6} + \text{Q10} + \text{Q14} + \text{Q18} + \text{Q19}}{6}, \tag{3.8}$$

$$\text{Multisensory} = \frac{\text{Q6} + \text{Q8} + \text{Q10} + \text{Q12} + \text{Q13} + \text{Q14}}{6}, \text{ and} \tag{3.9}$$

$$\text{Final score} = \frac{\text{Appearance} + \text{Response} + \text{Ownership} + \text{Multisensory}}{4}. \tag{3.10}$$

3.5.5 Correlations with EEG metrics and machine-learning accuracies

The VMIQ-2 was used to see whether there were statistically significant ($p < 0.05$) linear correlations between the answers to its items and the mERDs and LIs obtained for left- and right-hand trials, alpha

and beta waves, electrodes C3 and C4, and each condition. The significant correlations were put on a table, where the rows and columns were labeled with numbers to make the table easier to read.

The first 12 rows belonged to the VMIQ-2 items, and the last 5 belonged to the embodiment questionnaire: appearance, response, ownership, multisensory, and the final score (see Appendices A.2 and A.4). The table had 180 columns, which were different permutations between five or two sections, depending on the EEG metric.

For mERDs, there were five sections: the six conditions, side of the trial (left- or right-hand), electrode (C3 or C4), brain rhythm (alpha or beta), and VMIQ-2 section (IVI, EVI, and KI). The correlation values did not change when assessing the embodiment scores across the VMIQ-2 sections, nor did for the LIs; this redundancy was kept due to the script's already existing complexity.

Once the permutations ended for the mERDs of a specific condition, the next two columns computed the correlations for the alpha and beta LIs of that same condition. The columns would keep cycling through the many sections aforementioned until the last condition, *grazME*. For example:

1. grazMI – Left – C3 – Alpha – IVI
2. grazMI – Left – C3 – Alpha – EVI
3. grazMI – Left – C3 – Alpha – KI

   ⋮

23. grazMI – Right – C4 – Beta – EVI
24. grazMI – Right – C4 – Beta – KI
25. grazMI – Lateralization index – Alpha – IVI
26. grazMI – Lateralization index – Alpha – EVI

And so on until the 180th column, "grazME – Lateralization index – Beta – KI."

Additionally, the EEG metrics and the embodiment scores were also plotted in scatter plots to better observe any statistically significant correlations between the different conditions.

No *p*-value corrections were made; therefore, given the numerous possible correlation, trends in the results were analyzed instead of singular significant correlations, on the off chance that the they were falsely identified.

4

Results

Contents

The results were analyzed in an attempt to (1) answer which condition, or BCI–VR configuration, induces the strongest, most lateralized ERD (i.e., brain activation) for stroke rehabilitation and (2) which conditions and machine-learning algorithms lead to the most accurate models in BCIs, also for stroke rehabilitation.

The first results pertain to the EEG metrics, which are the alpha and beta mERDs and LIs. Then, the accuracies of the machine-learning models are shown, and correlations between them and the LIs are mentioned. Finally, questionnaire scores are presented, and correlations between them and EEG metrics are also mentioned.

4.1 Event-related desynchronizations

4.1.1 Power differences

4.1.1.A Mean event-related desynchronizations across conditions

The box plots of the mERDs in electrodes C3 and C4 are shown in Figure 4.1, which reveal the cortical activation for the different conditions. The mERD medians were all negative except *grazMI*'s ipsilateral alpha mERD (*Mdn* = 3.57%). The condition *grazME* had the strongest mERD medians of all conditions. The contralateral sample groups had overall lower distributions than the ipsilateral ones.

From the ipsilateral alpha mERD medians, *grazME* had the highest value (*Mdn* = −37.45%), followed by *neurowMIMOHP* (*Mdn* = −12.12%), *neurowMIMOVRHP* (*Mdn* = −8.69%), *neurowMIMO* (*Mdn* = −1.79%), *neurowMIMOVR* (*Mdn* = −1.48%), and *grazMI* (*Mdn* = 3.57%). Between the contralateral medians, *grazME* had the highest median (*Mdn* = −37.27%), followed by *neurowMIMOHP* (*Mdn* = −33.30%), *neurowMIMOVRHP* (*Mdn* = −22.86%), *neurowMIMOVR* (*Mdn* = −20.16%), *neurowMIMO* (*Mdn* = −12.92%), and *grazMI* (*Mdn* = −5.08%) (see Figure 4.1(a)).

From the ipsilateral beta mERD medians, *grazME* had the highest value (*Mdn* = −17.30%), followed by *neurowMIMOHP* (*Mdn* = −11.08%), *neurowMIMOVR* (*Mdn* = −8.70%), *neurowMIMOVRHP* (*Mdn* = −8.05%), *neurowMIMO* (*Mdn* = −7.50%), and *grazMI* (*Mdn* = −5.47%). Between the contralateral medians, *grazME* had the highest median (*Mdn* = −24.34%), followed by *neurowMIMOVR* (*Mdn* = −17.07%), *neurowMIMO* (*Mdn* = −15.39%), *neurowMIMOHP* (*Mdn* = −14.29%), *neurowMIMOVRHP* (*Mdn* = −13.76%), and *grazMI* (*Mdn* = −8.69%) (see Figure 4.1(b)).

According to the Kruskal–Wallis test, the alpha mERD was significantly different across all groups (ipsilateral: χ^2 = 33.92, $p < 0.001$; contralateral: χ^2 = 27.54, $p < 0.001$) but there were no significant differences between the beta mERDs (ipsilateral: χ^2 = 10.75, p = 0.057; contralateral: χ^2 = 10.30, p = 0.067). Specifically, according to Dunn's test for the post-hoc pairwise comparisons ($p < 0.05$), *grazMI* was significantly different from all the other conditions for contralateral electrodes (*neurowMIMO*: p = 0.043; *neurowMIMOHP*: $p < 0.001$; *neurowMIMOVR*: p = 0.012; *neurowMIMOVRHP*: $p < 0.001$;

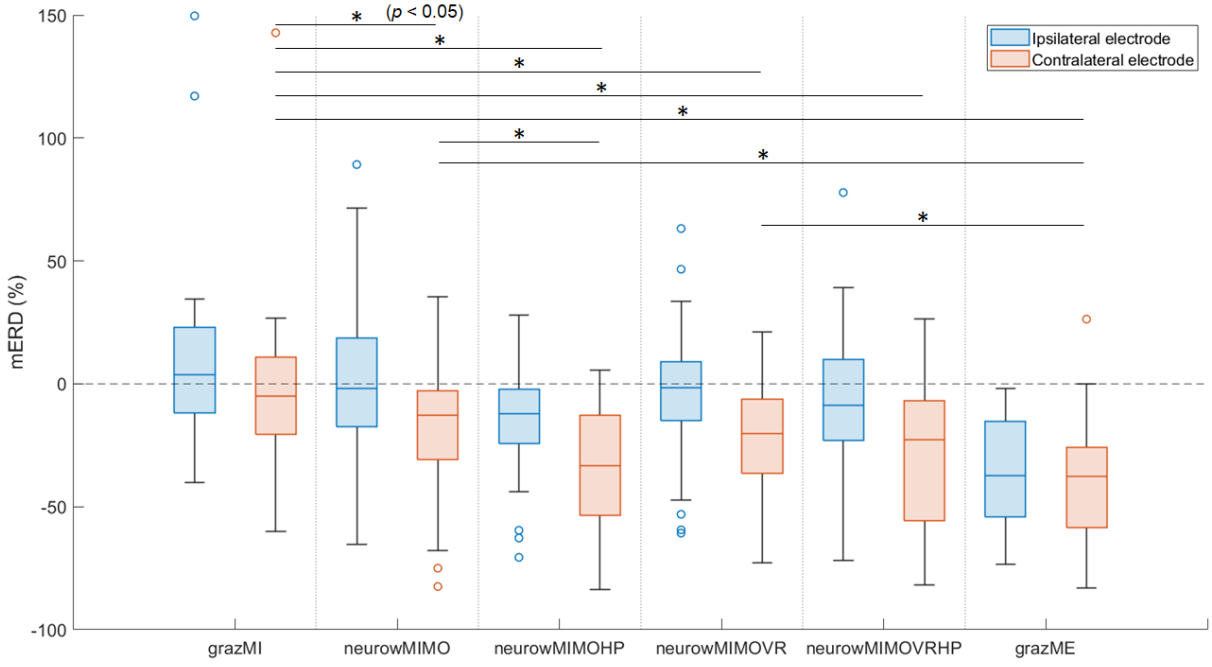

(a) Alpha mERDs

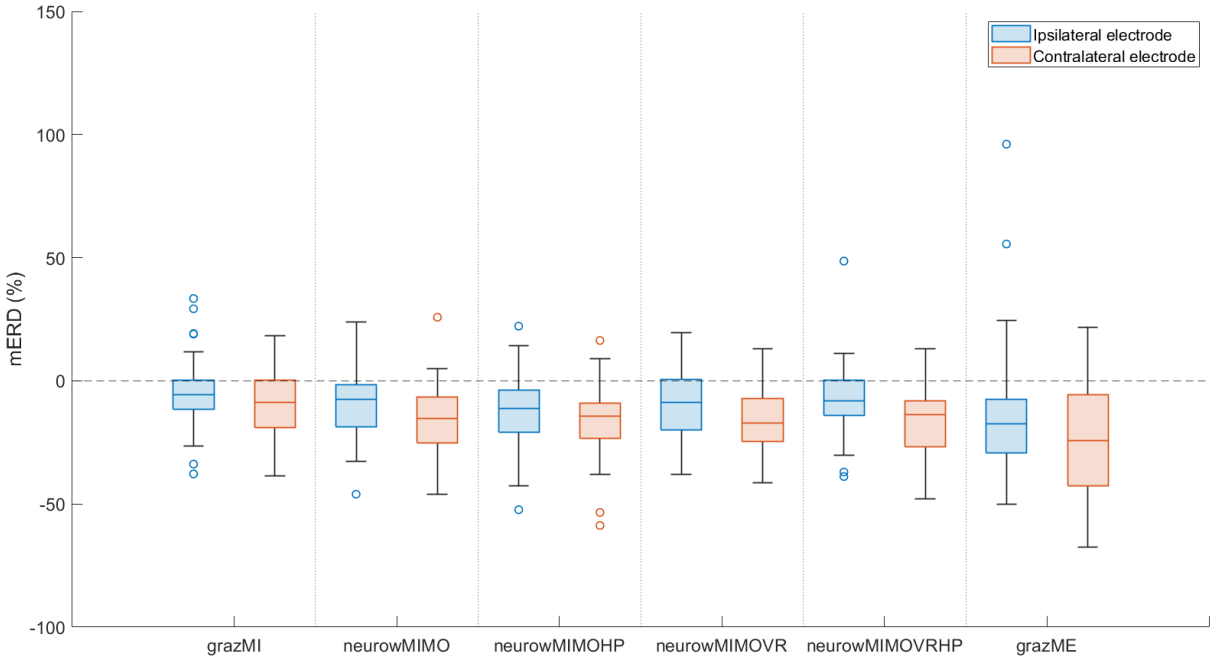

(b) Beta mERDs

Figure 4.1: mERDs for the different conditions, where each sample group contains both left- and right-hand trials for both (a) alpha and (b) beta bands. The asterisks indicate significant differences between the distributions of the contralateral electrodes. ($p < 0.05$)

Table 4.1: Relative percentages of the ipsi- and contralateral median mERDs between the motor-imagery conditions and *grazME*, where negative values (in bold) indicate early synchronization

	Relative median mERD (%)			
	Alpha rhythm		**Beta rhythm**	
Condition	**Ipsilateral**	**Contralateral**	**Ipsilateral**	**Contralateral**
grazME	100.00	100.00	100.00	100.00
grazMI	**−9.53**	13.63	31.62	35.70
neurowMIMO	4.78	34.67	43.35	63.23
neurowMIMOHP	32.36	89.34	64.05	58.71
neurowMIMOVR	3.95	54.09	50.29	70.13
neurowMIMOVRHP	23.20	61.34	46.53	56.53

grazME: $p < 0.001$), while *grazME* was significantly different from *grazMI* ($p < 0.001$) and the *NeuRow* conditions without haptic feedback, *neurowMIMO* ($p = 0.009$) and *neurowMIMOVR* ($p = 0.033$). On the other hand, the *NeuRow* conditions with haptic feedback were not significantly different from *grazME* for the contralateral electrodes (*neurowMIMOHP*: $p = 0.480$; *neurowMIMOVRHP*: $p = 0.153$). The condition *grazME* also had significantly different ipsilateral mERD distributions from all the other conditions (*neurowMIMOHP*: $p = 0.021$; the others: $p < 0.001$).

4.1.1.B Relative mERD

The relative mERD medians between the motor-imagery conditions and *grazME* are in Table 4.1. The percentages are relative to *grazME*'s ipsi- or contralateral distributions, which is, by definition, 100% for any of them. The *grazMI* alpha ipsilateral percentage was negative, which indicates an early alpha rebound. All the other values were positive, with *neurowMIMOHP* being the condition that had the closest alpha mERD and ipsilateral beta mERD medians to *grazME*. The *neurowMIMOHP*'s contralateral alpha mERD median was just short of 10.66%, which was distantly followed by *neurowMIMOVRHP*'s 38.66%.

4.1.1.C Spatial distribution of the mean event-related desynchronizations

The spatial distributions of the mERDs for alpha and beta waves are shown in Figure 4.2, which help get a better understanding of where the ERDs occurred. The desynchronization peaks were located in the region posterior to the sensorimotor cortex in the motor-imagery conditions, while *grazME*'s peaks

were slightly more anterior and closer to the sensorimotor cortex. The condition *grazMI* had a weak ERD spread in the posterior region of the sensorimotor cortex, while the *NeuRow* conditions had clearly defined desynchronization clusters around the contralateral electrodes. Conditions *neurowMIMOHP* and *neurowMIMOVRHP* had the most prominent ERD peaks of all motor-imagery conditions, particularly for alpha waves. The conditions *neurowMIMO* and *neurowMIMOVR* showed similar alpha ERDs, with intensities in-between those in *grazMI* and the *NeuRow* conditions with haptic feedback. Condition *grazME* had the strongest, most evident ERD for both waves. The motor-imagery conditions showed more lateralized alpha ERDs than *grazME*, albeit not as prominent. On the other hand, the desynchronizations were not as pronounced for beta waves as for alpha waves.

The standard deviations of the mERDs, which help understand which areas were more active than the others, are shown in Figure 4.3. They were generally higher for alpha waves while showing overall much lower values for beta waves. Some small peaks were located in the temporal regions, which can be seen in *neurowMIMOHP* and *neurowMIMOVRHP*. The occipital lobe and posterior parietal cortex had noticeably higher standard deviations in *grazMI*, especially for alpha waves; *neurowMIMOVR*; and *grazME*, crossing into the temporal lobe. There were clusters around electrodes C3 and C4, which can be clearly observed in the *NeuRow* conditions, but slightly less so in *neurowMIMOHP*.

The differences between the motor-imagery conditions' mERDs and *grazME*'s are shown in Figure 4.4. The *NeuRow* conditions had noticeably stronger ERDs than *grazME* in the regions posterior to the sensorimotor cortex, while *grazMI* had a much weaker ERD all around.

4.1.1.D Average event-related desynchronizations in time

The average alpha and beta ERD values in time are shown in Figure 4.5 for contralateral electrodes C3 or C4. All conditions led to ERDs after the arrow cue was shown to the subjects; however, the desynchronization in *grazMI* was not as sustained as in the other conditions. Its average ERD returned to the baseline, except for alpha waves in left-hand trials, which rebounded early. The ERD was generally the strongest for *grazME*. The conditions *neurowMIMOHP* and *neurowMIMOVRHP* showed similar ERDs to *grazME* for alpha waves and surpassed it momentarily in the right-hand trials. The beta waves were not as reactive, as seen by the weaker ERDs, especially in motor imagery.

4.1.2 Lateralization indices

The box plots of the LI sample groups are shown in Figure 4.6, which indicate the lateralization of the ERDs in each condition. The alpha LIs had mostly broader distributions and higher values than the beta LIs. The median alpha LI of *neurowMIMOVR* was the highest (*Mdn* = 15.2), followed by *neurowMIMOHP* (*Mdn* = 14.1), *neurowMIMOVRHP* (*Mdn* = 13.7), and *neurowMIMO* (*Mdn* = 10.8). The conditions *grazMI* and *grazME* had the lowest medians (*Mdn* = 5.3 and *Mdn* = 7.3, respectively).

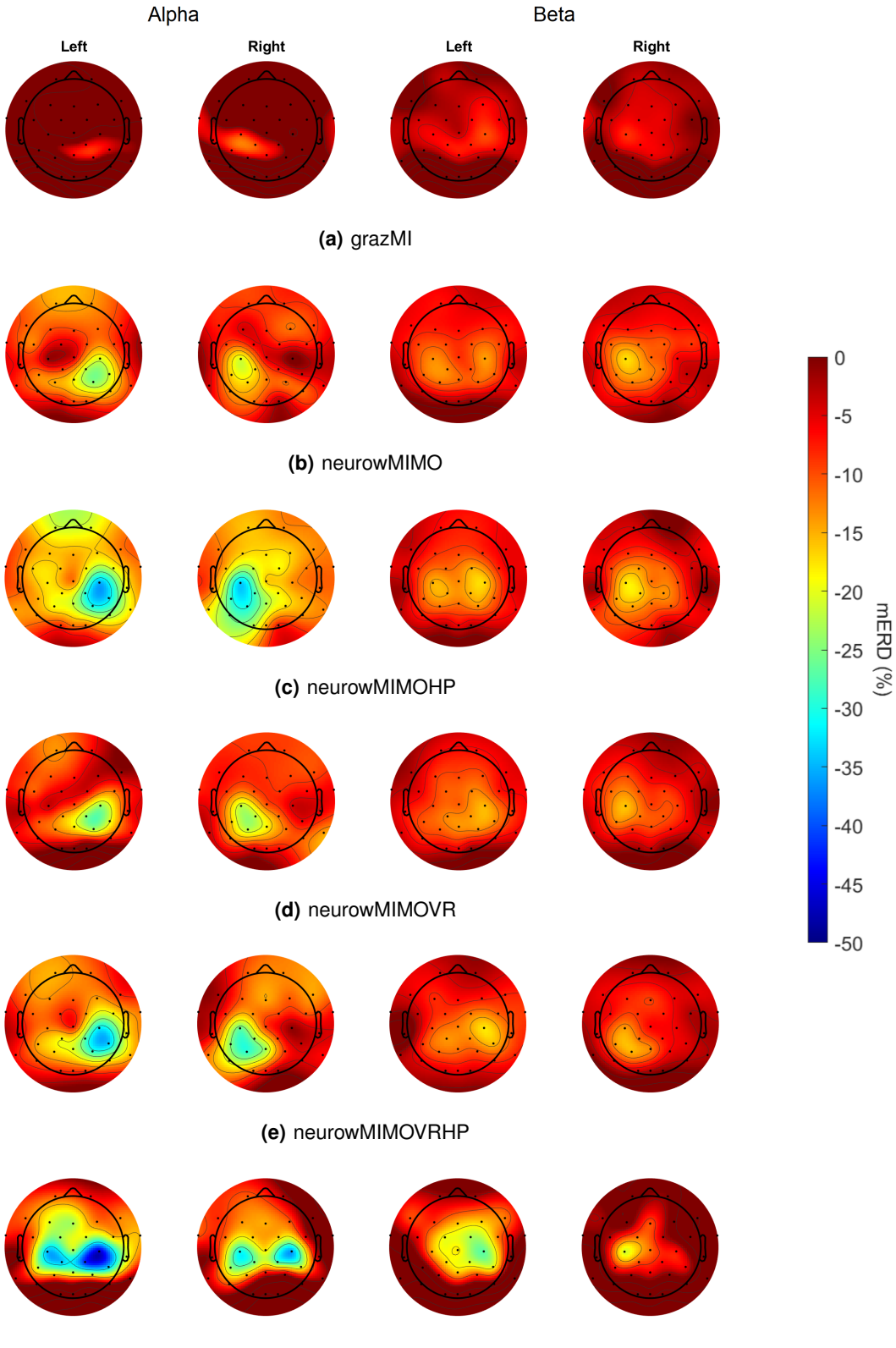

(a) grazMI

(b) neurowMIMO

(c) neurowMIMOHP

(d) neurowMIMOVR

(e) neurowMIMOVRHP

(f) grazME

Figure 4.2: Topographic plots of the mERDs averaged for all subjects in the different conditions

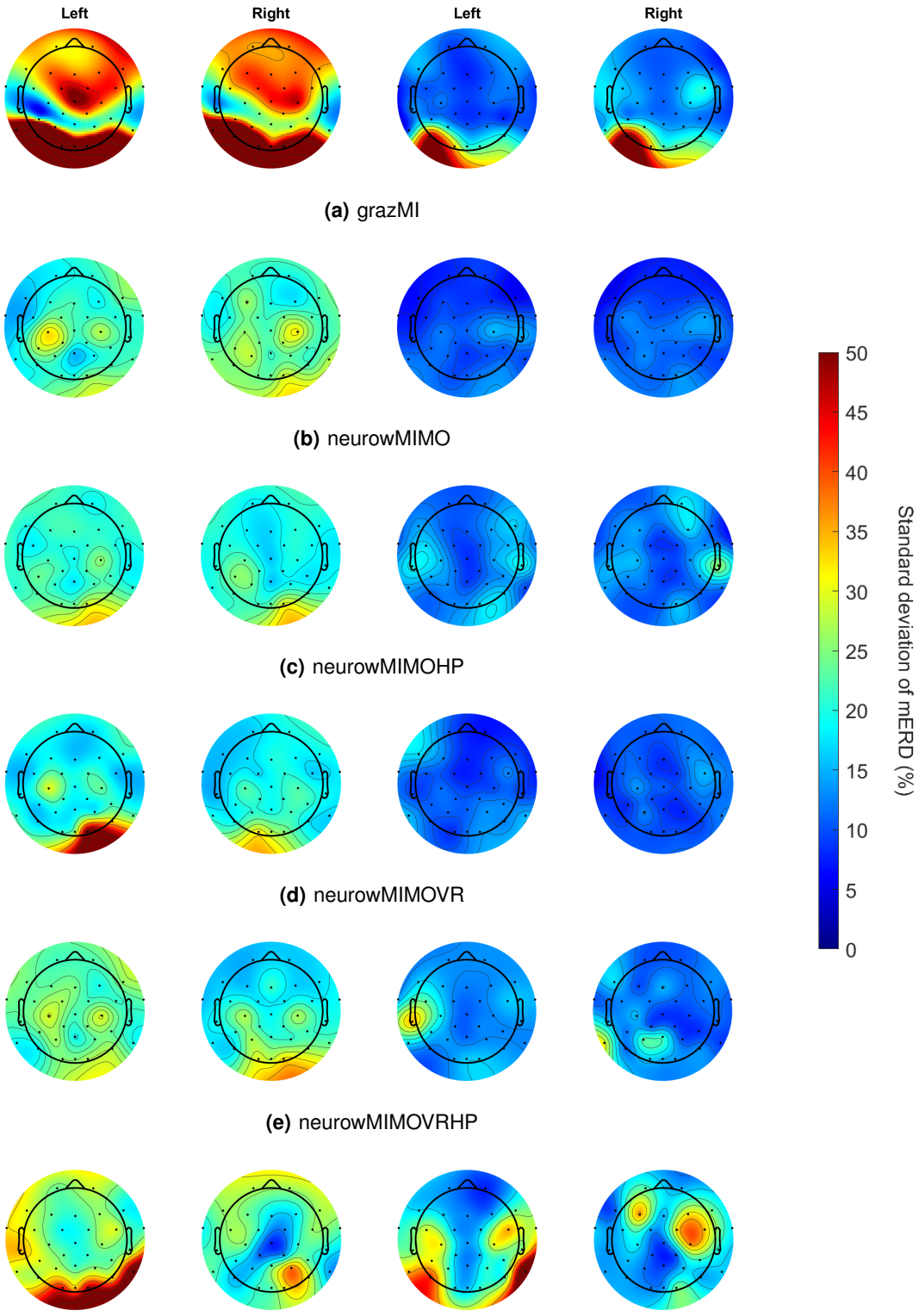

Figure 4.3: Topographic plots of the mERDs' standard deviations averaged for all subjects in the different conditions

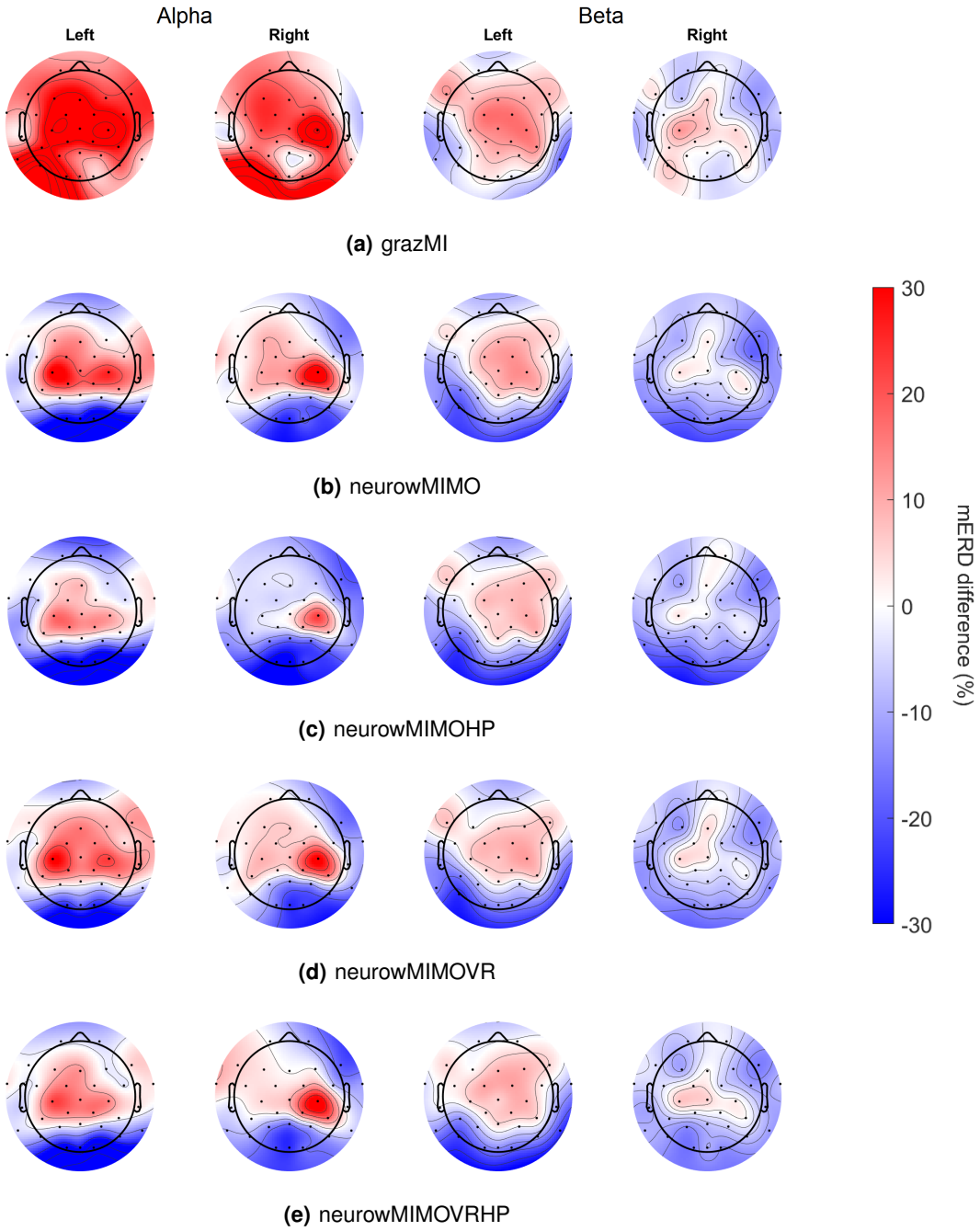

Figure 4.4: Subtraction topographic plots of the mERDs averaged for all subjects between the motor-imagery conditions and *grazME*, where positive and negative differences indicate weaker and stronger desynchronizations in the motor-imagery conditions, respectively

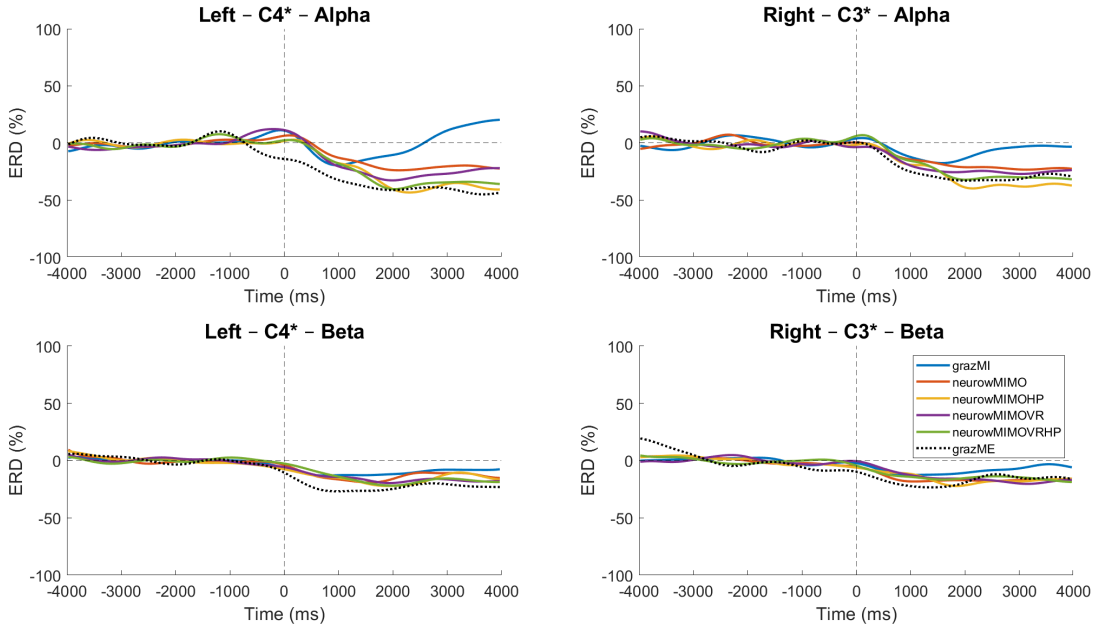

Figure 4.5: Average alpha and beta ERD values in time for contralateral electrodes C3 or C4

The condition *grazME* had the highest median beta LI (Mdn = 8.6) but also the broadest distribution. The motor-imagery conditions had similar distributions between themselves, with the conditions *neurowMIMOHP* and *neurowMIMOVRHP* having the highest medians (Mdn = 5.1 and Mdn = 5.4, respectively). However, all conditions included negative indices in their sample groups, which are found up to the lower quartile of the distributions.

According to the Kruskal–Wallis test ($p < 0.05$), none of the sample groups were significantly different (alpha: $\chi^2 = 6.06$, $p = 0.300$); beta: $\chi^2 = 3.77$, $p = 0.582$). However, there was a significant difference between the sample groups and a null LI, LI = 0 (alpha: $\chi^2 = 28.17$, $p < 0.001$; beta: $\chi^2 = 20.03$, $p = 0.003$). Dunn's test for pairwise comparisons found *grazMI* and the *NeuRow* conditions to have significantly different alpha LI sample groups from the null LI (*grazMI*: $p = 0.010$; *NeuRow* conditions: $p < 0.001$; *grazME*: $p = 0.057$), while all the beta LI sample groups were significantly different (*grazMI*: $p = 0.006$; *neurowMIMO* and *neurowMIMOHP*: $p = 0.005$; *neurowMIMOVR*: $p = 0.003$; *neurowMIMOVRHP* and *grazME*: $p < 0.001$).

4.2 Machine learning

4.2.1 Accuracies between conditions

The accuracies of the machine-learning models for each condition are shown in Figure 4.7. The condition *grazME* had lower distributions than the motor-imagery conditions for any of the algorithms. According

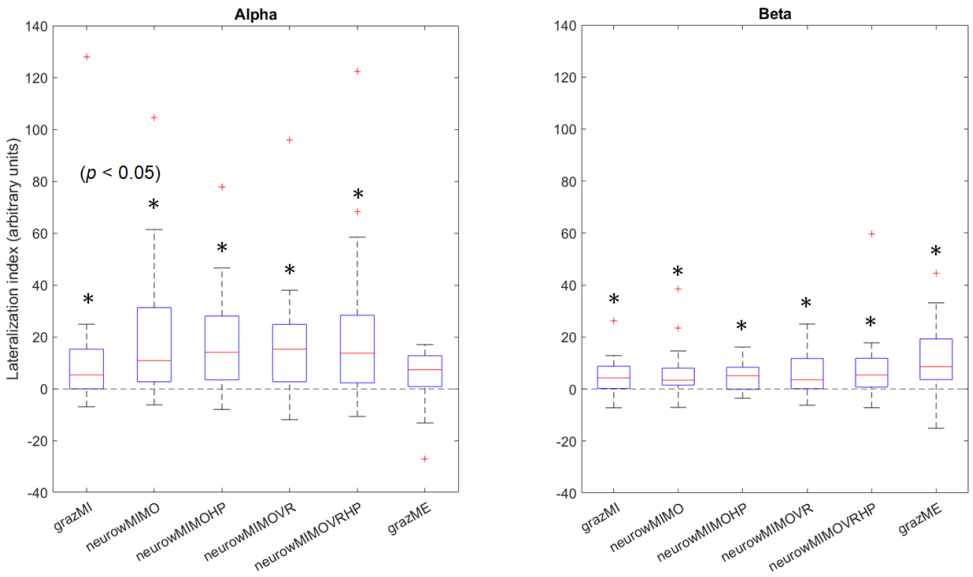

Figure 4.6: Box plots of the LIs for alpha and beta waves, where the asterisks show the distributions that are significantly different from the null LI, LI = 0 ($p < 0.05$)

to the Kruskal–Wallis test ($p < 0.05$), the conditions had significantly different accuracy distributions for algorithms LDA (χ^2 = 15.39, p = 0.009), SVC (χ^2 = 38.06, $p < 0.001$), MLP (χ^2 = 21.47, $p < 0.001$), random forest (χ^2 = 11.87, p = 0.037), and AdaBoost (χ^2 = 17.33, p = 0.004). The algorithms k-NN and Gaussian naive Bayes, on the other hand, did not have significantly different distributions (χ^2 = 8.14, p = 0.149 and χ^2 = 7.97, p = 0.158, respectively).

Further pairwise comparisons using Dunn's test say that *grazME* was significantly different from all motor-imagery conditions ($p < 0.05$) except *neurowMIMO* for LDA (p = 0.066), random forests (p = 0.204), and AdaBoost (p = 0.187); and *neurowMIMOHP* for random forests (p = 0.080). The condition *grazMI* was significantly different from *neurowMIMO* for random forests (p = 0.040) and AdaBoost (p = 0.020), and from *neurowMIMOHP* for SVC (p = 0.038). The condition *neurowMIMO* was significantly different from *neurowMIMOVR* (p = 0.035) and *neurowMIMOVRHP* (p = 0.028) for AdaBoost.

4.2.2 Accuracies between algorithms

The median accuracies of each model are shown in Figure 4.8. The algorithms SVC and MLP had the highest median-accuracy medians (*Mdn* = 68.46%), followed by AdaBoost (*Mdn* = 56.88%), LDA (*Mdn* = 55.77%), k-NN (*Mdn* = 53.46%), and Gaussian naive Bayes (*Mdn* = 47.63%). The algorithms SVC and MLP had the most compact distributions with a mean accuracy of 67.88% (SD = 1.29%) and 68.01% (SD = 1.38%), respectively. The median accuracies were identical for both algorithms except in *neurowMIMO*, which was 68.46% for SVC and 69.23% for MLP. The Gaussian naive Bayes was the only algorithm with all of its median accuracies below 50%.

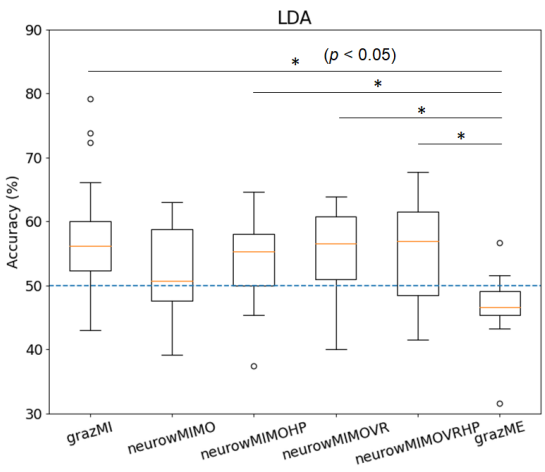

(a) Linear discriminant analysis

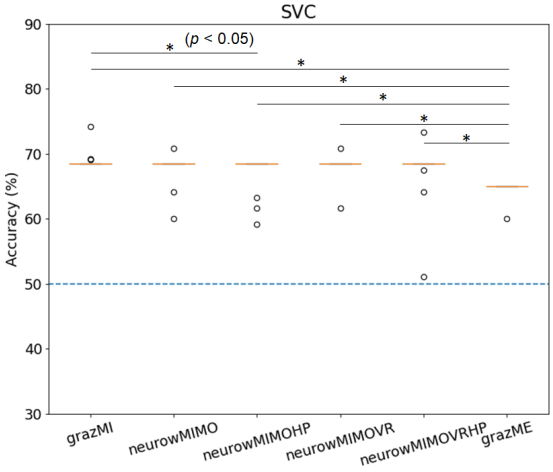

(b) Support-vector classifier

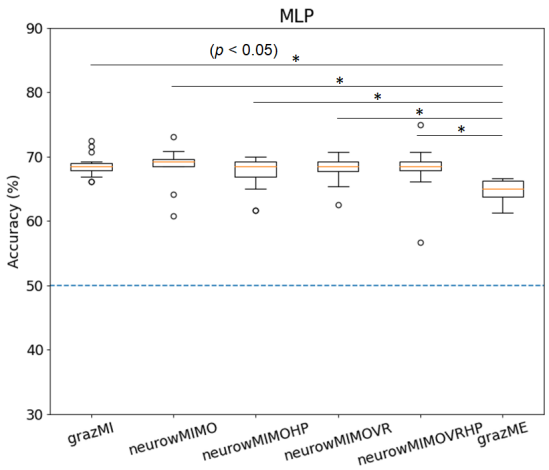

(c) Multilayer perceptron

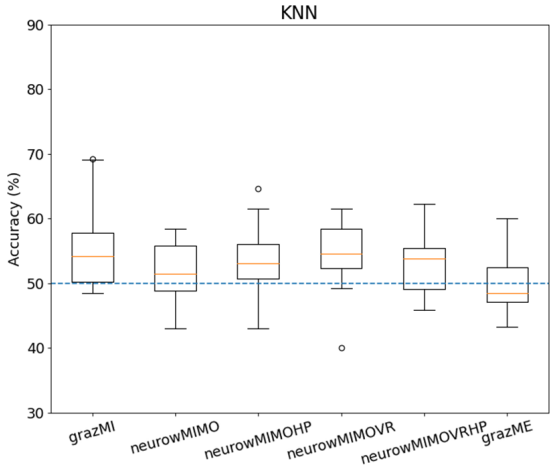

(d) *k*-nearest neighbors

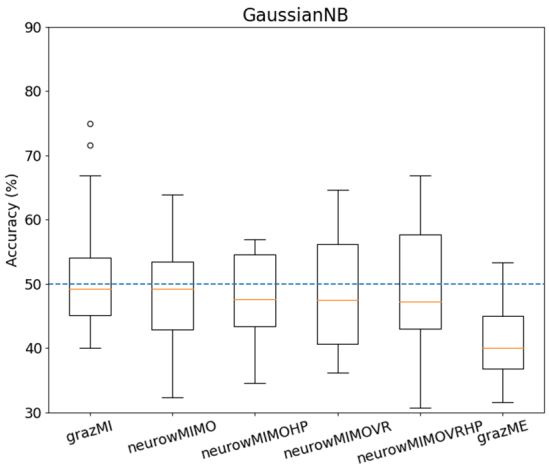

(e) Gaussian naive Bayes

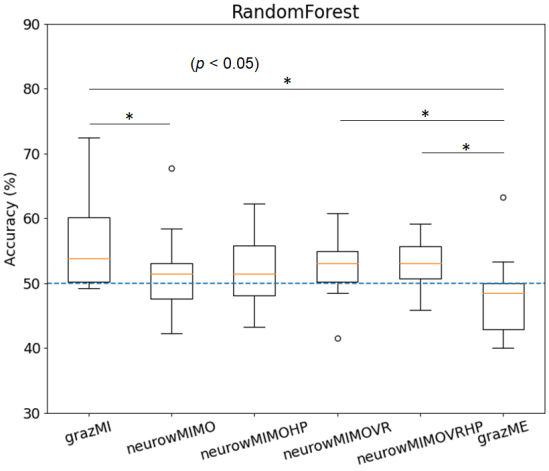

(f) Random forests

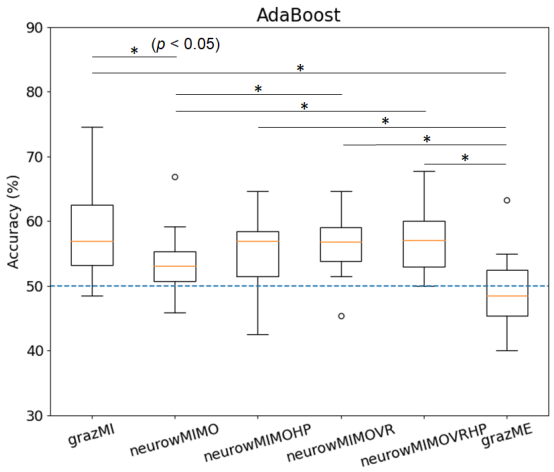

(g) AdaBoost

Figure 4.7: Box plots of the machine-learning models' accuracies for each condition, where the asterisk and horizontal lines indicate statistically significant pairwise sample group differences, for $p < 0.05$

The Kruskal–Wallis test showed a significant difference ($p < 0.05$) between the accuracy distributions ($\chi^2 = 32.08$, $p < 0.001$). The pairwise comparisons using Dunn's test further showed that LDA was significantly different from SVC ($p = 0.014$) and MLP ($p = 0.010$); SVC was significantly different from k-NN ($p = 0.006$), Gaussian naive Bayes ($p < 0.001$), and random forests ($p = 0.002$); MLP was significantly different from k-NN ($p = 0.004$), Gaussian naive Bayes ($p < 0.001$), random forests ($p = 0.001$), and AdaBoost ($p = 0.040$); and Gaussian naive Bayes was significantly different from AdaBoost ($p = 0.015$).

4.2.3 Correlations between the accuracies and the lateralization indices

A correlation analysis was done to see if the lateralization of the alpha and beta mERDs was contributing to the performance of the classifiers. Thus, the extracted LIs was used to compare their performances (%) as computed through the CSP's features.

The scatter plots with the models' accuracies and the LIs are shown in Figure 4.9. There were some significant correlations, most notably for *neurowMIMO*, but none for *grazMI* and *grazME*. The alpha LIs generally showed positive, albeit nonsignificant, correlations, more so than the beta LIs.

The number of statistically significant correlations illustrated in Figure 4.10 shows that the Gaussian naive Bayes classifier correlated in most of the conditions with both alpha LIs(3 out of 6) and beta LIs (4 out of 6). The extracted performance from SVC and MLP algorithms, unlike the others, did not have any significant correlations with LIs.

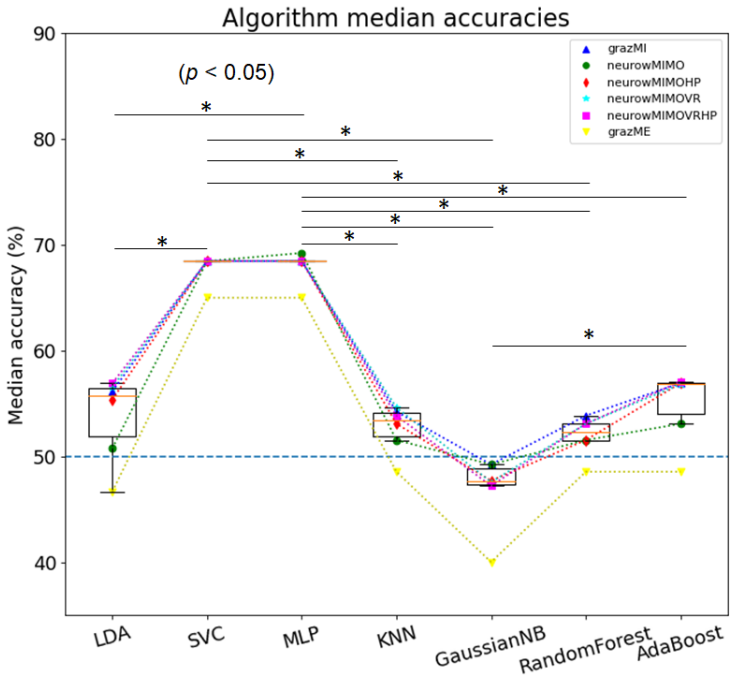

Figure 4.8: Box plots of the machine-learning models' median accuracies for all conditions, where the asterisk and horizontal lines indicate statistically significant pairwise sample group differences, for $p < 0.05$

4.3 Questionnaires

4.3.1 Condition preference

A questionnaire was issued to capture the subjects' preferences to assess their choices between the different conditions, given the equipment differences and setup complexity.

As shown in Figure 4.11, most subjects preferred *neurowMIMOVRHP*, while *grazMI* was the least preferred. The condition *neurowMIMO* was strongly voted as the second least preferred condition, and *neurowMIMOHP* and *neurowMIMOVR* fall in-between it and *neurowMIMOVRHP*, with the latter being slightly preferred over the former. The answers to all of the questionnaires, except the condition-preference questionnaire, which is shown in Figure 4.11, are in Appendix A.

4.3.2 Correlations of motor-imagery ability and embodiment with event-related desynchronizations

In order to assess possible relations between the extracted EEG and machine-learning metrics and the subjective experience of the subjects—given that user-related information is scarce in literature—a correlation analysis was done between the mERDs, LIs, and BCI performance with the VMIQ-2 and the embodiment questionnaire (both the subscale scores and the final score).

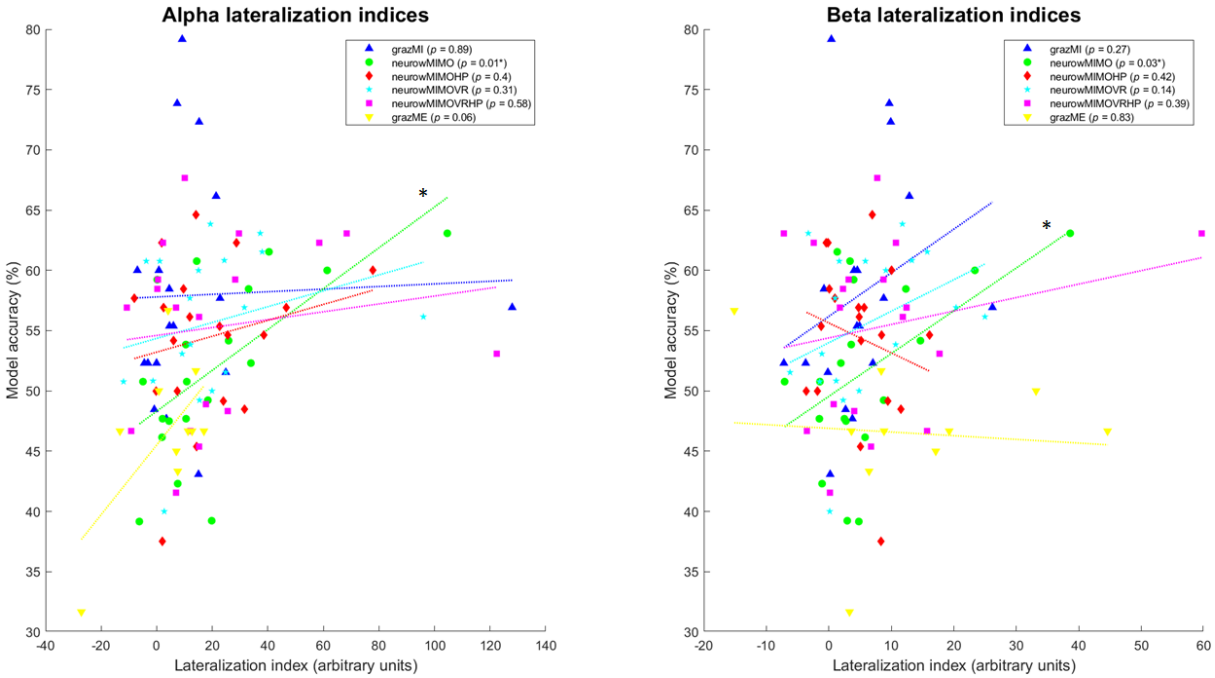

(a) Linear discriminant analysis

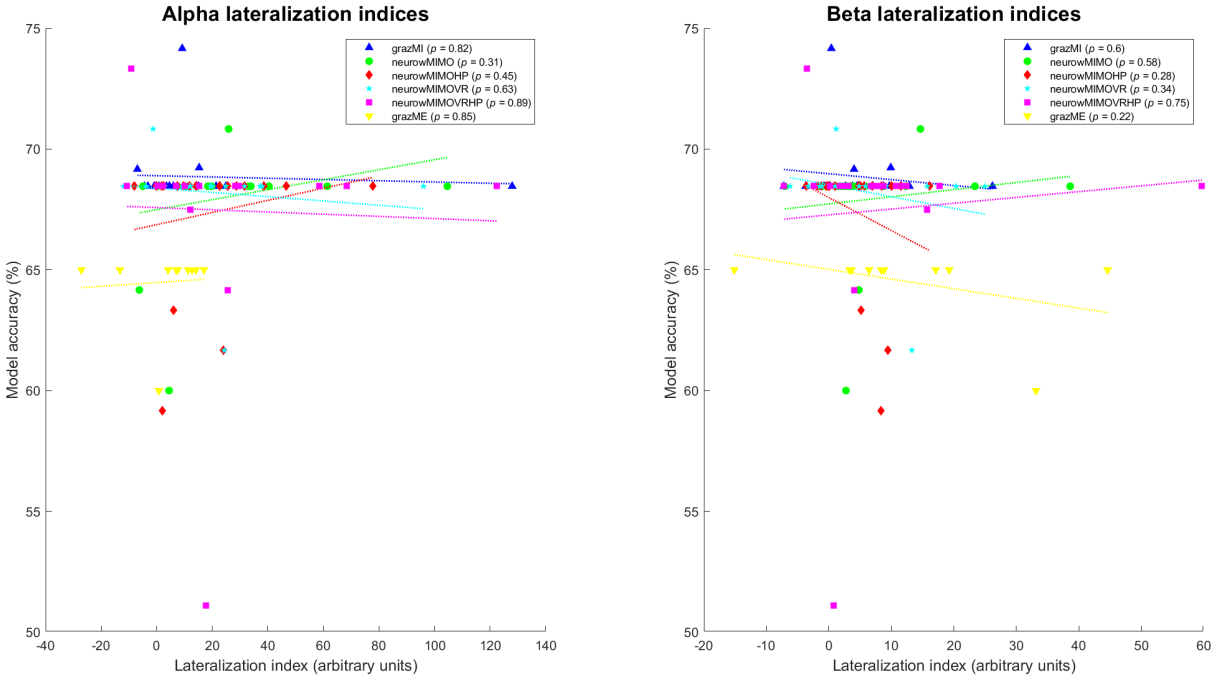

(b) Support-vector classifier

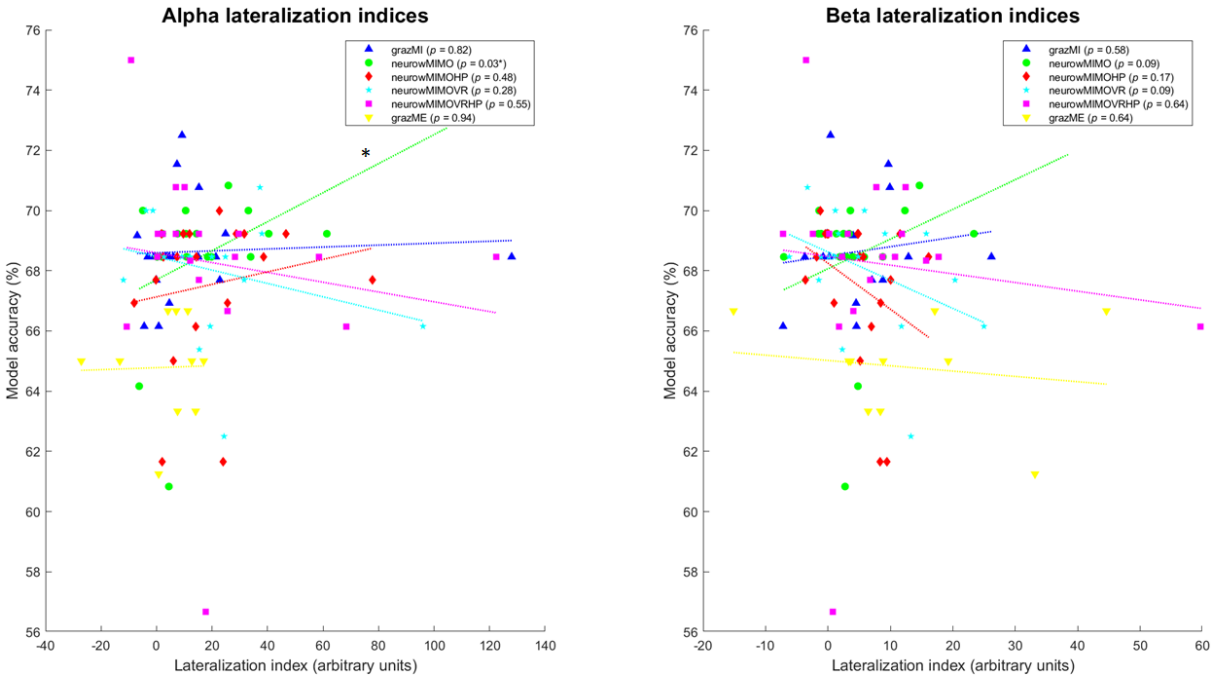

(c) Multilayer perceptron

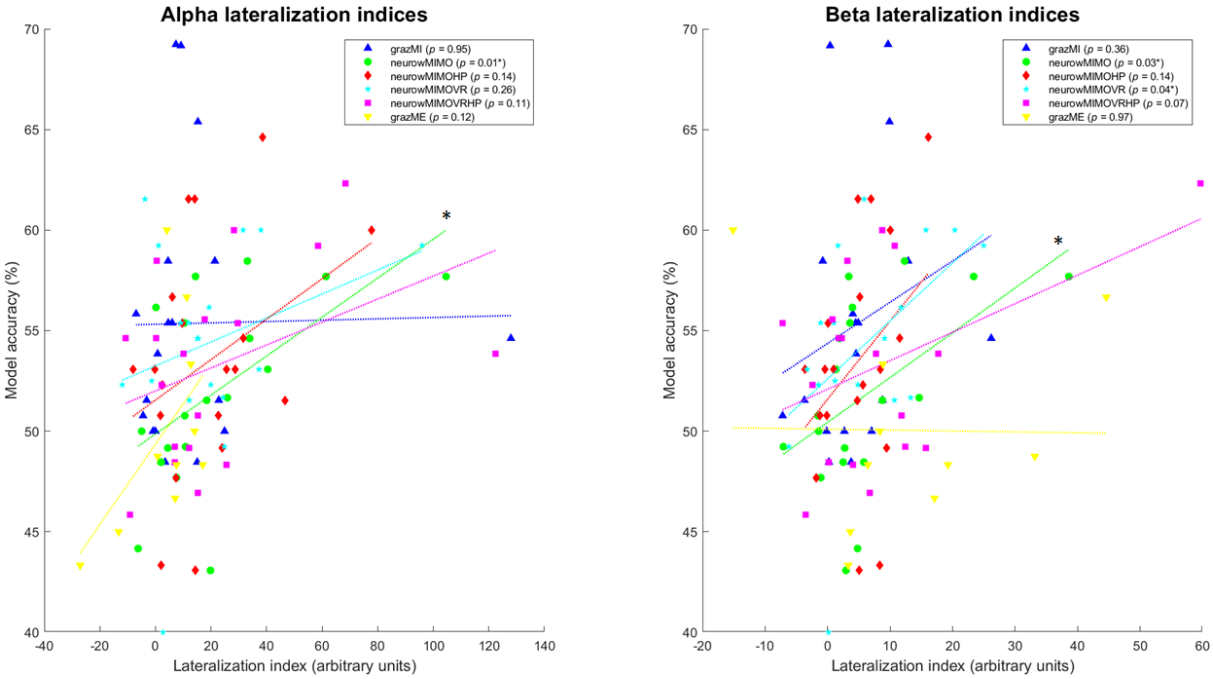

(d) *k*-nearest neighbors

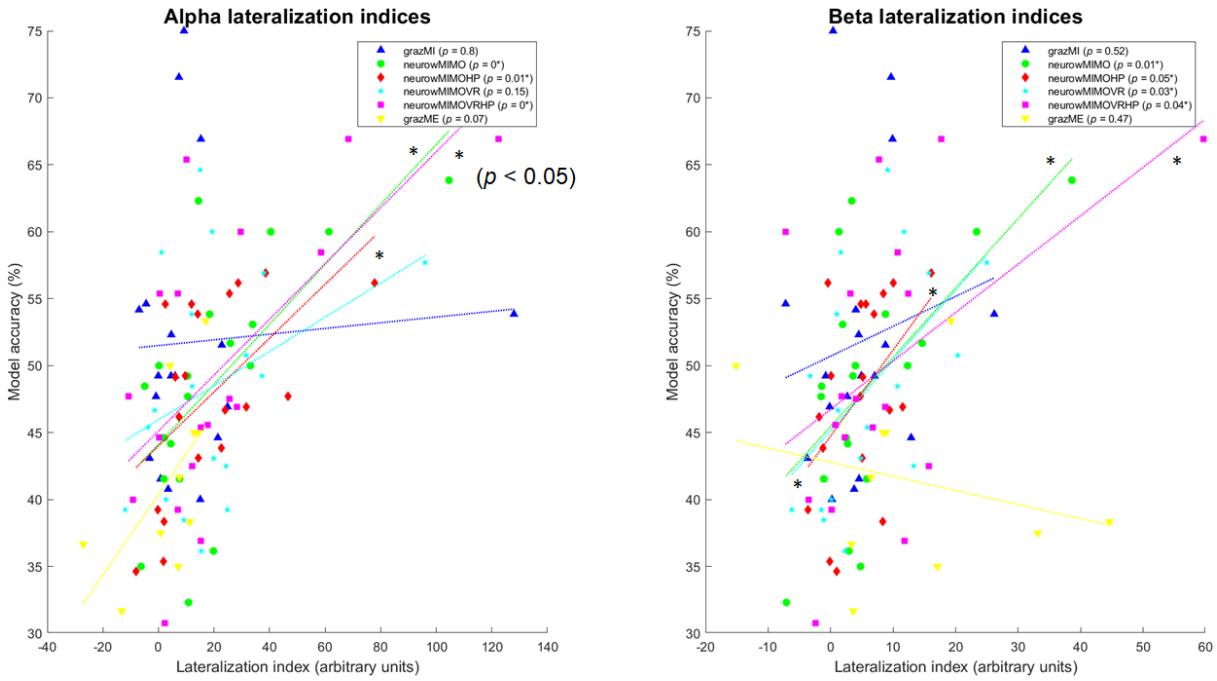

(e) Gaussian naive Bayes

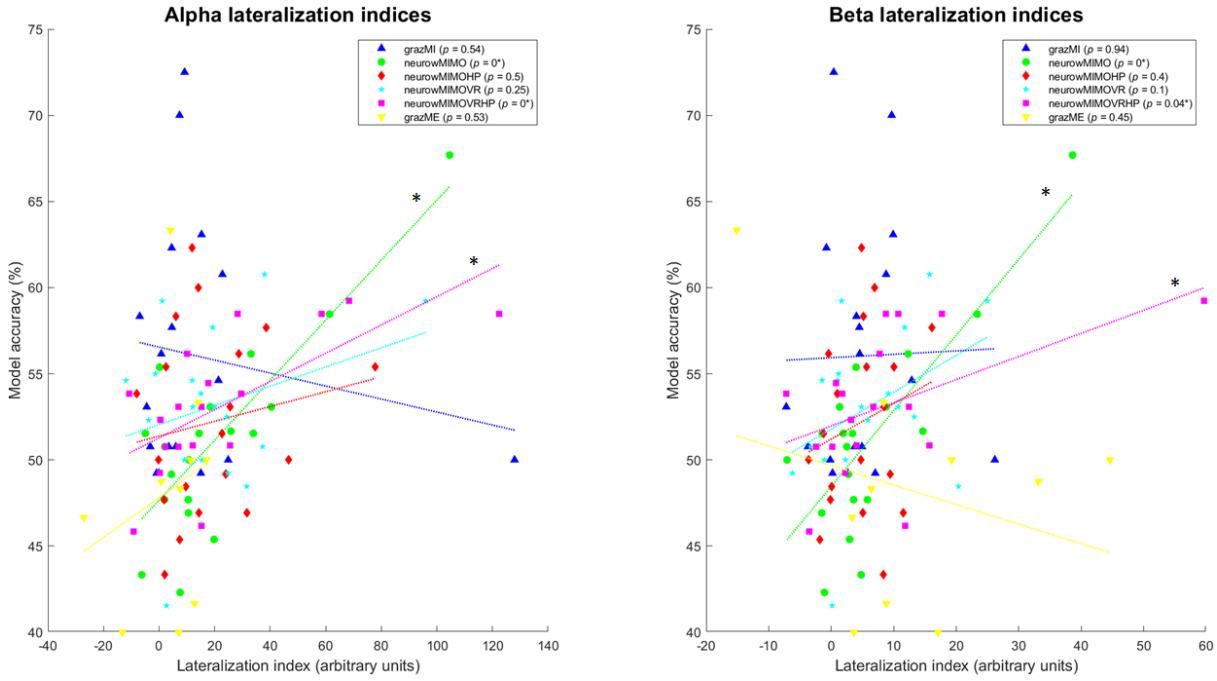

(f) Random forest

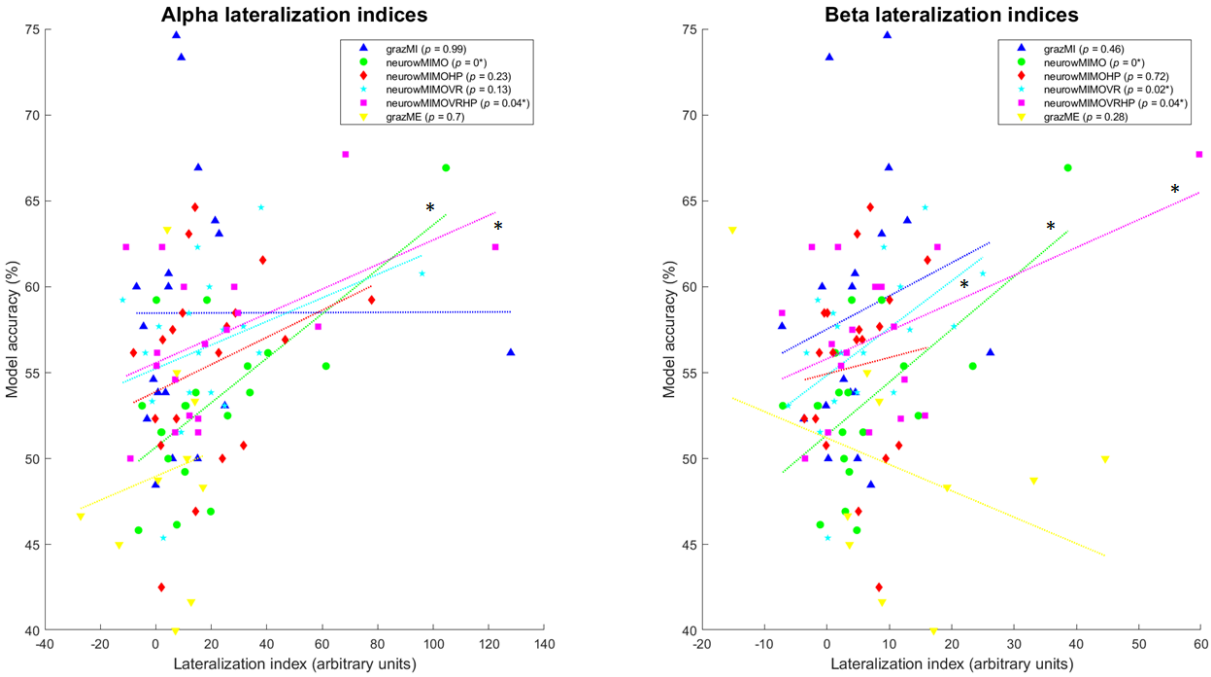

(g) AdaBoost

Figure 4.9: Scatter plots of the machine-learning models' accuracies and the LIs, where the asterisks indicate statistically significant correlations, for $p < 0.05$

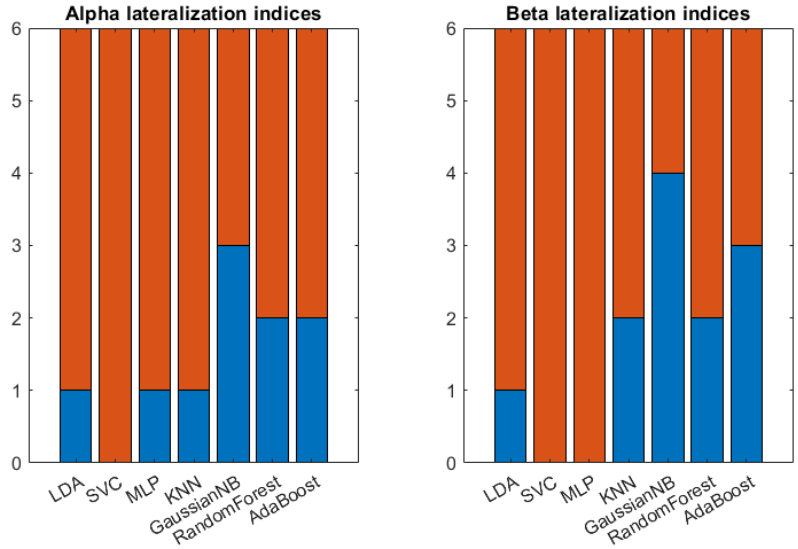

Figure 4.10: Number of statistically significant correlations ($p < 0.05$) in the scatter plots with the machine-learning accuracies and the LIs

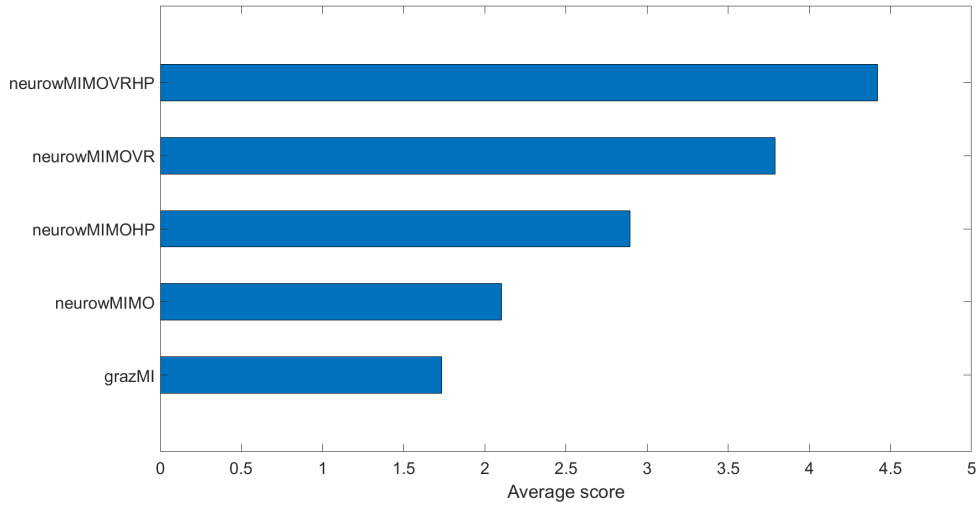

Figure 4.11: A chart of the conditions' ranking by their average scores

Current results show that there was a trend for *grazME* in which C3's alpha mERDs for left-hand trials and C4's alpha mERDs for both left- and right-hand trials had statistically significant negative correlations ($p < 0.05$) with all the VMIQ-2 items and sections (IVI, EVI, and KI), and embodiment scores. These trends can be observed in columns 157–159 (mean correlation coefficient, $\rho_m = -0.72$; mean p-value, $p_m = 0.004$), 163–165 ($\rho_m = -0.74$, $p_m = 0.002$), and 169–171 ($\rho_m = -0.75$, $p_m = 0.003$) of the heat map in Figure B.1.

The scatter plots with significant correlations between the embodiment scores and the LIs are shown in Figure B.2. There were some statistically significant linear correlations in *neurowMIMOVRHP* and *grazME* between some of the embodiment scores (appearance, ownership, response, multisensory, and the final score) and the LIs. In *neurowMIMOVRHP*, beta LI had a statistically significant negative correlation with ownership ($R^2 = 0.26$, $p = 0.04$). In *grazME*, on the other hand, the beta LIs had a statistically significant negative linear correlation between appearance ($R^2 = 0.42$, $p = 0.04$) and the final score ($R^2 = 0.43$, $p = 0.04$), the average of the other four embodiment scores.

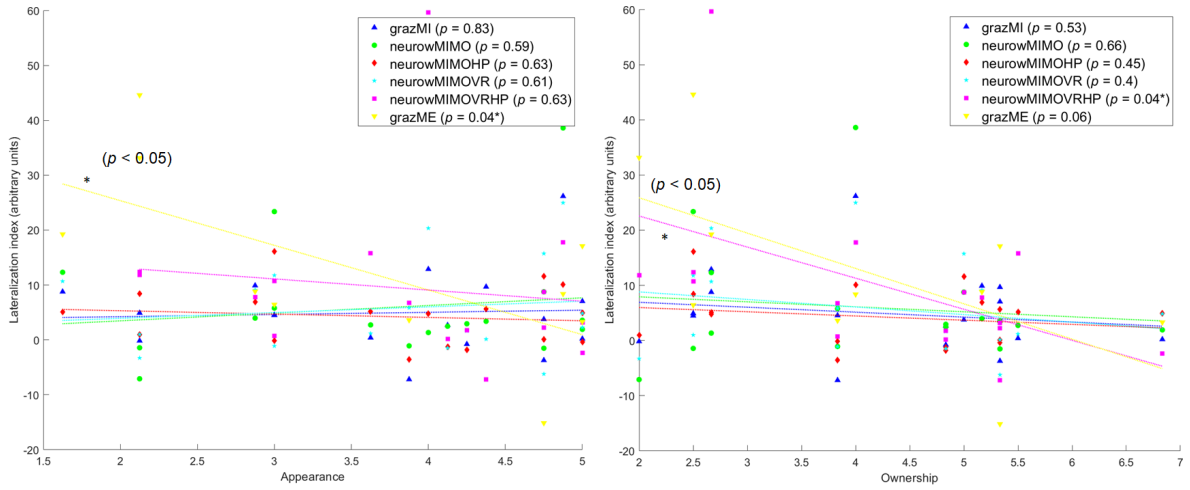

(a) Appearance vs. beta LIs

(b) Ownership vs. beta LIs

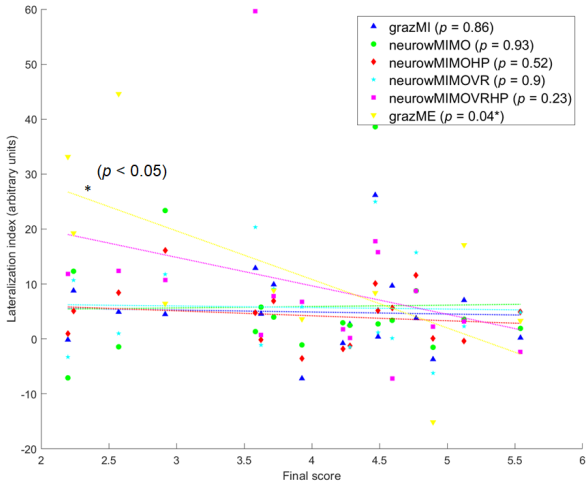

(c) Final score vs. beta LIs

Figure 4.12: Scatter plots with significant correlations ($p < 0.05$) between the LIs and the machine-learning accuracies

5

Discussion

Contents

There are two main questions posed in this thesis:

1. What are the BCI–VR configurations that maximize motor-related contralateral brain activation during motor imagery (i.e., ERD)?

2. What BCI–VR configurations, or conditions, provide the highest accuracies for the BCI, in any given condition? And, conversely, what machine-learning algorithms stand out in producing more accurate machine-learning models?

The data suggests that the conditions that use *NeuRow* with haptic feedback induce a stronger alpha ERD than the other motor-imagery conditions and that all of them produce a slightly, but not significantly, more contralateral desynchronization than the motor-execution condition, *grazME*.

The SVC and MLPs have the most accurate models compared to the other five algorithms. The motor-imagery conditions perform similarly, with *grazME* having the least accurate models for any of the algorithms. Additionally, the LIs—an important EEG metric for stroke rehabilitation—are not significantly correlated with the models' accuracies.

Last but not least, the relationship between the perceived embodiment or motor-imagery ability and the ERDs was analyzed, but the results are inconclusive.

5.1 What BCI–VR configurations lead to the strongest, most lateralized brain activation?

5.1.1 Strongest event-related desynchronizations

From all the motor-imagery conditions, the ones that use the VR environment (*neurowMIMO*, *neurowMIMOHP*, *neurowMIMOVR*, and *neurowMIMOVRHP*) led to significantly stronger alpha ERDs. That is, the left side of the sensorimotor cortex in right-hand trials and the right side in left-hand trials had stronger alpha desynchronizations after the subject began to perform motor imagery. However, the *NeuRow* conditions that use vibrotactile stimulation as haptic feedback (*neurowMIMOHP* and *neurowMIMOVRHP*) produced the strongest alpha ERDs, which are comparable with motor execution's equivalent (*grazME*). The abstract-feedback-only condition (*grazMI*) performed significantly worse than the *NeuRow* conditions, thus suggesting that *NeuRow* and haptic feedback, together or separately, lead to stronger alpha ERDs. Furthermore, there were no significant differences between *neurowMIMOHP* and *neurowMIMOVRHP*, which implies that, while having haptic feedback, the use of a VR headset does not lead to a significantly stronger desynchronization.

The alpha waves were much more reactive to the different configurations than the beta waves, as there were many more significant differences between the alpha ERDs than the beta counterparts.

Nevertheless, motor execution led to a slightly, though not significantly, stronger beta ERD than motor imagery. The ERD in beta waves has been observed shortly after performing both motor imagery or motor execution [46].

Every motor-imagery condition except *grazMI* was able to sustain, on average, their ERDs until the end of the trials. Not only is it important to invoke a strong desynchronization, but to also be able to sustain it, as the brain activation is consequently longer and the cortical reorganization more thorough. The ERDs in *neurowMIMOHP* and *neurowMIMOVRHP* could surpass *grazME*'s desynchronization toward the end of the trials, on average, which suggests that these conditions are competitive with motor execution at inducing a strong brain activation.

5.1.2 Most lateralized event-related desynchronizations

The LIs were not significantly different between each condition. However, they were significantly different from the null LI (LI = 0), except *grazME*'s alpha LIs. This is ideal in stroke rehabilitation, as the patient's brain activation should be similar to healthy subjects, who have a mostly contralateral alpha activation [81]. Although the motor-imagery conditions led to significantly contralateral brain activation, no significant differences were found between them. Thus, all the conditions may be capable of inducing similar lateralization. Nevertheless, there was a slight increase in the median LIs for the conditions that include a VR headset and haptic feedback, separately or together, which may become significantly different from the other two motor-imagery conditions, *grazMI* and *neurowMIMO*, if a larger sample is gathered.

The *grazME*'s alpha LIs were not significantly different from the null LI, as also hinted in the topographic plots, which is in accordance with upper-alpha and lower-beta ERDs being observed to become bilaterally symmetrical shortly before motor execution [46]. Nevertheless, *grazME*'s beta LIs were significantly contralateral, which were computed for both lower and upper beta bands.

5.1.2.A Spatial distribution of the event-related desynchronizations

Although ERDs occur in the sensorimotor cortex for motor imagery or execution, the desynchronization peaks in the motor-imagery conditions were detected in the region posterior to it, in the posterior parietal cortex. This can be explained by the possible misalignment of the electrodes with the cortex, as the bulk of the equipment was kept on the back of the subject's head throughout the whole session, which could last over an hour. Not only that, but the interpolation of the mERDs between the electrodes in the topographic plots could have erroneously implied such a shift, as electrodes C3 and C4 still had their mERDs within the peaks' contours.

That being said, *grazME*'s right-hand trials did show ERD peaks closer to electrodes C3 and C4, which may invalidate the reasons mentioned above. Given the different nature of the tasks, that of motor imagery and motor execution, the brain activation between the two does overlap in the sensorimotor

cortex, but the act of imagining movement has also been shown to activate broader regions of the brain [40].

Lastly, a stronger occipital alpha ERD was observed for the *NeuRow* conditions relative to motor execution, which could have originated from the visual feedback. As motor imagery is harder to perform than motor execution, especially considering that the subjects only had to perform finger tapping on the table, the desynchronization of alpha waves has been reported previously as occurring for complex tasks that demand higher attention [46].

5.2 What BCI–VR configurations and machine-learning algorithms lead to the most accurate models?

5.2.1 BCI–VR configurations

In all algorithms, *grazME* performed significantly worse than the motor-imagery conditions, which can be attributed to the fact that CSPs are not usually used for motor execution but prominently implemented in motor-imagery tasks [43]. There were some significant differences between the motor-imagery conditions for some of the algorithms, but these differences varied between them without a clear trend.

As such, the data does not suggest any conditions to perform consistently better for any of the algorithms. Nevertheless, abstract feedback coupled with vibrotactile stimulation has recently been reported to improve classification accuracy compared to abstract feedback only [74]. Moreover, FES, another type of haptic feedback, has also been used together with a VR headset with an improved classification percentage compared to using just the headset [71].

5.2.2 Machine-learning algorithms

Despite the LDA being commonly used in motor-imagery-based BCIs [82], it performed worse than the SVC and MLPs. The peculiar accuracy distribution of these two algorithms could require further analysis; for example, by looking at their hyperparameters. The use of nonlinear algorithms in BCIs is not commonly seen, as the LDA or SVC with a linear kernel are serviceable for online performance, despite attempts at implementing, for example, CNNs [49].

Although the accuracies were offline, most of them were close to chance level (i.e., 50% in a cue-based binary classifier that detects left- or right-hand movements). The analysis of the models' performances should also consider the fitting times, which is an important factor in online performance, but it was not analyzed in this study. Thus, the machine-learning aspect requires a more thorough investigation that involves online accuracies, fitting times, and possibly other metrics, as well as the analysis of the hyperparameters.

5.2.3 Correlations with lateralization indices

There were no significant correlations between the models' accuracies and the LIs. The CSPs used to train the models do not necessarily take into account the lateralization of the ERD, which leads to models not enforcing neurofeedback based on contralateral brain activation. The ERDs in the sensorimotor cortex are also not necessarily taken into account. Therefore, as the purpose of these BCIs is to aid patients in stroke rehabilitation, the CSPs, as is, may not be adequate features for machine-learning training. Alternatives include the relative alpha power detected before and after the cue in electrodes C3 and C4.

5.3 Relation between questionnaire answers and event-related desynchronizations

5.3.1 Condition preference

The subjects had a strong preference for *neurowMIMOVRHP*, followed by *neurowMIMOVR*. While both of these configurations make use of a VR headset to display *NeuRow*, haptic feedback induced the strongest ERDs. There were no significant desynchronization differences with or without haptic feedback while using a VR headset. However, the median alpha mERD in *neurowMIMOHP* was 89.34% of *grazME*'s, compared to *neurowMIMOVRHP*'s 61.34%, a difference of 28%. Despite the noticeable difference, the subjects preferred to use of a VR headset and had mixed opinions of *neurowMIMOHP*.

Most subjects did not have much experience using VR headsets, which induced a novelty factor observed in subjects who were enthusiastically experiencing the heightened immersion. Despite this and the strong preference for using a VR headset, *neurowMIMOVR*'s desynchronization was not significantly different from *neurowMIMO*'s.

5.3.2 Motor-imagery ability

Despite the VMIQ-2 being designed around motor imagery, the only noticeable trends were found for *grazME*. There were significant negative correlations between its alpha mERDs and the questionnaire's items, which suggests that greater motor-imagery ability correlates with stronger ERDs. Given that the task was that of motor execution, and that there no noticeable trends of correlations for the motor-imagery conditions, the results were inconclusive.

5.3.3 Embodiment

There were some significant correlations between *grazME*'s beta LIs and appearance and the final score, which, again, is a motor-execution task. Not only that but the correlations are negative, which

implies a weaker contralateral brain activation corresponds to a stronger overall embodiment. However, given that *grazME* did not make use of *NeuRow*, nor was it based on motor imagery, the results were inconclusive. There was, however, a significant negative correlation between *neurowMIMOVRHP*'s beta LI and ownership. But, given that beta waves were not as reactive as alpha waves in motor imagery, the correlation is also inconclusive. Furthermore, the negative correlation implies a worse sense of ownership of the avatar's body for more lateralized brain activation, which seems counterintuitive and, thus, requires a more thorough analysis.

The embodiment questionnaire did not distinguish the four *NeuRow* conditions, which could have helped find correlations between the EEG metrics and the embodiment scores. Particularly, the subjects reported the VR headset to improve their immersion in the virtual environment, which certainly would have influenced the embodiment scores for *neurowMIMOVR* and *neurowMIMOVRHP*.

5.4 Limitations

The most pronounced limitation of this study is that the BCIs were not closed loops; that is, the subjects do not control the avatar in *NeuRow*. Rather, the virtual environment assisted the subjects in performing motor imagery, by providing visual aid and vibrotactile stimulation. In stroke rehabilitation, the object of this study, using the more interactive closed-loop BCIs could prove to be more beneficial than displaying the avatar to the patient without any possible input from the patient. While *NeuRow* is capable of closing the loop, the experiment would have taken significantly longer to conduct with all of the conditions, due to the time needed to train the machine-learning models of the BCIs, as well as time constraints. Therefore, the study did not use closed-loop BCIs.

Another limitation of the study was the use of healthy subjects, given that the questions posed in this thesis pertain to stroke patients. Nevertheless, it would have been difficult to gather a meaningful number of stroke patients willing and capable of participating in the study, given the time constraints. Not only that, but the BCIs under study are mainly for stroke patients who have an inadequate motor ability for rehabilitation that requires arm movement, thus making the inclusion criteria even more selective. Therefore, the subjects were all healthy individuals, most of them in their 20s, who had not suffered a stroke before.

The small sample was also a limitation, which also fluctuated between the different conditions. While *neurowMIMO* and *neurowMIMOHP* had 19 runs, or subjects, *grazMI*, *neurowMIMOVR*, and *neurowMIMOVRHP* had 18 runs, and *grazME* only 10. As an immediate consequence, the conclusions obtained from the statistical tests were weaker; however, they could signal trends in the data that could be recognized and drawn conclusions from. Another consequence was the lack of demographic comparisons, which would have been too skewed to carry out.

The questionnaire correlations were also affected. The embodiment questionnaire was not answered by two of the pilot subjects, while the rest were answered by all of them. The correlation analysis was mostly affected by the number of runs in the conditions, as the comparison between the questionnaire scores and the mERDs and LIs could only be made for the subjects who not only had answered the questionnaires but also had runs for the targeted conditions.

Finally, the machine-learning analysis was not close to being exhaustive, due to time constraints, and only a select number of hyperparameters were tested. The analysis of the machine-learning algorithms and conditions that lead to the more robust and accurate models was, therefore, carried out in a broad, but not as deep, search. Not only that, but the accuracies analyzed were offline, as the BCIs did not let the subjects control the avatar in *NeuRow*.

5.5 Future research

Future studies should have a sample criterion that includes stroke patients with poor motor ability instead of healthy participants. They should also test different training features besides standard CSPs, so as to find alternatives that lead to not only accurate classifications in BCIs but also strong contralateral ERDs in the sensorimotor cortex.

Being a new field, the search for the best BCI–VR still requires studies of similar nature (i.e., that test different configurations), albeit with larger samples, the inclusion of stroke patients, and closed-loop BCIs. Haptic feedback, in particular, has seen limited use in research [10], despite the promising results obtained in this study.

Lastly, more studies should assess the sense of embodiment through a questionnaire, which is not normally employed in studies that make use of immersive VR technology. There were only a few singular statistically significant correlations between the EEG metrics, which were only the beta LI, and the embodiment scores in this study, but this could have been due to limitations such as the smaller-than-ideal sample. Particularly, this could also help answer the question of whether a VR headset is warranted in getting a stronger ERD for stroke rehabilitation, given its additional costs over a standard monitor.

6

Conclusion

This thesis aimed to find the BCI–VR configuration, or condition, that leads to the strongest, most lateralized brain activation, as well as the BCI–VR configurations and machine-learning algorithms that lead to the most accurate models of the BCIs.

Based on the acquisition of EEG signals and an analysis of the alpha and beta ERDs and LIs, the use of a virtual environment, *NeuRow*, and haptic feedback—implemented as vibrotactile stimulation in this study—led to significantly stronger contralateral ERDs, which were comparable to motor execution. Furthermore, the VR headset did not lead to such results by itself, being comparable to just using a monitor without haptic feedback. All motor-imagery conditions invoked similarly contralateral desynchronizations.

The SVC and MLPs had the most accurate models by a significant margin, but were not influenced by the conditions like the other algorithms such as the LDA and AdaBoost. Moreover, none of the conditions stood out in having more accurate models. Interestingly, however, was the weak correlations of the LIs and the median accuracies across conditions, which, by proxy, relate to the features used to train the models, the CSPs. Given the purpose of the BCI–VR systems, the features should be intimately connected with the brain activation, since the neurofeedback offered to the stroke patients should not only lead to accurate models but also strong contralateral ERDs.

Additionally, the questionnaires, despite arguably not showing interesting results besides the condition preference, were important to bridge the gap between the subjectivity of the subjects' perceived immersion and motor-imagery ability, as well as their preference for certain configurations, and the objectivity of the EEG analysis concerning their brain activation.

There was an attempt in figuring out the configurations and algorithms that led to the strongest brain activation and most accurate models, respectively, but there were several limitations. The absence of stroke patients; the open-loop BCI, as opposed to a closed-loop one; a small sample size; and, by any means, a non-exhaustive machine-learning analysis were some of them. Nevertheless, the promising results pertaining to haptic feedback contributed toward understanding this new field of research better, that of the BCI–VR systems for stroke rehabilitation, which hope to offer a good therapy option to patients who cannot take part in conventional or virtual rehabilitation.

Bibliography

[1] GBD 2019 Diseases and Injuries Collaborators, “Global burden of 369 diseases and injuries in 204 countries and territories, 1990–2019: a systematic analysis for the global burden of disease study 2019,” *The Lancet*, vol. 396, pp. 1204–1222, October 2020.

[2] K. K. Ang and C. Guan, “Brain–computer interface in stroke rehabilitation,” *Journal of Computing Science and Engineering*, vol. 7, pp. 139–146, June 2013.

[3] A. Aminov, J. M. Rogers, S. Middleton, K. Caeyenberghs, and P. H. Wilson, “What do randomized controlled trials say about virtual rehabilitation in stroke? A systematic literature review and meta-analysis of upper-limb and cognitive outcomes,” *Journal of NeuroEngineering and Rehabilitation*, vol. 15, March 2018.

[4] J. R. Wolpaw, N. Birbaumer, D. J. McFarland, G. Pfurtscheller, and T. M. Vaughan, “Brain–computer interfaces for communication and control,” *Clinical Neurophysiology*, vol. 113, pp. 767–791, June 2002.

[5] M. L. Martini, E. K. Oermann, N. L. Opie, F. Panov, T. Oxley, and K. Yaeger, “Sensor modalities for brain–computer interface technology: A comprehensive literature review,” *Neurosurgery*, vol. 86, pp. 108–117, February 2020.

[6] F. Pichiorri, G. Morone, M. Petti, J. Toppi, I. Pisotta, M. Molinari, S. Paolucci, M. Inghilleri, L. Astolfi, F. Cincotti, and D. Mattia, “Brain–computer interface boosts motor imagery practice during stroke recovery,” *Annals of Neurology*, vol. 77, pp. 851–865, 2015.

[7] J. J. Daly and J. R. Wolpaw, “Brain–computer interfaces in neurological rehabilitation,” *The Lancet Neurology*, vol. 7, pp. 1032–1043, 2008.

[8] M. Ortiz, E. Iáñez, J. L. Contreras-Vidal, and J. M. Azorín, “Analysis of the EEG rhythms based on the empirical mode decomposition during motor imagery when using a lower-limb exoskeleton: A case study,” *Frontiers in Neurorobotics*, vol. 14, pp. 1–13, August 2020.

[9] A. Vourvopoulos, C. Jorge, R. Abreu, P. Figueiredo, J.-C. Fernandes, and S. B. i Badia, “Efficacy and brain imaging correlates of an immersive motor imagery BCI-driven VR system for upper limb motor rehabilitation: A clinical case report,” *Frontiers in Human Neuroscience*, vol. 13, July 2019.

[10] M. Fleury, G. Lioi, C. Barillot, and A. Lécuyer, “A survey on the use of haptic feedback for brain–computer interfaces and neurofeedback,” *Frontiers in Neuroscience*, vol. 14, June 2020.

[11] G. Pfurtscheller, C. Neuper, G. R. Muller, B. Obermaier, G. Krausz, A. Schlögl, R. Scherer, B. Graimann, C. Keinrath, D. Skliris, M. Wortz, G. Supp, and C. Schrank, “Graz-BCI: state of the art and clinical applications,” *IEEE Transactions on Neural Systems and Rehabilitation Engineering*, vol. 11, pp. 177–180, 2003.

[12] A. Vourvopoulos, A. Ferreira, and S. B. i Badia, “NeuRow: An immersive VR environment for motor-imagery training with the use of brain–computer interfaces and vibrotactile feedback,” in *Proceedings of the 3rd International Conference on Physiological Computing Systems*, Lisbon, Portugal, July 2016, pp. 43–53.

[13] G. Pfurtscheller and F. H. L. da Silva, in *Niedermeyer’s Electroencephalography: Basic Principles, Clinical Applications, and Related Fields*, 6th ed.

[14] J. Ferro. A cerebrovascular accident: what should you do? [Online]. Available: https://www.hospitaldaluz.pt/en/health-dictionary/a-cerebrovascular-accident-what-should-you-do- (accessed Dec. 22, 2021).

[15] Stroke. [Online]. Available: https://www.nhlbi.nih.gov/health-topics/stroke (accessed Dec. 22, 2021).

[16] *Global Stroke Fact Sheet 2022*, World Stroke Organization.

[17] S. Li, “Spasticity, motor recovery, and neural plasticity after stroke,” *Frontiers in Neurology*, vol. 8, 2017.

[18] S. C. Cramer, G. Nelles, R. R. Benson, J. D. Kaplan, R. A. Parker, K. K. Kwong, D. N. Kennedy, S. P. Finklestein, and B. R. Rosen, “A functional MRI study of subjects recovered from hemiparetic stroke,” *Stroke*, vol. 28, pp. 2518–2527, December 1997.

[19] H. A. Wafa, C. D. A. Wolfe, E. Emmett, G. A. Roth, C. O. Johnson, and Y. Wang, “Burden of stroke in Europe: Thirty-year projections of incidence, prevalence, deaths, and disability-adjusted life years,” *Stroke*, vol. 51, pp. 2418–2427, August 2020.

[20] King’s College London, “The burden of stroke in Europe,” Stroke Alliance for Europe, Tech. Rep., 2017.

[21] S. C. Johnston, S. Mendis, and C. D. Mathers, “Global variation in stroke burden and mortality: estimates from monitoring, surveillance, and modelling,” *The Lancet Neurology*, vol. 8, pp. 345–354, February 2009.

[22] M. Hallett, “Plasticity of the human motor cortex and recovery from stroke,” *Brain Research Reviews*, vol. 36, pp. 169–174, October 2001.

[23] P. Thirumala, D. B. Hier, and P. Patel, “Motor recovery after stroke: Lessons from functional brain imaging,” *Neurological Research*, vol. 24, pp. 453–458, July 2002.

[24] J. Young and A. Forster, “Review of stroke rehabilitation,” *BMJ*, vol. 334, pp. 86–90, January 2007.

[25] Stroke rehabilitation: What to expect as you recover. [Online]. Available: https://www.mayoclinic.org/diseases-conditions/stroke/in-depth/stroke-rehabilitation/art-20045172 (accessed Dec. 22, 2021).

[26] V. Mathiowetz, “Task-oriented approach to stroke rehabilitation,” in *Stroke Rehabilitation: A Function-Based Approach*. Elsevier, 2016, ch. 3, pp. 59–78.

[27] C. Grefkes and G. R. Fink, “Recovery from stroke: current concepts and future perspectives,” *Neurological Research and Practice*, vol. 2, pp. 1–10, June 2020.

[28] H. S. Jørgensen, H. Nakayama, H. O. Raaschou, J. Vive-Larsen, M. Støier, and T. S. Olsen, “Outcome and time course of recovery in stroke. Part II: Time course of recovery. the Copenhagen stroke study,” *Archives of Physical Medicine and Rehabilitation*, vol. 76, pp. 406–412, May 1995.

[29] S. E. Fasoli, H. I. Krebs, and N. Hogan, “Robotic technology and stroke rehabilitation: Translating research into practice,” *Topics in Stroke Rehabilitation*, vol. 11, pp. 11–19, September 2015.

[30] S. Yang, R. Li, H. Li, K. Xu, Y. Shi, Q. Wang, T. Yang, and X. Sun, “Exploring the use of brain–computer interfaces in stroke neurorehabilitation,” *BioMed Research International*, vol. 2021, June 2021.

[31] How do rehab facilities make life easier for stroke survivors? [Online]. Available: https://www.holidayretirement.com/how-do-rehab-facilities-make-life-easier-for-stroke-survivors/ (accessed Jan. 27, 2022).

[32] Stroke recovery. [Online]. Available: https://generationsneighbors.com/rehabilitation/stroke-recovery/ (accessed Jan. 27, 2022).

[33] J. N. Mak and J. R. Wolpaw, “Clinical applications of brain–computer interfaces: Current state and future prospects,” *IEEE Reviews in Biomedical Engineering*, vol. 2, pp. 187–199, December 2009.

[34] S. Silvoni, A. Ramos-Murguialday, M. Cavinato, C. Volpato, G. Cisotto, A. Turolla, F. Piccione, and N. Birbaumer, "Brain–computer interface in stroke: A review of progress," *Clinical EEG and Neuroscience*, vol. 42, pp. 245–252, 2011.

[35] A. Vourvopoulos, E. Niforatos, S. B. i Badia, and F. Liarokapis, "Brain–computer interfacing with interactive systems—Case study 2," in *Intelligent Computing for Interactive System Design: Statistics, Digital Signal Processing, and Machine Learning in Practice*. Association for Computing Machinery, February 2021, ch. 6, pp. 237–272.

[36] P. L. Nunez, R. Srinivasan, A. F. Westdorp, R. S. Wijesinghe, D. M. Tucker, R. B. Silberstein, and P. J. Cadusch, "EEG coherency I: statistics, reference electrode, volume conduction, Laplacians, cortical imaging, and interpretation at multiple scales," *Electroencephalography and Clinical Neurophysiology*, vol. 103, pp. 499–515, November 1997.

[37] M. Jeannerod, "Mental imagery in the motor context," *Neuropsychologia*, vol. 33, pp. 1419–1432, November 1995.

[38] Tomaton124. 21 electrodes of international 10-20 system for EEG. [Online]. Available: https://pt.wikipedia.org/wiki/Ficheiro:21_electrodes_of_International_10-20_system_for_EEG.svg (accessed Feb. 17, 2022).

[39] Pancrat. Human motor cortex. [Online]. Available: https://commons.wikimedia.org/wiki/File:Human_motor_cortex.jpg (accessed Oct. 21, 2022).

[40] K. J. Miller, G. Schalk, E. E. Fetz, M. den Nijs, J. G. Ojemann, and R. P. N. Rao, "Cortical activity during motor execution, motor imagery, and imagery-based online feedback," *Proceedings of the National Academy of Sciences of the United States of America*, vol. 9, pp. 4430–4435, March 2009.

[41] C. S. Nam, A. Nijholt, and F. Lotte, "Brain–computer interface: An emerging interaction technology," in *Brain–Computer Interfaces Handbook: Technological and Theoretical Advances*. CRC Press, August 2019, p. 27.

[42] G. Pfurtscheller, C. Neuper, A. Schlögl, and K. Lugger, "Separability of EEG signals recorded during right and left motor imagery using adaptive autoregressive parameters," *IEEE Transactions on Rehabilitation Engineering*, vol. 6, pp. 316–325, 1998.

[43] C. S. Nam, A. Nijholt, and F. Lotte, "Introduction: Evolution of brain–computer interfaces," in *Brain–Computer Interfaces Handbook: Technological and Theoretical Advances*. CRC Press, August 2019, p. 3.

[44] H. Cho, M. Ahn, K. Kim, and S. C. Jun, “Increasing session-to-session transfer in a brain–computer interface with on-site background noise acquisition,” *Journal of Neural Engineering*, vol. 12, October 2015.

[45] N. E. Crone, D. L. Miglioretti, B. Gordon, J. M. Sieracki, M. T. Wilson, S. Uematsu, and R. P. Lesser, “Functional mapping of human sensorimotor cortex with electrocorticographic spectral analysis. i. alpha and beta event-related desynchronization,” *Brain*, vol. 121, pp. 2271–2299, December 1997.

[46] G. Pfurtscheller and F. H. L. da Silva, “Event-related EEG/MEG synchronization and desynchronization: basic principles,” *Clinical Neurophysiology*, vol. 110, pp. 1842–1857, 1999.

[47] G. Pfurtscheller, “Event-related synchronization (ERS): an electrophysiological correlate of cortical areas at rest,” *Electroencephalography and Clinical Neurophysiology*, vol. 83, pp. 62–69, 1992.

[48] H. Cho, M. Ahn, S. Ahn, M. Kwon, and S. C. Jun, “EEG datasets for motor imagery brain–computer interface,” *GigaScience*, vol. 6, July 2017.

[49] T. Karácsony, J. P. Hansen, H. K. Iversen, and S. Puthusserypady, “Brain computer interface for neurorehabilitation with deep learning classification and virtual reality feedback,” in *ACM International Conference Proceeding Series*, Reims, France, March 2019.

[50] M. A. Khan, R. Das, H. K. Iversen, and S. Puthusserypady, “Review on motor imagery based BCI systems for upper limb post-stroke neurorehabilitation: From designing to application,” *Computers in Biology and Medicine*, vol. 123, pp. 1–17, June 2020.

[51] M. da Silva Cameirão, S. B. i Badia, E. Duarte, and P. F. M. J. Verschure, “Virtual reality based rehabilitation speeds up functional recovery of the upper extremities after stroke: a randomized controlled pilot study in the acute phase of stroke using the Rehabilitation Gaming System,” *Restorative Neurology and Neuroscience*, vol. 29, 2011.

[52] S. B. i Badia, G. G. Fluet, R. Llorens, and J. E. Deutsch, “Virtual reality for sensorimotor rehabilitation post stroke: Design principles and evidence,” in *Rehabilitation Applications Using Virtual Reality for Persons with Residual Impairments Following Stroke*. Springer, June 2014, ch. 28, pp. 119–144.

[53] M. Erhardsson, M. A. Murphy, and K. S. Sunnerhagen, “Commercial head-mounted display virtual reality for upper extremity rehabilitation in chronic stroke: a single-case design study,” *Journal of NeuroEngineering and Rehabilitation*, vol. 17, 2020.

[54] M. Park, M. Ko, S. Oh, J. Lee, Y. Ham, H. Yi, Y. Choi, D. Ha, and J. Shin, “Effects of virtual reality-based planar motion exercises on upper extremity function, range of motion, and health-related quality of life: a multicenter, single-blinded, randomized, controlled pilot study,” *Journal of NeuroEngineering and Rehabilitation*, vol. 16, 2019.

[55] M. F. Levin, O. Snit, D. G. Liebermann, H. Weingarden, and P. L. Weiss, “Virtual reality versus conventional treatment of reaching ability in chronic stroke: clinical feasibility study,” *Neurology and Therapy*, vol. 1, pp. 1–15, December 2012.

[56] J. Shin, M. Kim, J. Lee, Y. Jeon, S. Kim, B. Seo, and Y. Choi, “Effects of virtual reality-based rehabilitation on distal upper extremity function and health-related quality of life: a single-blinded, randomized controlled trial,” *Journal of NeuroEngineering and Rehabilitation*, vol. 13, 2016.

[57] J. M. Rogers, J. Duckworth, S. Middleton, B. Steenbergen, and P. H. Wilson, “*Elements* virtual rehabilitation improves motor, cognitive, and functional outcomes in adult stroke: evidence from a randomized controlled pilot study,” *Journal of NeuroEngineering and Rehabilitation*, vol. 16, 2019.

[58] P. L. Jackson, M. F. Lafleur, F. Malouin, C. Richards, and J. Doyon, “Potential role of mental practice using motor imagery in neurologic rehabilitation,” *Clinical Implications of Basic Research*, vol. 82, pp. 1133–1141, August 2001.

[59] G. Pfurtscheller, R. Scherer, R. Leeb, C. Keinrath, C. Neuper, F. Lee, and H. Bischof, “Viewing moving objects in virtual reality can change the dynamics of sensorimotor EEG rhythms,” *Presence*, vol. 16, pp. 111–118, February 2007.

[60] S. B. i Badia, A. G. Morgade, H. Samaha, and P. F. M. J. Verschure, “Using a hybrid brain computer interface and virtual reality system to monitor and promote cortical reorganization through motor activity and motor imagery training,” *IEEE Transactions on Neural Systems and Rehabilitation Engineering*, vol. 21, pp. 174–181, November 2012.

[61] M. S. Cameirão, S. B. i Badia, E. D. Oller, and P. F. M. J. Verschure, “Neurorehabilitation using the virtual reality based Rehabilitation Gaming System: methodology, design, psychometrics, usability and validation,” *Journal of NeuroEngineering and Rehabilitation*, vol. 7, September 2010.

[62] D. Achanccaray, K. Acuña, E. Carranza, and J. Andreu-Perez, “A virtual reality and brain computer interface system for upper limb rehabilitation of post stroke patients,” in *IEEE International Conference on Fuzzy Systems*, Naples, Italy, July 2017.

[63] W. Cho, A. Heilinger, R. Ortner, N. Murovec, R. Xu, J. Swift, M. Zehetner, S. Schobesberger, G. Edlinger, and C. Guger, “Motor rehabilitation for hemiparetic stroke patients using a brain–computer interface method,” in *Proceedings of 2018 IEEE International Conference on Systems, Man, and Cybernetics*, Miyazaki, Japan, October 2018.

[64] M. Sebastián-Romagosa, R. Ortner, E. Udina-Bonet, J. Dinarès-Ferran, K. Mayr, F. Cao, and C. Guger, “Laterality coefficient: An EEG parameter related with the functional improvement in

stroke patients," in *Proceedings of the 2019 IEEE EMBS International Conference on Information Technology Applications on Biomedicine*, Chicago, IL, USA, May 2017.

[65] Y. Miao, S. Chen, X. Zhang, J. Jin, R. Xu, I. Daly, J. Jia, X. Wang, A. Cichocki, and T.-P. Jung, "BCI-based rehabilitation on the stroke in sequela stage," *Neural Plasticity*, vol. 2020, December 2020.

[66] A. E. Voinas, R. Das, M. A. Khan, I. Brunner, and S. Puthusserypady, "Motor imagery EEG signal classification for stroke survivors rehabilitation," in *Proceedings of the 10th International Winter Conference on Brain–Computer Interface (BCI)*, Gangwon-do, Republic of Korea, February 2022.

[67] J. M. Juliano, R. P. Spicer, A. Vourvopoulos, S. Lefebvre, K. Jann, T. Ard, E. Santarnecchi, D. M. Krum, and S.-L. Liew, "Embodiment is related to better performance on a brain–computer interface in immersive virtual reality: A pilot study," *Sensors*, vol. 20, February 2020.

[68] R. G. Lupu, D. C. Irimia, F. Ungureanu, M. S. Poboroniuc, and A. Moldoveanu, "BCI and FES based therapy for stroke rehabilitation using VR facilities," *Wireless Communications and Mobile Computing*, vol. 2018, April 2018.

[69] TRAVEE: Visual therapist with augmented feedback for neuromotor rehabilitation. [Online]. Available: https://travee.upb.ro/ (accessed Mar. 19, 2022).

[70] A. Vourvopoulos, O. M. Pardo, S. Lefebvre, M. Neureither, D. Saldana, E. Jahng, and S.-L. Liew, "Effects of a brain–computer interface with virtual reality (VR) neurofeedback: A pilot study in chronic stroke patients," *Frontiers in Human Neuroscience*, vol. 13, June 2019.

[71] D. Achanccaray, S.-I. Izumi, and M. Hayashibe, "Visual-electrotactile stimulation feedback to improve immersive brain–computer interface based on hand motor imagery," *Computational Intelligence and Neuroscience*, vol. 2021, February 2021.

[72] M. Sebastián-Romagosa, W. Cho, R. Ortner, N. Murovec, T. V. Oertzen, K. Kamada, B. Z. Allison, and C. Guger, "Brain computer interface treatment for motor rehabilitation of upper extremity of stroke patients—A feasibility study," *Frontiers in Neuroscience*, vol. 14, October 2020.

[73] X. Shu, S. Chen, J. Meng, L. Yao, X. Sheng, J. Jia, D. Farina, and X. Zhu, *IEEE Transactions on Biomedical Engineering*, pp. 1987–1995.

[74] Y. Zhong, L. Yao, J. Wang, and Y. Wang, "Tactile sensation assisted motor imagery training for enhanced BCI performance: A randomized controlled study," *IEEE Transactions on Biomedical Engineering*, pp. 1–9, August 2022.

[75] A. Vourvopoulos, S. Legeay, and P. Figueiredo, “NeuXus: A biosignal processing and classification pipeline for real-time brain–computer interaction,” 2020.

[76] R. C. Oldfield, “The assessment and analysis of handedness: The Edinburgh inventory,” *Neuropsychologia*, vol. 9, pp. 97–113, March 1971.

[77] R. Roberts, N. Callow, L. Hardy, D. Markland, and J. Bringer, “Movement imagery ability: Development and assessment of a revised version of the vividness of movement imagery questionnaire,” *Journal of Sport & Exercise Psychology*, vol. 30, pp. 200–221, 2008.

[78] T. C. Peck and M. Gonzalez-Franco, “Avatar embodiment. A standardized questionnaire,” *Frontiers in Virtual Reality*, vol. 1, February 2021.

[79] J. Rapela. [Eeglablist] A question on ERS / ERD. [Online]. Available: https://sccn.ucsd.edu/pipermail/eeglablist/2012/004755.html (accessed Jul. 15, 2022).

[80] D. S. Batista. Hyperparameter optimization across multiple models in scikit-learn. [Online]. Available: https://www.davidsbatista.net/blog/2018/02/23/model_optimization/ (accessed Jun. 12, 2022).

[81] J. E. Downey, K. M. Quick, N. Schwed, J. M. Weiss, G. F. Wittenberg, M. L. Boninger, and J. L. Collinger, “The motor cortex has independent representations for ipsilateral and contralateral arm movements but correlated representations for grasping,” *Cerebral Cortex*, vol. 30, pp. 5040–5409, October 2020.

[82] C. S. Nam, A. Nijholt, and F. Lotte, “A step-by-step tutorial for a motor imagery-based BCI,” in *Brain–Computer Interfaces Handbook: Technological and Theoretical Advances*. CRC Press, August 2019, p. 454.

A

Questionnaires

The four questionnaires answered by the subjects are found in this appendix, together with the responses to all questionnaires except the condition-preference one, which is shown in the Results chapter.

A.1 Edinburgh Handedness Inventory

Please indicate your preferences in the use of hands in the following activities by checking off in the appropriate column. When the preference is so strong that you would never try to use the other hand unless absolutely forced to, put a check mark on columns with "++"; otherwise, put it on columns with "+." If in any case you are really indifferent, put the check mark on both columns with "+." Some of the activities require both hands. In these cases, the part of the task, or object, for which hand preference is wanted is indicated in brackets. Please try to answer all the questions, and only leave a blank if you have no experience at all with the object or task.

Task	**Left ++**	**Left +**	**Right +**	**Right ++**
1. Writing				
2. Drawing				
3. Throwing				
4. Scissors				
5. Toothbrush				
6. Knife (without a fork)				
7. Spoon				
8. Broom (upper hand)				
9. Striking a match (match)				
10. Opening a box (lid)				
i. Which foot do you prefer to kick with?				
ii. Which eye do you use when using only one?				

Responses

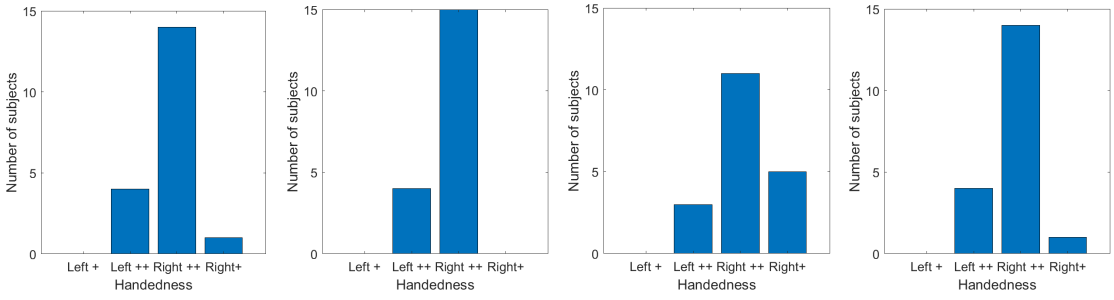

(a) Writing **(b)** Drawing **(c)** Throwing **(d)** Scissors

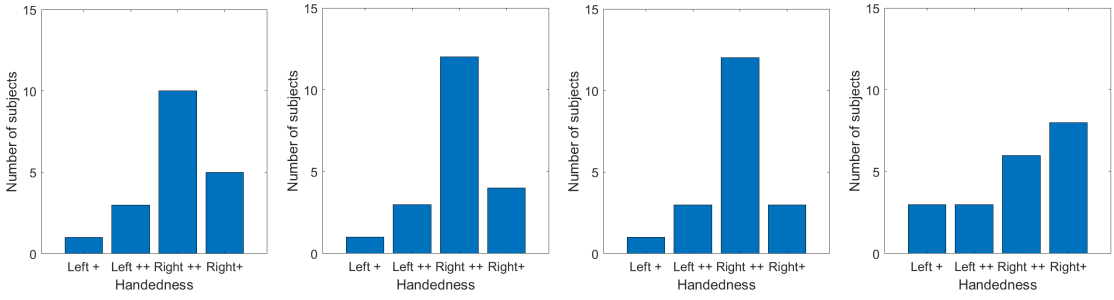

(e) Toothbrush **(f)** Knife (without a fork) **(g)** Spoon **(h)** Broom (upper hand)

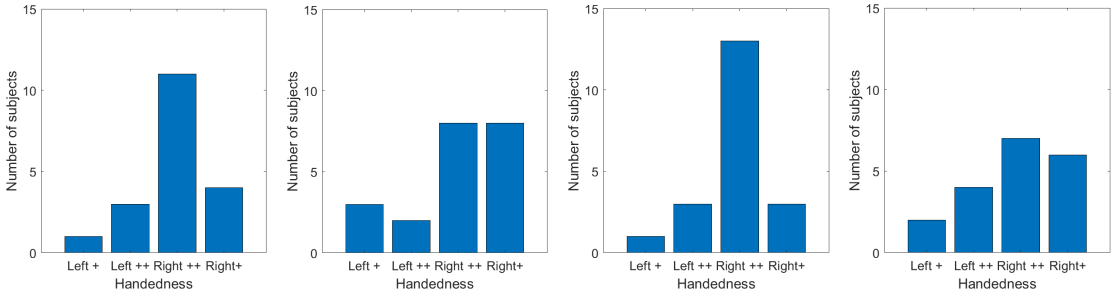

(i) Striking a match (match) **(j)** Opening a box (lid) **(k)** Which foot do you prefer to kick with? **(l)** Which eye do you use when using only one?

Figure A.1: Bar charts of the answers to the Edinburgh Handedness Inventory

A.2 Vividness of Movement Imagery Questionnaire-2 (VMIQ-2)

Movement imagery refers to the ability to imagine a movement. The aim of this questionnaire is to determine the vividness of your movement imagery. The items of the questionnaire are designed to bring certain images to our mind. You are asked to rate the vividness of each item by reference to the 5-point scale. After each item, circle the appropriate number in the boxes provided. The first column is for an image obtained watching yourself performing the movement from an external point of view (external visual imagery), and the second column is for an image obtained from an internal point of view as if you were looking out through your own eyes while performing the movement (internal visual imagery). The third column is for an image obtained by feeling yourself do the movement (kinesthetic imagery). Try to do each item separately, independently of how you may have done other items. Complete all items from an external visual perspective, and then return to the beginning of the questionnaire and complete all of the items from an internal visual perspective, and finally return to the beginning of the questionnaire and complete the items while feeling the movement. The three ratings for a given item may not in all cases be the same. For all items, please have your eyes closed.

Rating scale

Think of each of the following acts that appear on the next page, and classify the images according to the degree of clearness and vividness as shown on the rating scale. The image aroused by each item might be:

Rating	Description
1	Perfectly clear and as vivid as normal vision or feel of movement
2	Clear and reasonably vivid
3	Moderately clear and vivid
4	Vague and dim
5	No image at all; you only “know” that you are thinking of the skill

External visual imagery (EVI), internal visual imagery (IVI), or kinesthetic imagery (KI)

(The following items appear thrice: once for external visual imagery, which is imagining oneself watching their body perform the movement from an outside perspective; once for internal visual imagery, which is imagining performing the movement while observing it through one's own eyes; and another for kinesthetic imagery, which is imagining the feeling of performing the movement.)

Skill	**1**	**2**	**3**	**4**	**5**
1. Walking					
2. Running					
3. Kicking a stone					
4. Bending to pick up a coin					
5. Running up the stairs					
6. Jumping sideways					
7. Throwing a stone into the water					
8. Kicking a ball in the air					
9. Running downhill					
10. Riding a bike					
11. Swinging on a rope					
12. Jumping off a high wall					

Responses

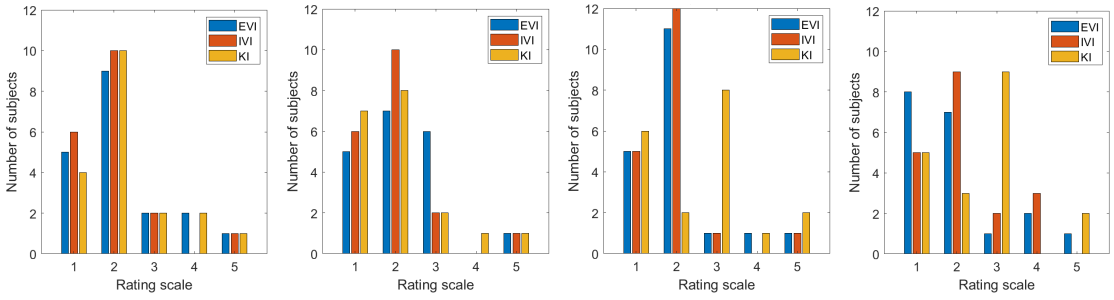

(a) Walking **(b)** Running **(c)** Kicking a stone **(d)** Bending to pick up a coin

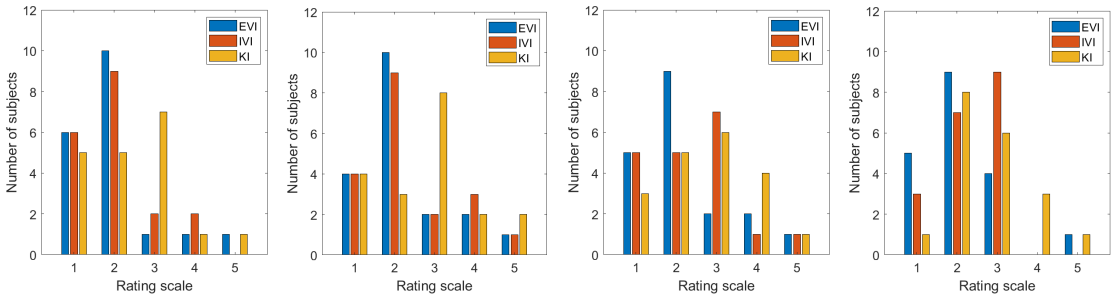

(e) Running up the stairs **(f)** Jumping sideways **(g)** Throwing a stone into the water **(h)** Kicking a ball in the air

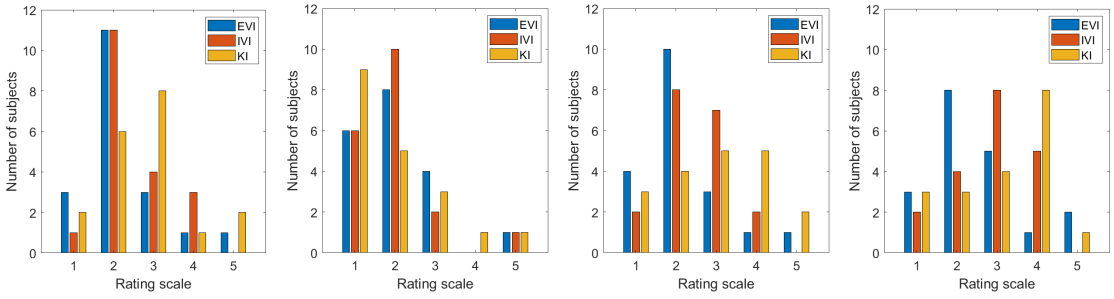

(i) Running downhill **(j)** Riding a bike **(k)** Swinging on a rope **(l)** Jumping off a high wall

Figure A.2: Bar charts of the answers to the VMIQ-2

A.3 Condition-preference questionnaire

Please indicate your training preference based on the setup that helped you perform good and vivid motor imagery.

Condition	**1 (best)**	**2**	**3**	**4**	**5 (worst)**
Graz					
NeuRow PC screen					
NeuRow PC screen + Haptics					
NeuRow VR					
NeuRow VR + Haptics					

A.4 Embodiment questionnaire

Please select your level of agreement with the following statements:

Levels of agreement

Strongly disagree	**Disagree**	**Somewhat disagree**	**Neither agree nor disagree**	**Somewhat agree**	**Agree**	**Strongly agree**
−3	−2	−1	0	1	2	3

Embodiment questionnaire

Please select your level of agreement with the following statements, “During the experiment, there were moments in which . . . ”:

Statement	**−3**	**−2**	**−1**	**0**	**1**	**2**	**3**
Q1. I felt as if the virtual body I saw when I looked down was my body							
Q2. It felt as if the virtual body I saw was someone else							
Q3. It seemed as if I might have more than one body							
Q4. I felt as if the virtual body I saw when looking in the mirror was my own body							
Q5. I felt as if the virtual body I saw when looking at myself in the mirror was another person							
Q6. It felt like I could control the virtual body as if it was my own body							
Q7. The movements of the virtual body were caused by my movements							
Q8. I felt as if the movements of the virtual body were influencing my own movements							
Q9. I felt as if the virtual body was moving by itself							

Statement	−3	−2	−1	0	1	2	3
Q10. It seemed as if I felt the touch of the row in the location where I saw the virtual body touched							
Q11. It seemed as if the touch I felt was located somewhere between my physical body and the virtual body							
Q12. It seemed as if the touch I felt was caused by the row touching the virtual body							
Q13. It seemed as if my body was touching the boat							
Q14. I felt as if my body was located where I saw the virtual body							
Q15. I felt out of my body							
Q16. I felt as if my (real) body were drifting towards the virtual body or as if the virtual body were drifting towards my (real) body							
Q17. It felt as if my (real) body were turning into an “avatar” body							
Q18. At some point, it felt as if my real body was starting to take on the posture or shape of the virtual body that I saw							
Q19. At some point, it felt that the virtual body resembled my own (real) body, in terms of shape, skin tone or other visual features							
Q20. I felt like I was wearing different clothes from when I came to the laboratory							
Q21. I felt that my own body could be affected by the movement of the boat							
Q22. I felt a movement sensation in my body when I saw the hands rowing							
Q23. When the boat movement happened, I felt the instinct to row							
Q24. I had the feeling that I might be harmed by the water							

Responses

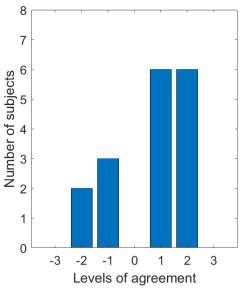

(a) Question 1

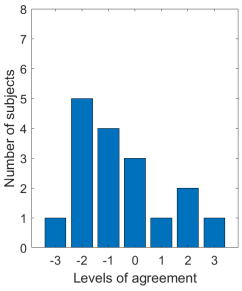

(b) Question 2

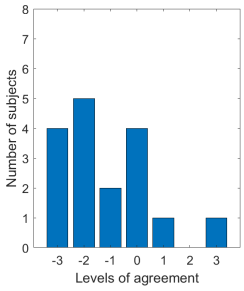

(c) Question 3

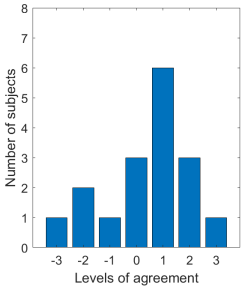

(d) Question 4

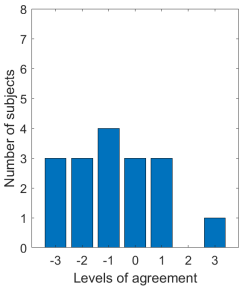

(e) Question 5

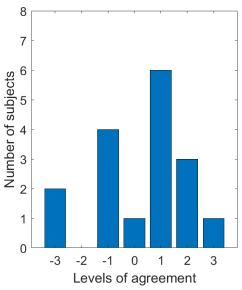

(f) Question 6

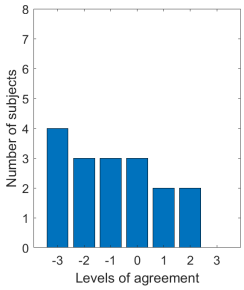

(g) Question 7

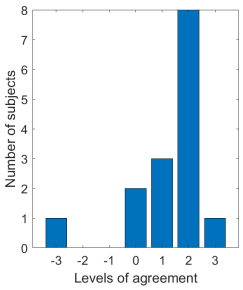

(h) Question 8

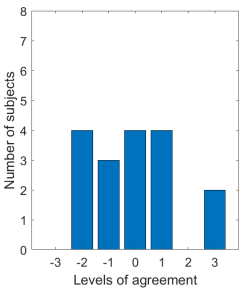

(i) Question 9

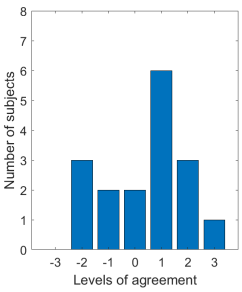

(j) Question 10

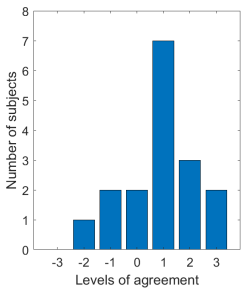

(k) Question 11

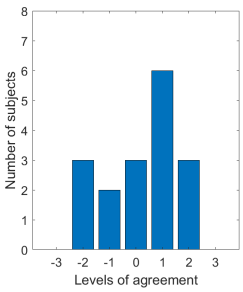

(l) Question 12

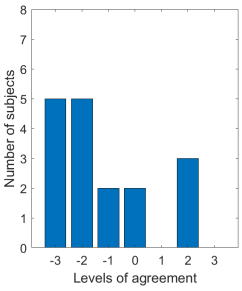

(m) Question 13

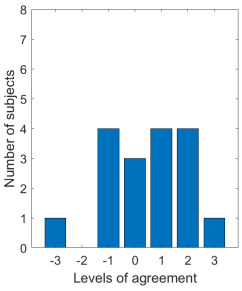

(n) Question 14

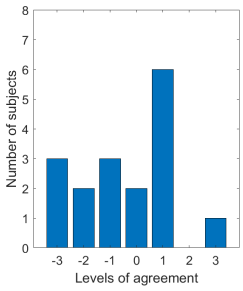

(o) Question 15

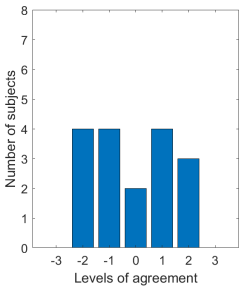

(p) Question 16

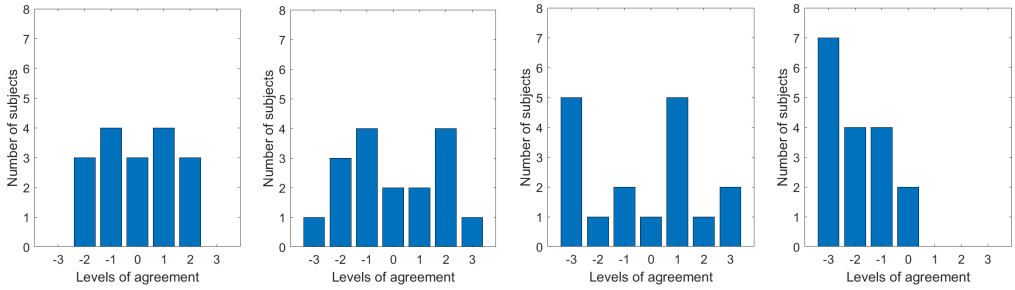

(q) Question 17 **(r)** Question 18 **(s)** Question 19 **(t)** Question 20

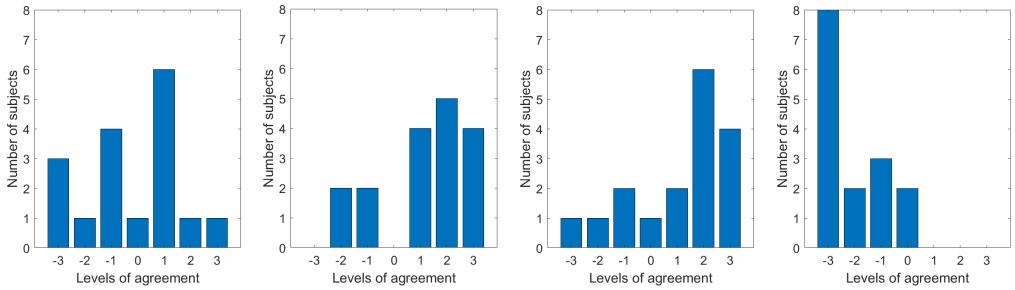

(u) Question 21 **(v)** Question 22 **(w)** Question 23 **(x)** Question 24

Figure A.3: Bar charts of the answers to the embodiment questionnaire

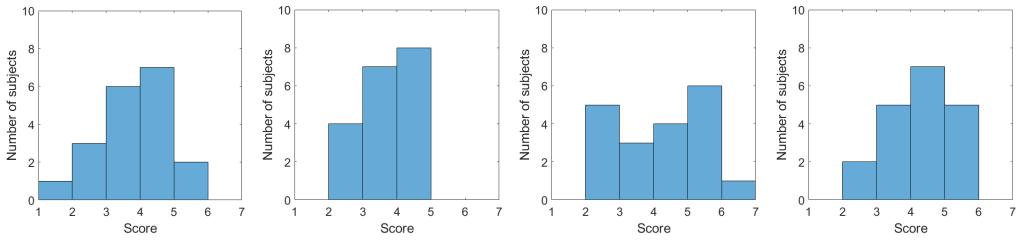

(a) Appearance **(b)** Response **(c)** Ownership **(d)** Multisensory

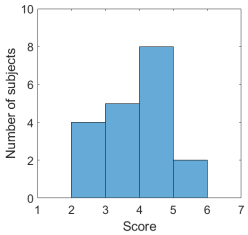

(e) Final score

Figure A.4: Histograms of the embodiment scores computed from the questionnaire

B

Supplementary Figures

This appendix has figures with results from the questionnaire correlations that were either not particularly important to show in the Results chapter, took up a significant number of pages in the main body of the thesis, or both.

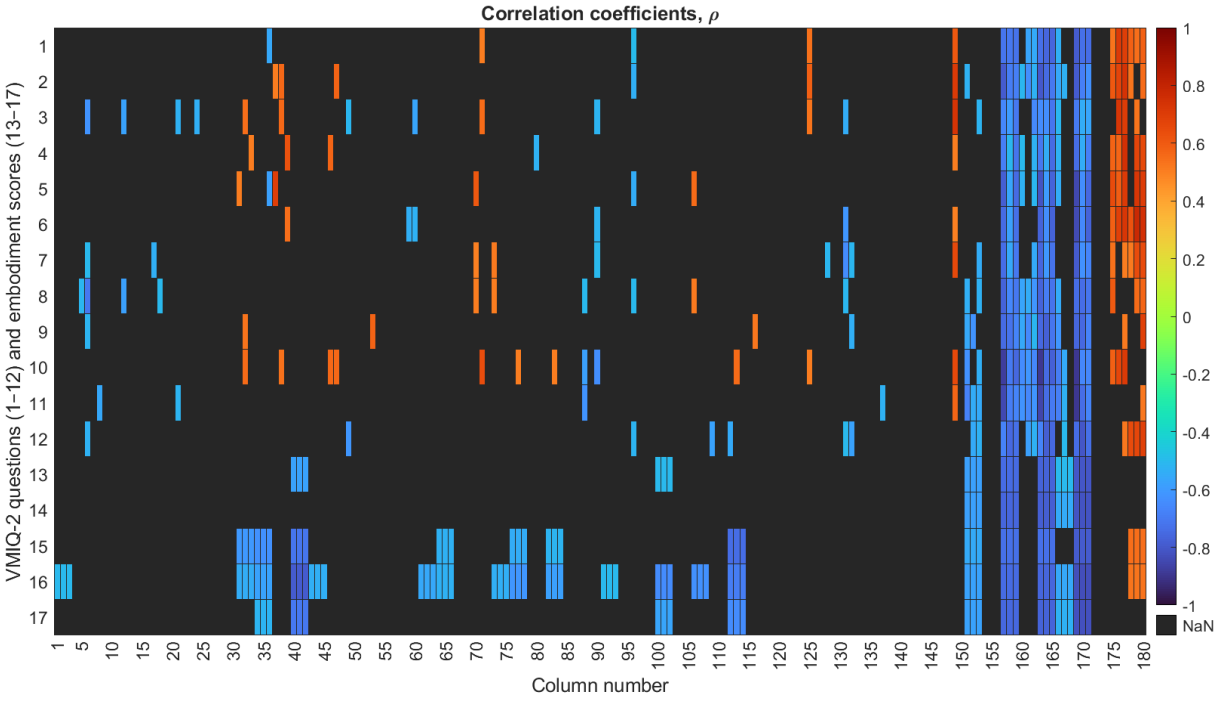

Figure B.1: Heat map of statistically significant ($p < 0.05$) correlations between VMIQ-2 items and embodiment scores (appearance, response, ownership, multisensory, and the final score) and the EEG metrics, ERDs and LIs

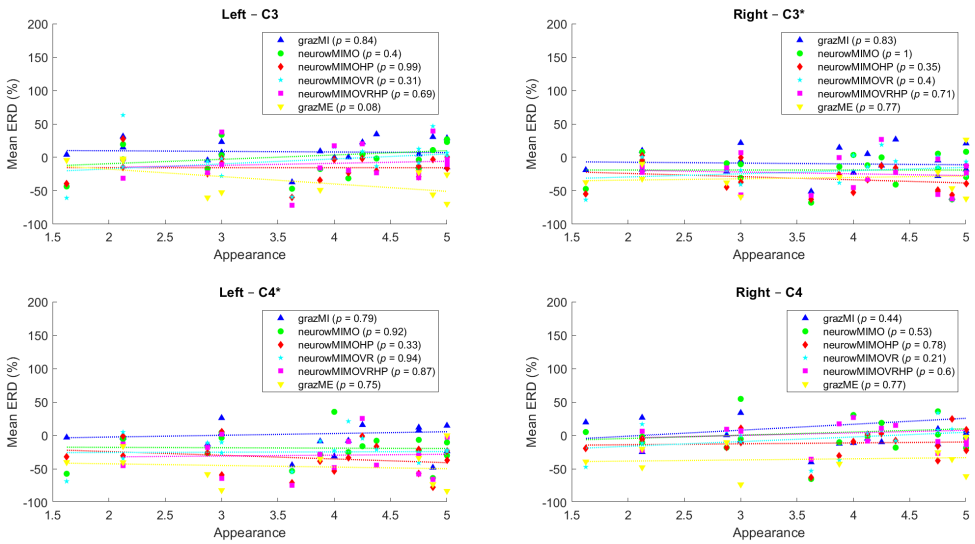

(a) Appearance vs. alpha mERD

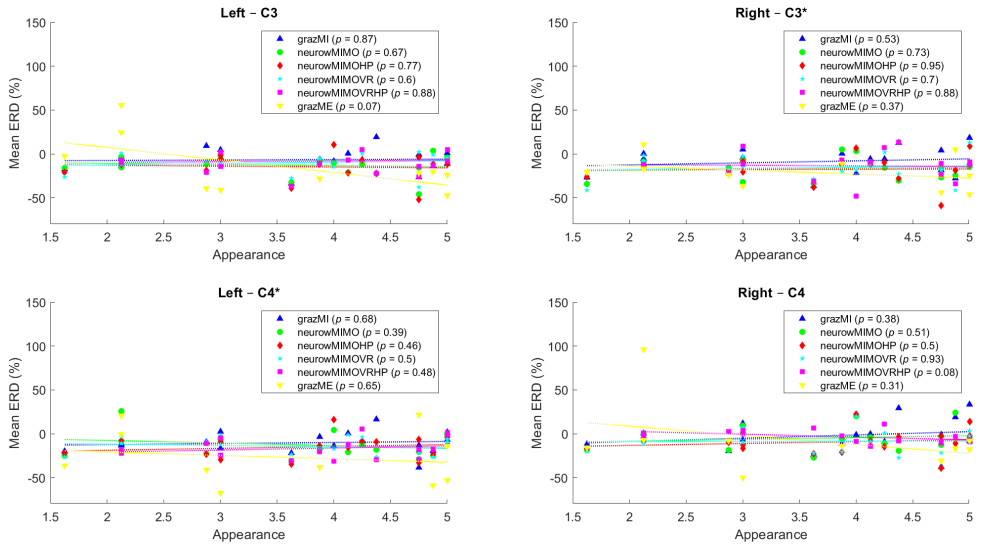

(b) Appearance vs. beta mERD

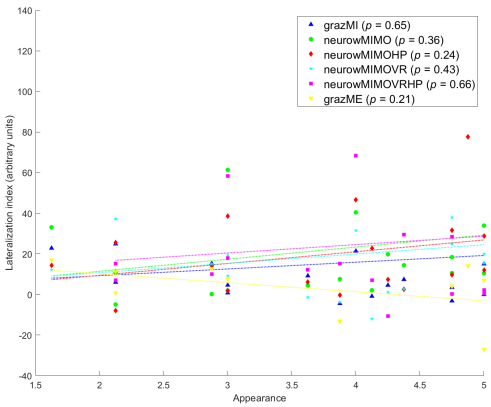

(c) Appearance vs. alpha LIs

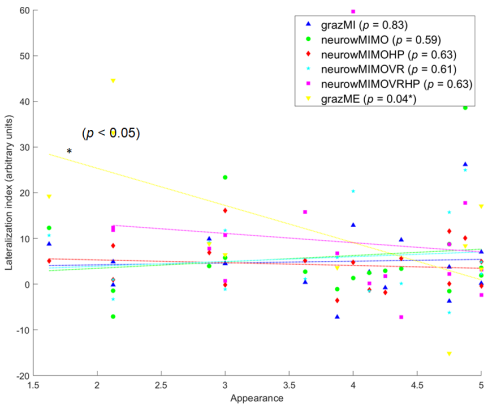

(d) Appearance vs. beta LIs

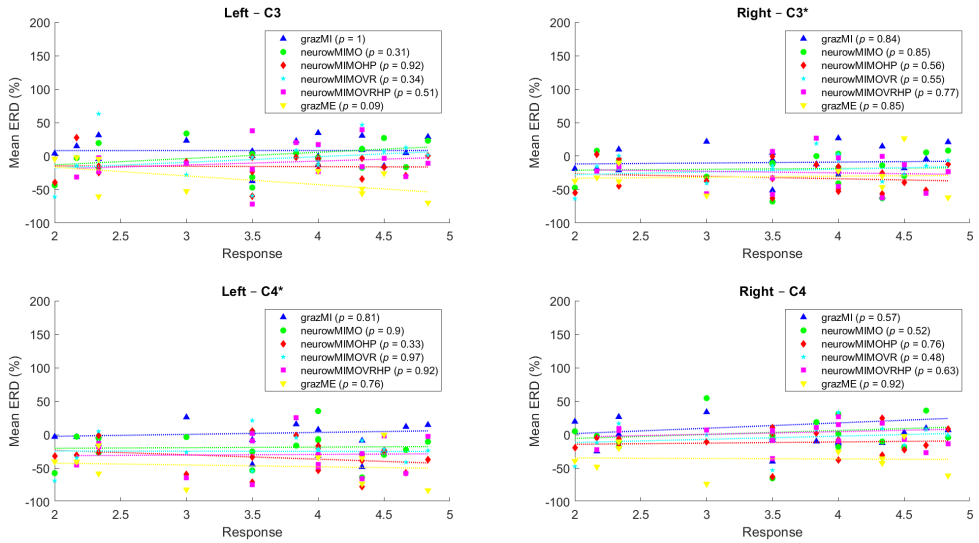

(e) Response vs. alpha mERD

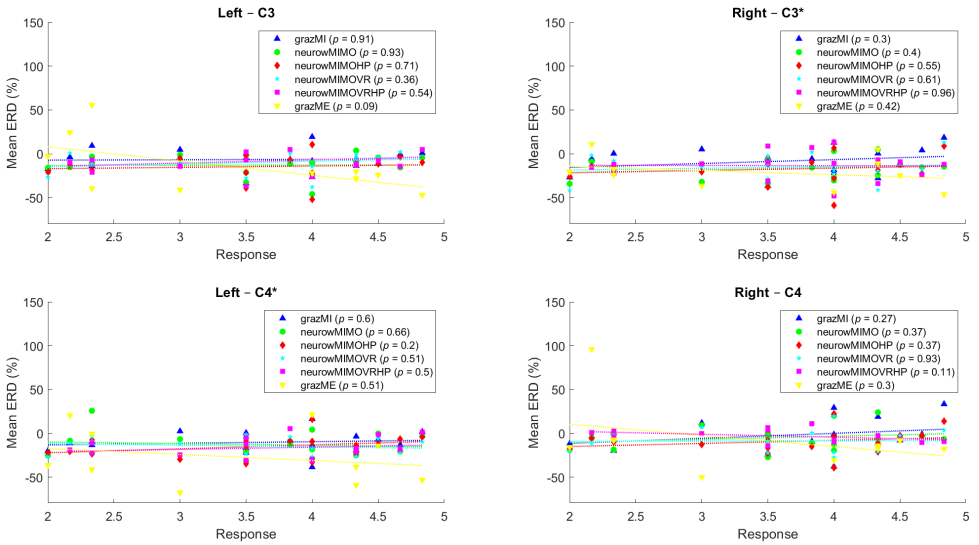

(f) Response vs. beta mERD

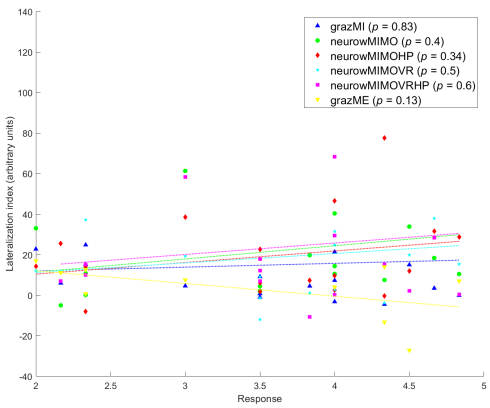

(g) Response vs. alpha LIs

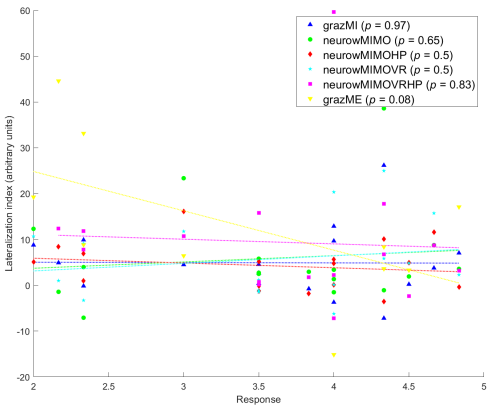

(h) Response vs. beta LIs

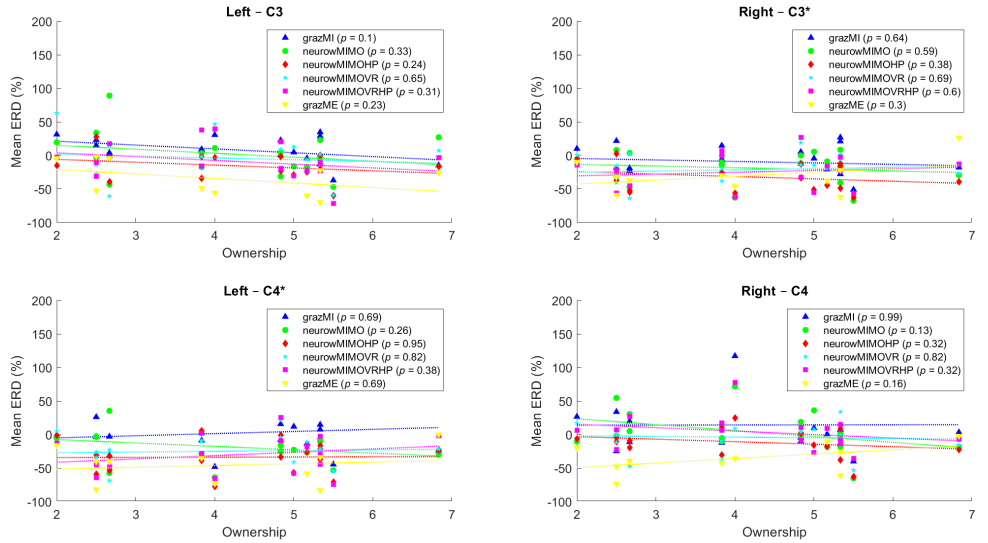

(i) Ownership vs. alpha mERD

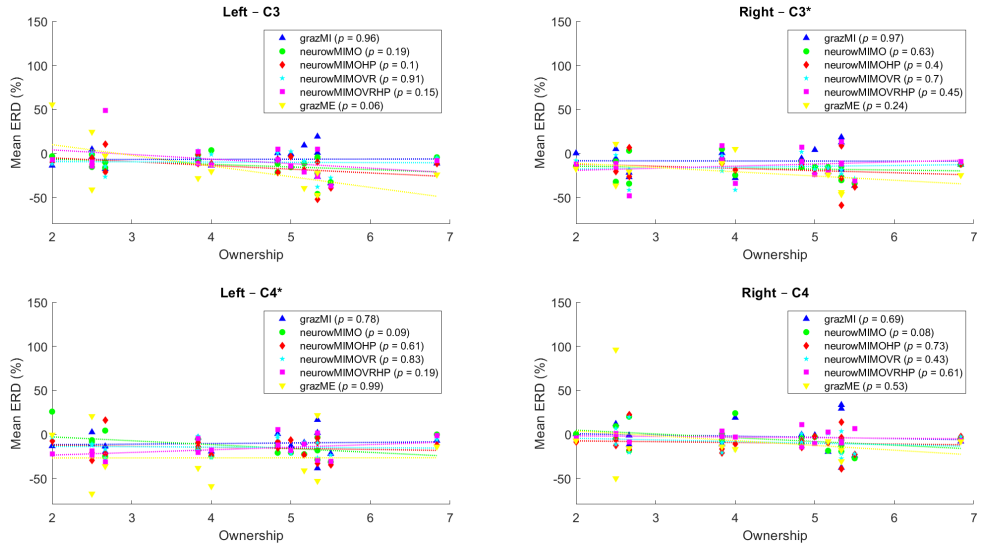

(j) Ownership vs. beta mERD

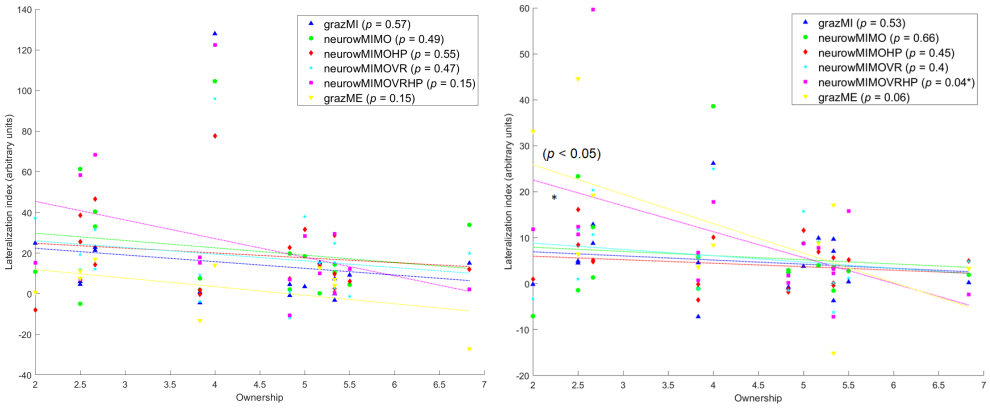

(k) Ownership vs. alpha LIs

(l) Ownership vs. beta LIs

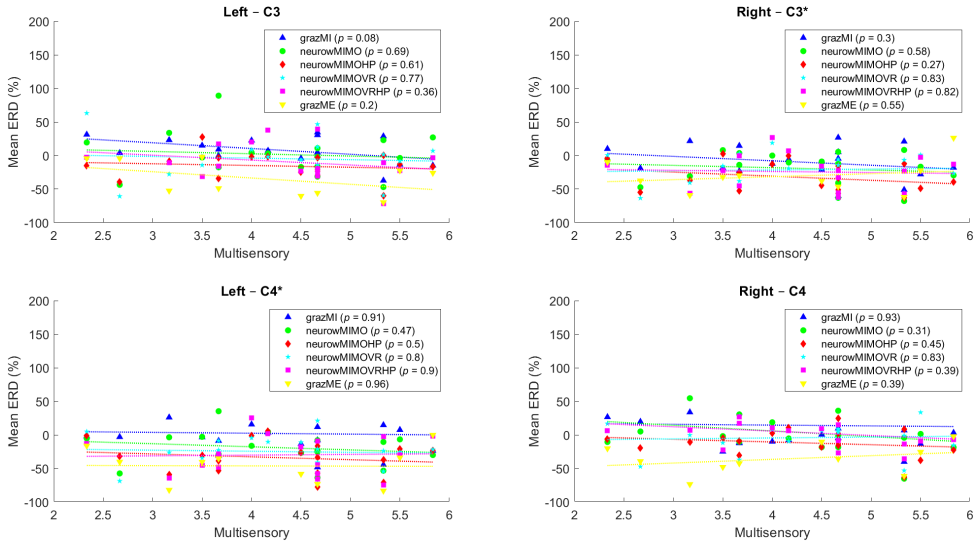

(m) Multisensory vs. alpha mERD

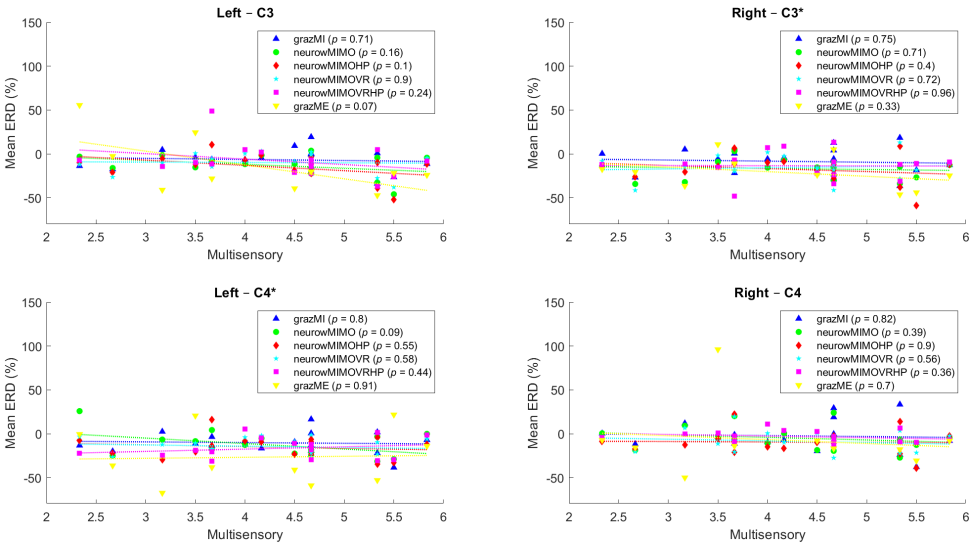

(n) Multisensory vs. beta mERD

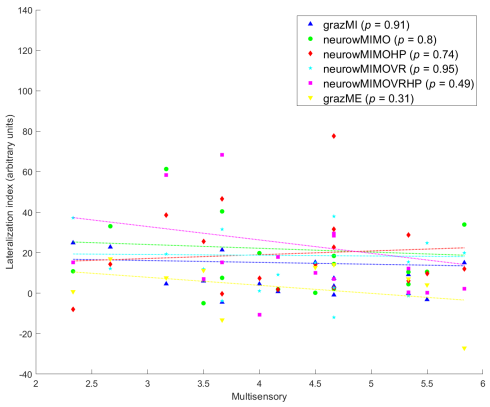

(o) Multisensory vs. alpha LIs

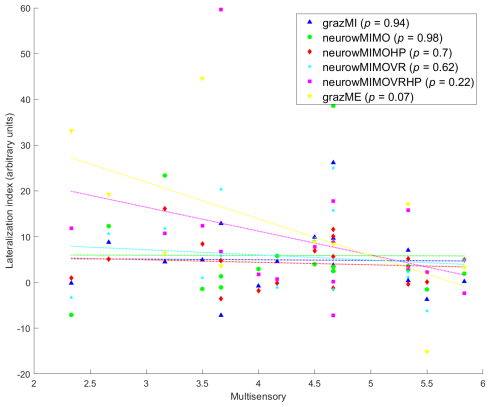

(p) Multisensory vs. beta LIs

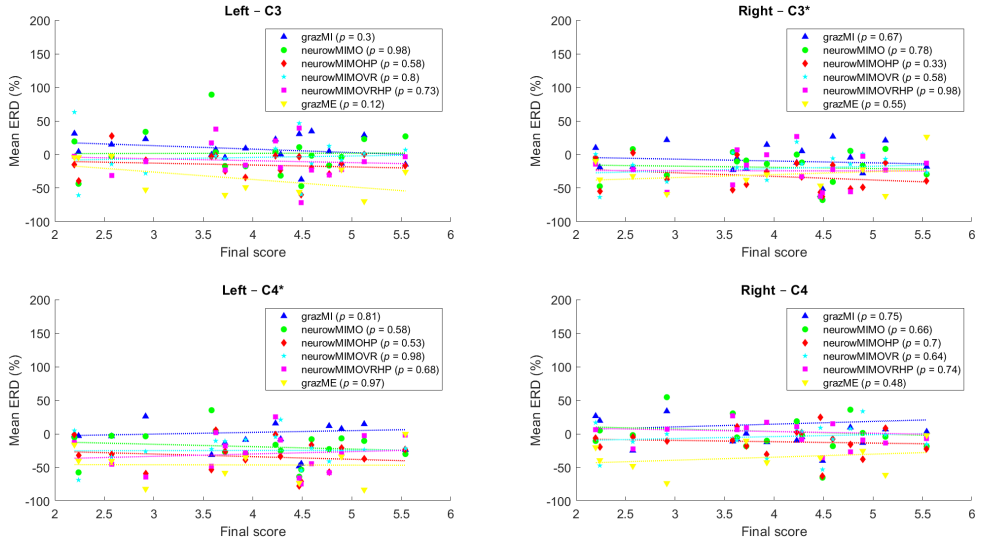

(q) Final score vs. alpha mERD

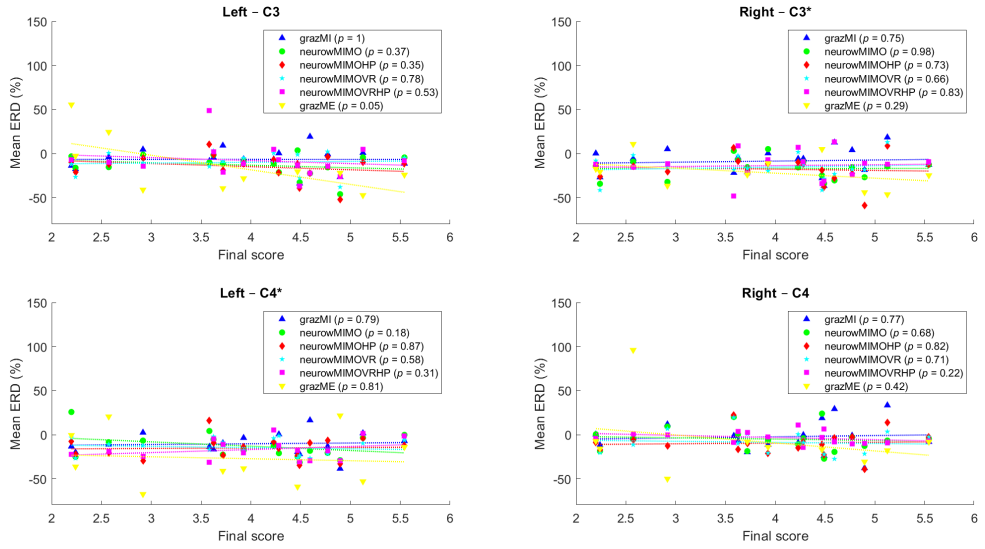

(r) Final score vs. beta mERD

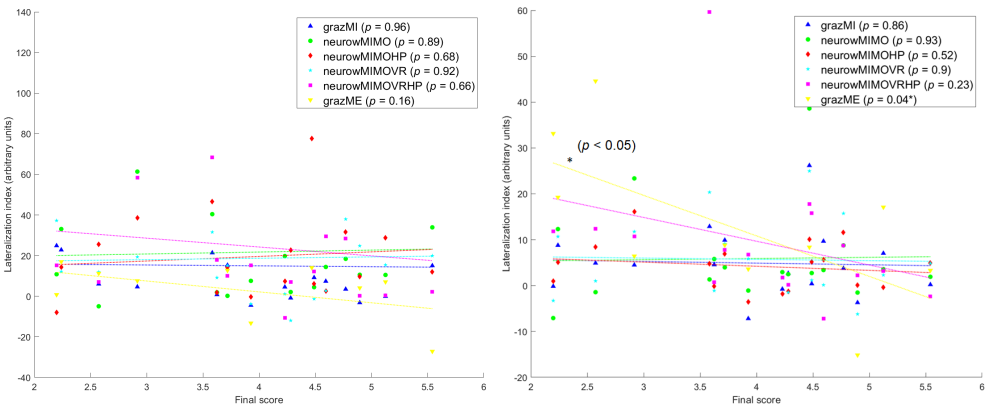

(s) Final score vs. alpha LIs

(t) Final score vs. beta LIs

Figure B.2: Scatter plots of the EEG-metric values and the embodiment-questionnaire scores, where the asterisks show statistically significant correlations ($p < 0.05$)